Analysis of Phonon-Drag Thermomagnetic Effects in n-Type Germanium*

By C. HERRING, T. H. GEBALLE and J. E. KUNZLER

(Manuscript received November 12, 1958)

A study has been made of the Nernst effect and the variation of thermoelectric power with magnetic field for single-crystal samples of n-type germanium of various orientations and impurity concentrations, at fields up to 18,000 gauss and temperatures from 275° to 60°K and below. Except at the highest temperatures, both effects arise predominantly from that part of the thermoelectric power which is due to phonon drag. All observations can be quantitatively accounted for by theory. They yield information about the dependence of the relaxation times for phonon-phonon scattering on the frequency of the phonons, and establish with some certainty the conclusion that four-phonon collisions are much less important than three-phonon collisions in the pertinent range of temperatures and phonon frequencies. Auxiliary investigations have shown that the quantization of electron orbits in a magnetic field has only a small effect on transport properties when the cyclotron level spacing is less than thermal energy. The mean free path of electrons is shown to be energy-independent, as acoustic-scattering theory predicts. The absolute mobility can be predicted to within 10 per cent or better from data on the fractional changes of resistance with stress and magnetic field.

A more detailed summary of the conclusions and implications of the present work is given in Section IX.

1. INTRODUCTION

In a recent paper[1] we have presented measurements of the Nernst effect and the change of thermoelectric power in a magnetic field for n-type germanium of high purity. These two effects were shown to be

* This paper, though complete in itself, constitutes part II of a study, part I of which was presented in Ref. 1. In addition to describing the phenomena and the physical principles underlying them, Ref. 1 develops the background of the present study and gives details of the measuring techniques.

compounded out of electron-diffusion and phonon-drag contributions, the latter being the predominant one in the range near liquid-air temperature. Now the phonon-drag phenomenon[2] — the pushing of charge carriers from hot to cold by the asymmetric phonon distribution which a thermal gradient produces — depends on the details of both the electron-phonon interaction and the processes which scatter phonons. The anisotropies of these interactions and their dependences on wave number enter in different ways into the several thermomagnetic quantities which one can measure. Thus, an analysis of thermomagnetic data should make it possible to sort out the different factors involved in phonon drag, and to obtain information not previously available about electron-phonon and phonon-phonon interactions. In our first paper we used qualitative arguments to draw a number of semiquantitative conclusions about these interactions. Our object in the present paper is to make these conclusions as quantitative as possible, by comparing the observations with explicit theoretical formulas.

1.1 *Basic Concepts*

Following our previous practice,[1] we shall formulate the theory in terms of the Peltier tensor $\mathbf{\Pi}$ of the electrons, which is related to the thermoelectric power tensor $\mathbf{Q}$ in a magnetic field $\mathbf{H}$ by

$$\mathbf{Q}_{\alpha\beta}(\mathbf{H}) = \frac{\mathbf{\Pi}_{\beta\alpha}(-\mathbf{H})}{T}. \tag{1}$$

Here, $\mathbf{\Pi}$ is defined as the tensor relating the energy flux $\mathbf{F}$, relative to the Fermi level, to the current density $\mathbf{j}$:

$$\mathbf{F} = \mathbf{\Pi} \cdot \mathbf{j}. \tag{2}$$

In terms of the Q-tensor, the change of thermoelectric power in the α direction, due to $\mathbf{H}$, is

$$\Delta Q = Q_{\alpha\alpha}(\mathbf{H}) - Q_{\alpha\alpha}(\mathbf{0}). \tag{3}$$

The Nernst coefficient $\mathrm{B}(\mathbf{H})$ is defined — for the symmetrical orientations considered here — by

$$\mathbf{E}_N = -B\mathbf{H} \times \nabla T, \tag{4}$$

where $\mathbf{E}_N$ is the open-circuit field transverse to the temperature gradient. We shall obtain B from (1) and the relation

$$BH = -Q_{yx}, \tag{5}$$

which applies if ∇T is in the x-direction and $\mathbf{H}$ in the z-direction.

The model which we shall use as a basis for our calculations is the "electron-group" model described in our previous paper.[1] In this, the possible states of motion of the charge carriers are divided into a number of groups, g, and the assumption is made that for each such group the distribution function over the group is determined by the contribution, $\mathbf{j}_g$, which the states of this group make to the current density. Carriers of all groups are, of course, subject to the same electric and magnetic fields.

For a multivalley semiconductor like n germanium, a natural choice is to let a group g consist of the states in an ellipsoidal shell of the Brillouin zone, of energy range ϵ to $\epsilon + d\epsilon$, in a particular valley. Each such group g has its characteristic Peltier tensor $\mathbf{\Pi}_g$; this must be independent of $\mathbf{H}$ if, as we are assuming, $\mathbf{H}$ affects the $\mathbf{j}_g$'s of the different groups but not the distribution function for a given $\mathbf{j}_g$. The total Peltier tensor of the medium can be compounded out of those of the different groups. Explicitly,

$$\mathbf{\Pi}(\mathbf{H}) = \Sigma_g \mathbf{\Pi}_g \cdot \mathfrak{o}_g(\mathbf{H}) \cdot \mathfrak{g}(\mathbf{H}), \tag{6}$$

where $\mathfrak{o}_g$ is the conductivity tensor of group g and $\mathfrak{g} = (\Sigma_g \mathfrak{o}_g)^{-1}$ is the total resistivity tensor.

For any one of the ellipsoidal shells just mentioned, the Peltier tensor $\mathbf{\Pi}_g$ must have the symmetry of the valley, which for n germanium is axial symmetry about a [111]-type direction. Thus, $\mathbf{\Pi}_g$ is describable in terms of its two principal components, $\Pi_\parallel(\epsilon)$, along this direction (the high-mass direction), and $\Pi_\perp(\epsilon)$, normal to it. Each of these components, in turn, is a sum of an electron-diffusion term (subscript e) and a phonon-drag term (subscript p). Here, $\Pi_{e\parallel} = \Pi_{e\perp}$ and is a linear function of ϵ, while $\Pi_{p\parallel}(\epsilon) \neq \Pi_{p\perp}(\epsilon)$. Our task is to relate these functions of energy explicitly to the low- and high-field values of the Nernst coefficient B and the change ΔQ in the thermoelectric power.

1.2 *Qualitative Properties of* $\Pi_{p\parallel}$ *and* $\Pi_{p\perp}$

As we formulate the detailed theory in the following sections, it will be helpful to keep in mind two qualitative conclusions which can be drawn from our earlier study.[1] The first of these concerns the anisotropy ratio of the phonon-drag Peltier coefficient. It is that

$$\frac{\Pi_{p\parallel}(\epsilon)}{\Pi_{p\perp}(\epsilon)} \gg 1 \quad \text{but} \quad < \frac{m^*_\parallel \tau_\perp}{m^*_\perp \tau_\parallel} \approx 17, \tag{7}$$

where $m^*_\parallel$, $m^*_\perp$ are the principal effective masses and $\tau_\parallel$, $\tau_\perp$ are the

acoustic-scattering relaxation times[3] for current contributions in the corresponding directions. A large anisotropy of this sort is to be expected, since, if all the phonon modes had the same velocity and relaxation time τ_{ph}, the ratio $\Pi_{p\parallel}/\Pi_{p\perp}$ would be the ratio of the rates of crystal-momentum loss to the lattice for unit currents in the high-mass and low-mass directions, and this is just $m^*_{\parallel}\tau_{\perp}/m^*_{\perp}\tau_{\parallel}$.

Our second conclusion had to do with the energy dependence of $\Pi_{p\parallel}$ and $\Pi_{p\perp}$. All the quantities which we have measured correspond to various kinds of weighted averages of $\Pi_{\parallel}$ and $\Pi_{\perp}$. A typical such average of $\Pi_{p\parallel}$ and $\Pi_{p\perp}$, considered as a function of energy ϵ, decreases as ϵ increases, at a rate distinctly slower than $\epsilon^{-\frac{1}{2}}$. This was shown to correspond to a frequency dependence of the relaxation time τ_{ph} of the pbonon modes intermediate between ω^{-1} and ω^{-2} and nearer to the former.

1.3 *Program*

In Section II and Appendix A we shall discuss critically the adequacy of the electron-group model, reporting several auxiliary experimental and theoretical investigations which bear on this question. After establishing that the model should be quite good for pure n germanium at liquid-air temperature and above, we shall describe in Section III the procedures used for deriving the formulas for B and ΔQ. The explicit derivations will be given in Appendix B in a form applicable to any multivalley medium (e.g., n silicon); the formulas we need for the present application will be summarized in Section IV. In Section V we shall present the raw experimental data and discuss the corrections which need to be applied to them before comparing them with the theory. In Sections VI and VII we shall make the comparison for temperatures in the range 60° to 131°K, with the object of deducing from it as much information as possible about the functions $\Pi_{p\parallel}(\epsilon)$ and $\Pi_{p\perp}(\epsilon)$. In Section VIII we shall discuss various further observations, such as the behavior of B at high fields and the thermomagnetic effects above 200°K. These observations, which for experimental or theoretical reasons are less amenable to precise analysis, still are in good accord with the conclusions previously drawn, and allow them to be slightly extended. Section IX will summarize the arguments and give a few remarks on the significance of the conclusions for the theories of electron-phonon and phonon-phonon interactions, topics which we hope to treat more fully in later publications.

II. CRITIQUE OF THE ELECTRON-GROUP MODEL

For a multivalley semiconductor the electron-group model, described above and in our earlier paper,[1] is based on two assumptions: (a) that the distribution function in any particular ellipsoidal energy shell can be approximated by a linear function of the crystal momentum over the shell and (b) that this distribution function is determined only by the external fields, being independent of the distribution functions of other shells. We must first examine critically the adequacy of this model; then we shall consider further specializations of it.

The adequacy of the electron-group model depends on the answers to the following questions:

i. Is it legitimate to use a transport equation in crystal-momentum space?

ii. How accurately can one separate the transport problems for different energy shells?

iii. How well is the distribution function in a single shell approximated by a linear function of the crystal momentum?

As regards i, there are two things which might undermine the validity of a transport equation in crystal-momentum space alone — inhomogeneities and orbital quantization. Distortion of the current distribution by inhomogeneities in the specimen may make it necessary to consider the transport problem in position as well as in velocity space. This trivial but annoying difficulty in the interpretation of experiments will be discussed at length by one of the authors in another place;[4] it causes the transverse magnetoresistance to fail to saturate as $H \rightarrow \infty$, but has very little effect on thermoelectric and thermomagnetic properties. The reason for the difference is simple. When a current flows, portions of the specimen with different carrier concentrations try to set up different Hall fields, and can only adjust to one another by a distortion of the current lines, which becomes large as $H \rightarrow \infty$. Thermoelectric and thermomagnetic effects, on the other hand, are measured at zero average current, and set up fields which are much less sensitive to inhomogeneities than the Hall field is. The fields also remain finite as $H \rightarrow \infty$, whereas the Hall field does not. For this reason, and because measurements on different pairs of side-arms showed the gross homogeneity of our specimens to be quite good, we believe the effect of inhomogeneity on our results to be negligible.

A less trivial objection to the use of a transport equation in crystal-momentum space is the fact of orbital quantization, which is known to make the high-field magnetoresistance qualitatively different from the

predictions of a transport theory formulated in crystal-momentum space.[5-11] It can be argued theoretically that this is not serious until the spacing, $\hbar\omega_c$, of the cyclotron levels becomes comparable with kT; however, for n germanium with 18,000 gauss along a [100] axis, $\hbar\omega_c$ corresponds to kT at about 25°K, and one may wonder whether this is negligible for experiments at 77°. Fortunately, theoretical and empirical evidence, which we have gathered together in Appendix A, indicates that for our specimens the effect of orbital quantization on the resistance and thermoelectric power is probably not more than 5 per cent or so at 18,000 gauss and 77°, and that for many orientations it is probably considerably less. The main arguments can be summarized as follows:

1. The theory of longitudinal magnetoresistance,[7] when interpreted with allowance for the energies of the phonons which do the scattering,[8] predicts only rather small departures from the unquantized theory as long as $\hbar\omega_c < kT$. Observations[12] support this conclusion.

2. Both for longitudinal and transverse cases the phonon-drag part Π_p of the Peltier coefficient is proportional to the product of the resistivity, the average relaxation time of the phonon modes which scatter the electrons, and the average squared velocity of these modes. As the effect of orbital quantization on the average relaxation time and velocity is probably rather less than on the resistivity, the quantization effect should be of similar magnitude for electrical and for thermoelectric measurements.

3. Although the theory for transverse magnetoresistance is more complicated than for longitudinal magnetoresistance, a combination of reasonable arguments with empirical evidence yields a rough upper bound for the orbital quantization effect. Contradictory approaches to the theory have been elaborated for the case of acoustic scattering by Klinger and Voronyuk,[9]* Argyres[10] and Wolff;[11] the resulting formulas can be evaluated for high fields ($\hbar\omega_c \gg kT$), but become very cumbersome at lower fields. A plausible presumption is that for constant carrier concentration and in the limit of small scattering (Hall angle practically $\pi/2$) the departure from the resistivity given by the older transport theory varies at least as fast as $\hbar\omega_c/kT$, as long as this quantity is rather less than unity. The size of the factor of proportionality cannot be estimated reliably from the nonsaturation of transverse magnetoresistance,

* These authors evaluate their expressions only for the limiting case of fields so large that the energy of an average phonon causing transitions of the electrons is $\gg kT$. However, it is easy to show that, for the case $\hbar\omega_c/kT \gg 1$ and phonon energies negligible, this approach yields a magnetoresistance that goes very nearly as H^2. (*Note added in proof:* We are indebted to E. N. Adams and T. Holstein for communicating to us an as-yet-unpublished analysis that shows the approach of Ref. 9 to be the correct one.)

since this can be shown to arise in large part from other effects. However, the factor can be estimated from thermoelectric data at liquid-hydrogen and intermediate temperatures.

4. The fair agreement of theory and experiment on high-field transverse magnetoresistance would be spoiled if orbital quantization increased the resistivity by any sizable amount. The resulting discrepancy would be hard to explain away, as most perturbing effects (inhomogeneities, surface conduction, etc.) also increase the magnetoresistance.

Turning to question ii at the beginning of this section, we must consider scattering processes which change the energy. In highly doped material the most important processes of this sort are electron-electron collisions. There is also another effect: at carrier concentrations high enough to make the low-frequency phonons have an effective drift velocity comparable with that of the electrons — the so-called saturation effect[2] on Π_p — the contribution of any electron group to Π is reduced by the unbalance of the distribution function of the phonons with which it interacts. Since this unbalance is influenced by the interactions of these phonons with all other electron groups, it is no longer possible at such concentrations to separate $\mathbf{\Pi} \cdot \mathbf{j}$ into a sum of $\mathbf{\Pi}_g \cdot \mathbf{j}_g$. At low carrier concentrations, however, both these effects become negligible, and the only type of energy change on scattering which must be considered is that due to the finiteness of the energies of the phonons. Only acoustical phonons need to be investigated, since scattering by intervalley or nonpolar optical modes occurs with almost equal probability to all final states in an energy shell,[13] and therefore is describable by a relaxation time dependent only on the initial state.

The most detailed study which has appeared on the effect of acoustic-phonon energies is that of Dorn.[14] He estimated the effect on the distribution function for a simple-model semiconductor in an electric field, using both a high-temperature expansion method and a variational method. He found that, as one expects, the fractional alteration in the mobility due to the phonons having finite rather than zero energy is very small in the temperature range of interest to us. The alteration is of the order of m^*c^2/kT, where m^* is the effective mass and c the velocity of sound. With a reasonable average m^* for n germanium, m^*c^2/k is only a small fraction of a degree. However, Dorn's expressions show that the fractional alteration in the current of a shell of energy ϵ is of order m^*c^2/ϵ for $\epsilon \ll kT$ but $\gg m^*c^2$. Since for pure lattice scattering the low-field magnetoresistance and ΔQ effects are dominated by the behavior of low-energy carriers, the effects of the phonon energies may be expected to be considerably more serious for these than for the mobility in the ab-

sence of a magnetic field. A quantitative estimate of these effects in a magnetic field and with anisotropic masses would be of some interest. However, it seems likely that they are still small. The fractional alteration in the H^2 term in the current of a shell should still be of order m^*c^2/ϵ, although perhaps with a sligbtly larger coefficient than for Dorn's case. Since, for a shell ϵ to $\epsilon + d\epsilon$ containing dn carriers, this H^2 term goes as $\epsilon\tau^3 dn \propto d\epsilon$ for $\epsilon \ll kT$, the phonon-energy correction should involve $\int d\epsilon/\epsilon$. Thus, we guess that

$$\text{fractional correction to magnetoresistance} \approx \frac{m^*c^2}{kT} \ln \frac{kT}{m^*c^2}. \quad (8)$$

Since the phonon-drag Peltier coefficients of the different shells do not vary much witb energy, (8) should apply to the thermoelectric power also. For n germanium in the range near liquid-air temperature, the value of (8) is at most a few per cent.

We can now give a prescription for answering question iii, the last of the three posed at the start of this section. This question had to do with the legitimacy of approximating the distribution function in each energy shell by a linear function of crystal momentum. Since questions i and ii have by now received favorable answers, we need only to solve tbe transport equation for an energy shell under the influence of arbitrary electric and magnetic fields, and see how well the current and Peltier-heat contributions from the accurate solution agree with those from the electron-group approximation. Now the latter approximation amounts to retaining only $l = 1$ spherical harmonics in the distribution function in a new set of variables which take the ellipsoidal energy surfaces into spheres[3] — variables which we have used for other purposes in Appendix A. The terms in the scattering operator which mix $l = 1$ with higher l values — call these S_{1l} — can be shown[3] to affect the electric current only to the second order, i.e., $|S_{1l}|^2$. They may, however, affect tbe Peltier flux to order $S_{1l}T_l$, where T_l measures the Peltier flux which would be produced by a distribution with the l value in question. Now the longitudinal and transverse branches individually contribute quite anisotropic scattering, but their combined effect in germanium is almost isotropic, so the S_{1l} for $l \neq 1$ are small. But since the relative contributions of the two branches to the phonon-drag Peltier effect are not known, it is quite conceivable that the $S_{1l}T_l$ for $l \neq 1$ are not negligible, even though tbe $|S_{1l}|^2$ are. A detailed investigation of this question using deformation-potential theory has been made for the case $l = 3$ and, to some extent, for larger l, and will be reported elsewhere.[15] The result is that, for germanium, both the S_{1l} and the T_l are quite small, and that the retention

of only the $l = 1$ term in the distribution function should be a very good approximation for all conduction and thermoelectric phenomena, with or without a magnetic field.

III. PROCEDURE FOR COMPUTING B AND ΔQ

Having satisfied ourselves that the electron-group model described in Section I is a good approximation for the cases we wish to analyze, let us now use this model to evaluate explicitly the expressions for B and ΔQ which were given there. In both cases the task is to evaluate (6). This determines the Nernst coefficient B, or the Nernst field (4), via (1) and (5). Similarly, it determines ΔQ via (1) and (3). Since each group g consists of the set of states in the energy range ϵ to $\epsilon + d\epsilon$ in some valley i, it is appropriate to replace the conductivity $\mathfrak{d}_g$ of this group by the infinitesimal $d\mathfrak{d}^{(i)}$, and to rewrite (6) in the form

$$\mathbf{\Pi}(\mathbf{H}) = \Sigma_i \left[\int \mathbf{\Pi}^{(i)}(\epsilon) \cdot d\mathfrak{d}^{(i)}(\mathbf{H}) \right] \cdot \varrho(\mathbf{H}), \tag{9}$$

where the tensor $\mathbf{\Pi}^{(i)}(\epsilon)$ has principal components $\Pi_\parallel(\epsilon)$ and $\Pi_\perp(\epsilon)$ in the principal-axis system of valley i, and where the integration is really over energies ϵ. The tensor $d\mathfrak{d}^{(i)}(\mathbf{H})$ can be obtained by solving the transport equation relating the isothermal current $d\mathbf{j}^{(i)}$ in the energy shell to the electric field $\mathbf{E}$ producing it, and expressing the solution in the form

$$d\mathbf{j}^{(i)} = d\mathfrak{d}^{(i)} \cdot \mathbf{E}.$$

For the case of nondegenerate statistics, which we shall assume throughout, the transport equation for $d\mathbf{j}^{(i)}$ is easily written down, in the electron-group approximation, by equating the rates of gain and loss of crystal momentum in the shell. Anisotropic scattering can be taken into account[3] by assigning to the shell a relaxation-time tensor $\boldsymbol{\tau}$, with principal components $\tau_\parallel(\epsilon)$, $\tau_\perp(\epsilon)$ along and normal to the axis of the valley. The resulting transport equation — in which, for simplicity, we omit the valley suffix i — is[3]

$$\boldsymbol{\tau}^{-1} \cdot \mathbf{m}^* \cdot d\mathbf{j} \pm \left(\frac{e}{c}\right) d\mathbf{j} \times \mathbf{H} = e^2 \left(\frac{\epsilon}{\langle\epsilon\rangle}\right) \mathbf{E}\, dn, \tag{10}$$

where dn is the number of carriers in the shell, $\mathbf{m}^*$ is the effective-mass tensor and $\langle\epsilon\rangle = (3kT)/2$ is the mean energy, and where the upper sign is for electrons, the lower for holes. For small H this can be solved by iteration to give the contributions (48) and (49) of Appendix B to the

conductivity tensor $d\mathfrak{d}$. As $H \to \infty$ the part of **E** normal to **H** becomes interpretable as the Hall field, and the asymptotic value of the part of $d\mathbf{j}$ normal to **H** can be determined by taking the cross product of (10) with **H** and throwing away the first term on the left. This part of $d\mathbf{j}$ is of order H^{-1}; the H^{-1} part of $d\mathbf{j}$ parallel to **H** can be determined from it by dotting (10) with **H**. Higher powers in the expansion of $d\mathbf{j}$ in H^{-1} can be obtained by further iteration. The resulting contributions to $d\sigma$ are given in (68) through (72) of Appendix B.

The resistivity tensor $\mathfrak{\rho}(\mathbf{H})$ occurring in (9) is just the reciprocal of $\Sigma_i \int d\mathfrak{d}^{(i)}(\mathbf{H})$. A few properties of $\mathfrak{\rho}$ and $d\mathfrak{d}^{(i)}$ are worth listing for reference. With superscripts 0, 1, 2, $\cdots$ to denote coefficients of $1, H, H^2, \cdots$ in the expansion of $\mathfrak{\rho}$ or $d\mathfrak{d}$ in powers of H, and $+1, \infty, -1, \cdots$ to denote coefficients of $H, 1, H^{-1}, \cdots$ in the expansion in powers of H^{-1}, we have, for a cubic crystal,

$$\rho_{\alpha\beta}{}^{(1)} = -R(0)\Sigma_\gamma \delta_{\alpha\beta\gamma} H_\gamma , \tag{11}$$

$$\rho_{\alpha\beta}{}^{(+1)} = -R(\infty)\Sigma_\gamma \delta_{\alpha\beta\gamma} H_\gamma , \tag{12}$$

where $R(0)$ and $R(\infty)$ are the limiting values of the Hall constant at $H = 0$ and $H = \infty$, respectively, and where $\delta_{\alpha\beta\gamma} = \pm 1$ when $\alpha\beta\gamma$ is an even (odd) permutation of 123, zero otherwise. For n even (odd), $\mathfrak{\rho}^{(n)}$ and $d\mathfrak{d}^{(n)}$ are symmetrical (antisymmetrical). The symmetrical tensor $\mathfrak{\rho}^{(\infty)}$ is finite and positive definite, but the only nonvanishing component of $d\mathfrak{d}^{(\infty)}$ is the HH component.

The procedure of Appendix B is thus to get the high- and low-field expansions of $d\mathfrak{d}^{(i)}(\mathbf{H})$ by solving (10); to use these, when necessary, to get the corresponding expansions of $\mathfrak{\rho}(\mathbf{H})$; to substitute into (9) to get the expansions for various components of $\mathbf{\Pi}(\mathbf{H})$; and thence to compute the high- and low-field B and ΔQ for various orientations. The results, containing integrals over $\Pi_\parallel(\epsilon)$ and $\Pi_\perp(\epsilon)$, can be expressed in a great variety of forms. Although in Appendix B expressions are obtained for B and ΔQ valid for arbitrary functional forms of $\Pi_\parallel$, $\Pi_\perp$, and for valleys of either the [111] or [100] types in a cubic crystal, these expressions are cumbersome in their most general forms. These forms involve Maxwellian averages of quantities $\epsilon\Pi_{\parallel,\perp} f^{(n)}(\tau_\parallel, \tau_\perp)$, where $f^{(n)}$ is a homogeneous function of degree n in its arguments. These forms therefore simplify greatly if the Π's and τ's are each proportional to some power of the energy ϵ. Now $\Pi_{\epsilon\parallel} = \Pi_{\epsilon\perp}$ is linear in ϵ, while our previous analysis[1] indicates that $\Pi_{p\parallel}$ and $\Pi_{p\perp}$ probably vary at a rate between constancy and $\epsilon^{-\frac{1}{2}}$. Moreover, for ideal acoustic scattering and negligible phonon energies $\tau_\parallel$ and $\tau_\perp$ are $\propto \epsilon^{-\frac{1}{2}}$. Thus, specialization of the formulas to power-law dependences of the Π's and τ's can give a fair picture of

the behavior of $\mathbf{\Pi}_e$ and $\mathbf{\Pi}_p$ separately, although not as accurate a picture as we shall need for our final analysis. We shall give such a specialization in the next section, before discussing more complete formulas.

IV. COMPILATION OF FORMULAS

Tables I through IV give formulas for high- and low-field B_e, B_p, ΔQ_e and ΔQ_p, as obtained by the procedure just described for various cases corresponding to energy-independent anisotropies. The formulas are for [111] valleys and are specialized to the cases $\Pi_{p\parallel,\perp} \propto \epsilon^{-\frac{1}{2}}$ or independent of ϵ, and $\tau_{\parallel,\perp} \propto \epsilon^{-\frac{1}{2}}$ or independent of ϵ. Comparison of the latter two alternatives makes possible a crude estimate of the effect of impurity scattering. Although these special cases do not give as accurate a representation of the data as we shall ultimately wish to use, they do give a fair representation. They are worth listing because their comparative simplicity makes it easy to see how sensitive the various measurable quantities are to the assumed anisotropies and energy dependences. All the tables contain references to equations of Appendix B. Most of these equations are more general expressions for the quantities tabulated, valid even when the anisotropies are not energy-independent. Also, they are applicable to multivalley band structures different from that of germanium.

The formulas for the low-field Nernst coefficient (see also Equation B.4 of Ref. 1) are most conveniently expressed in terms of the dimensionless coefficients ζ_e and ζ_p, defined by

$$B_e = \zeta_e \left(\frac{k}{e}\right)\left(\frac{\mu_H}{c}\right), \qquad B_p = \zeta_p \mid Q_p \mid \left(\frac{\mu_H}{c}\right), \tag{13}$$

where, as always, B_e and B_p represent, respectively, the electronic and phonon-drag contributions to B. Table I gives the expressions obtained in Appendix B for ζ_e and ζ_p for the case of energy-independent anisotropies. Note that $(1 + \zeta_p)$ is the product of a factor dependent only on the energy variations of the Π's and τ's by a factor dependent only on their anisotropies. The anisotropy factor is unity when the tensor $\mathbf{m}^* \cdot \boldsymbol{\tau}^{-1}$ is isotropic, and likewise when the tensor $\mathbf{\Pi}_{pq}$ is isotropic ($\Pi_{p\parallel} = \Pi_{p\perp}$); the energy factor is unity if either $\boldsymbol{\tau}$ or $\mathbf{\Pi}_{pq}$ is independent of energy. Fig. 1 shows the dependence of the anisotropy factor in $(1 + \zeta_p)$ on $p = \Pi_{p\parallel}/\Pi_{p\perp}$. Curves are drawn for several values of the anisotropy w of $\mathbf{m}^* \cdot \boldsymbol{\tau}^{-1}$, chosen to encompass the ranges likely to occur for germanium and silicon.

TABLE I

Values of the dimensionless coefficients ζ_e, ζ_p, related by (13) to the electronic and phonon-drag parts of the low-field Nernst coefficient, respectively. The expressions given apply when the ratios $w = \tau_\parallel m_\perp^*/\tau_\perp m_\parallel^*$ and $p = \Pi_{p\parallel}/\Pi_{p\perp}$ are independent of energy. They are valid for any type of valleys in a cubic crystal (e.g., n silicon or n germanium). Angular brackets represent Maxwellian averages, i.e., averages with weight $\epsilon^{1/2} \exp(-\epsilon/kT)$. For τ, one may take either $\tau_\parallel$ or $\tau_\perp$, and, for Π_p, either $\Pi_{p\parallel}$ or $\Pi_{p\perp}$.

	ζ_e	$1 + \zeta_p$
General formula	$\frac{3}{2}\left[\frac{\langle\epsilon^2\tau^2\rangle}{\langle\epsilon\tau^2\rangle\langle\epsilon\rangle} - \frac{\langle\epsilon^2\tau\rangle}{\langle\epsilon\rangle\langle\epsilon\tau\rangle}\right]$	$\frac{\langle\epsilon\Pi_p\tau^2\rangle\langle\epsilon\tau\rangle}{\langle\epsilon\Pi_p\tau\rangle\langle\epsilon\tau^2\rangle}\left[\frac{(2+w)(1+w+pw)}{(1+2w)(2+pw)}\right]$
Reference, Appendix B	(57), (50)	(57), (51)
Value for: $\tau \propto \epsilon^{-1/2}$, $\Pi_p \propto \epsilon^{-1/2}$	$-\frac{1}{2}$	$4/\pi$ [as above]
τ independent of ϵ, any $\Pi_p(\epsilon)$	0	1 [as above]
Any $\tau(\epsilon)$, Π_p independent of ϵ	—	1 [as above]

Table II gives the part of BH going as H^{-1} when $H \to \infty$, for certain special directions of **H** and **j**, again as obtained by specializing the formulas of Appendix B to the case of [111] valleys and energy-independent anisotropies. Note that at high fields the electronic contribution to the Nernst field is anisotropic and depends on the anisotropy w of $\mathbf{m}^* \cdot \boldsymbol{\tau}^{-1}$, whereas at low fields it does not. Fig. 2 shows the dependence of the phonon-drag contribution on $p = \Pi_{p\parallel}/\Pi_{p\perp}$, for two assumptions about the energy dependence of $\Pi_{p\parallel,\perp}$. Several features of the graphs and formulas are worth noting:

i. The high-field Nernst coefficient is very much larger when **H** is in an [011]-type direction than in an [001]-type. This could have been anticipated from the familiar difference in rapidity of saturation of the Hall coefficient in these two directions, and the close relationship of the Nernst and Hall effects.[1] The cause in both cases is the fact that, for **H** along [011], two of the four valleys have a high-mass direction exactly normal to **H**, and so require large fields to obtain Hall angles near $\pi/2$.

ii. The theoretical behavior of the Nernst coefficient differs from that of the Hall coefficient in that, when **H** is along [011], the value of B is

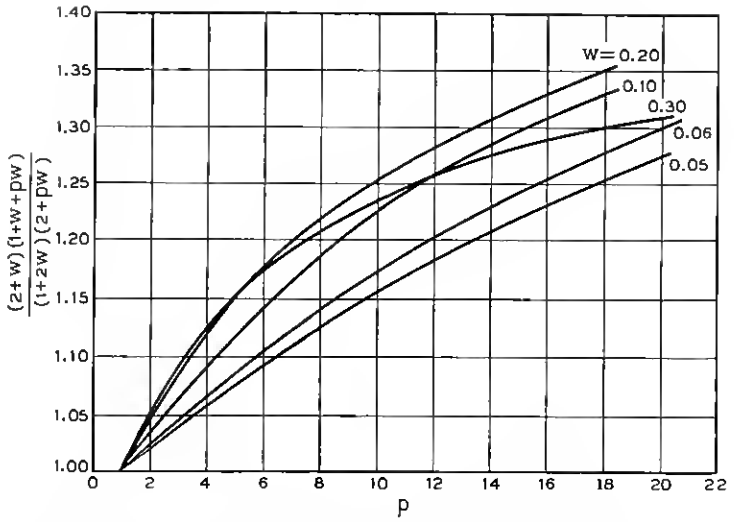

Fig. 1 — Dependence of the anisotropy factor in the expression of Table I for $1 + \zeta_p$ on $p = \Pi_{p\parallel}/\Pi_{p\perp}$, for various values of $w = m^*_{\perp}\tau_{\parallel}/m^*_{\parallel}\tau_{\perp}$.

slightly different for ∇T along [100] and [01$\bar{1}$]. Equality of Hall coefficients for these two directions of **j** is required by the Onsager relations (principle of microscopic reversibility), but equality of the Nernst coefficients is not.[1] For the phonon-drag B_p the theoretical difference is very small when $\Pi_{p\parallel} \gg \Pi_{p\perp}$, but for the electronic B_e it is sizable, e.g., a factor 1.62 for acoustic scattering and $w = 0.06$.

iii. From Tables I and II it follows that the ratio of B_p to B_e is not usually the same at high fields as at low. For most specimens, therefore, there should be a range of temperatures — near that for which $B_p + B_e = 0$ — where the sign of the Nernst voltage will change with increase of H. Substitutions in the formulas give the result that, for any values of the anisotropies in the neighborhood of those obtaining for pure germanium ($p \approx 10$, $w \approx 0.06$), the ratio $|B_p/B_e|$ is greater at high fields than at low fields whenever H is along [011]. When H is along [001], this ratio is less at high fields than at low if $\Pi_{p\parallel,\perp}$ increase with decreasing energy, but becomes the same at high and low fields if $\Pi_{p\parallel,\perp}$ are independent of energy.

The electronic part of the thermoelectric power, $Q_e(\mathbf{H})$, behaves very simply as $H \to \infty$. When **H** and **j** are parallel, the energy distribution of the current is the same at $H = \infty$ and $H = 0$. So, for $\mathbf{H} \parallel \nabla T$,

$$Q_e(\infty) = Q_e(0) = \mp \frac{3}{2}\left(\frac{k}{e}\right)\frac{\langle \epsilon^2 \tau \rangle}{\langle \epsilon \rangle \langle \epsilon \tau \rangle} \qquad (14)$$

TABLE II

Asymptotic behavior of the Nernst voltage as $H \to \infty$ for certain special directions of $\mathbf{H}$ and ∇T, as derived from (86) of Appendix B. Assumptions and notations are the same as for Table I except that the expressions apply only for [111] valleys (n-germanium). In addition, μ is the drift mobility for $H = 0$.

Π, ΔT	Quantity	Value if $\tau \propto \epsilon^{-1/2}$, $\Pi_p \propto \epsilon^{-1/2}$	Value if $\tau \propto \epsilon^{-1/2}$, Π_p independent of ϵ	Value if τ independent of ϵ, any $\Pi_p(\epsilon)$
[001], any $\perp \mathbf{H}$	$\frac{e}{k}\left[\frac{\partial(B_e H)}{\partial(c/\mu H)}\right]_\infty$	$-\frac{16}{9\pi}\left[\frac{(2+w)^2}{3(1+2w)}\right]$	same as at left	0
	$\lvert Q_p \rvert^{-1}\left[\frac{\partial(B_p H)}{\partial(c/\mu H)}\right]_\infty$	$\left[\frac{256}{81\pi^2}\frac{(2+w)^3(1+w+pw)}{(1+2w)^2(2+pw)} - \frac{8}{9\pi}\frac{(2+w)^2}{(1+2w)}\right]$	$\frac{32}{27\pi}\left[\frac{w(1-w)(2+w)^2(p-1)}{(1+2w)^2(2+pw)}\right]$	$\frac{1}{3}$ [as at left]
[011], [100]	$\frac{e}{k}\left[\frac{\partial(B_e H)}{\partial(c/\mu H)}\right]_\infty$	$-\frac{16}{9\pi}\frac{(2+w)(1+2w)}{9w}$	same as at left	0
	$\lvert Q_p \rvert^{-1}\left[\frac{\partial(B_p H)}{\partial(c/\mu H)}\right]_\infty$	$\left[\frac{256}{729\pi^2}\frac{(2+w)(1+2w)(5+p+w+2pw)}{w(2+pw)} - \frac{8}{27\pi}\frac{(2+w)(1+2w)}{w}\right]$	$\frac{32}{243\pi}\cdot\left[\frac{(2+w)(1+2w)(1-w)(p-1)}{w(2+pw)}\right]$	$\frac{1}{27}$ [as at left]
[011], [01$\bar{1}$]	$\frac{e}{k}\left[\frac{\partial(B_e H)}{\partial(c/\mu H)}\right]_\infty$	$-\frac{16}{9\pi}\left[\frac{w^2+7w+1}{9w}\right]$	same as at left	0
	$\lvert Q_p \rvert^{-1}\left[\frac{\partial(B_p H)}{\partial(c/\mu H)}\right]_\infty$	$\left[\frac{256}{729\pi^2}\frac{(w^2+7w+1)(2+w)(p+2)}{w(2+pw)} - \frac{8}{27\pi}\frac{(2+w)(pw^2+2pw+5w+1)}{w(2+pw)}\right]$	$\frac{32}{243\pi}\cdot\left[\frac{(2+w)(1+2w)(1-w)(p-1)}{w(2+pw)}\right]$	$\frac{1}{27}$ [as at left]

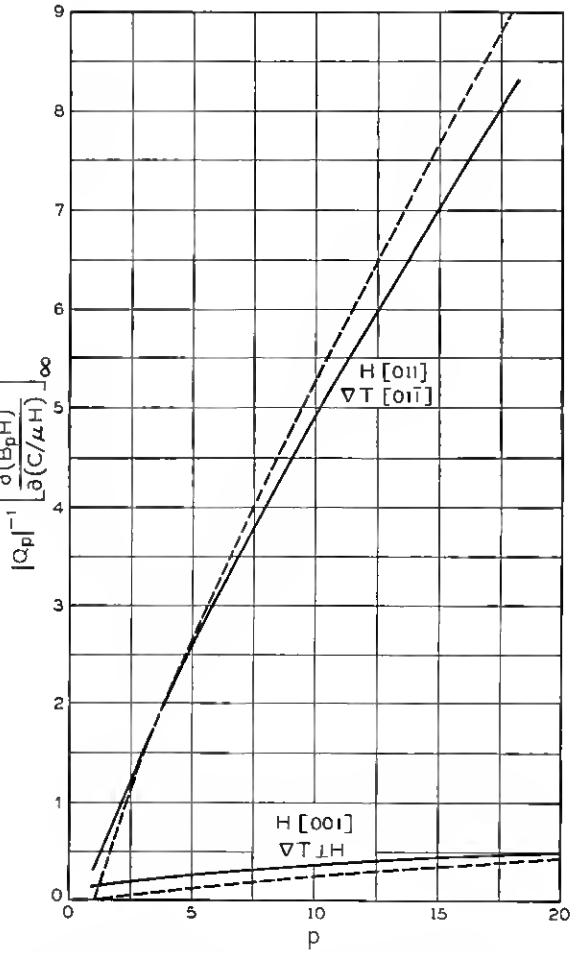

Fig. 2 — Dependence on $p = \Pi_{p\parallel}/\Pi_{p\perp}$ of the phonon-drag part of the Nernst coefficient at high magnetic fields, for two orientations of a cubic crystal with [111] valleys. All curves have been computed assuming $w = m^*_{\perp}\tau_{\parallel}/m^*_{\parallel}\tau_{\perp} = 0.06$, and pure acoustic scattering ($\tau \propto \epsilon^{-1/2}$). The full curves apply for $\Pi_p \propto \epsilon^{-1/2}$, the dashed for Π_p independent of energy. The curves are fairly insensitive to the energy dependence of τ, but depend strongly on w, the lower curves being for small w almost proportional to w, the upper to w^{-1}. For **H** along [011] and ∇T along [100] (not shown) the dashed curve would coincide with that for [011][01$\bar{1}$], while the full curve would differ by only a few per cent over most of the range shown.

TABLE III

Values of the saturation ratio $Q_p(H \to \infty)/Q_p(0)$, for special directions of $\mathbf{H}$ and ∇T. Assumptions and notations are the same as for Table I, except that the expressions apply only for [111] valleys (n germanium). The energy factor $\langle \epsilon \Pi_p \rangle \langle \epsilon \tau \rangle / \langle \epsilon \rangle \langle \epsilon \Pi_p \tau \rangle$ has the value $8/(3\pi) = 0.849$ when $\Pi_p \propto \epsilon^{-1/2}$, and the value 1 when either Π_p or τ is independent of energy.

H, ∇T	Reference, Appendix B	Value, General
[001], [001]	(78)	$\frac{(2+w)(p+2)}{3(2+pw)}$
[011], [011]	(79)	$\frac{(2+w)(1+w+pw)}{(1+2w)(2+pw)}$
[111], [111]	(80)	$\frac{(2+w)(6+p+2pw)}{(7+2w)(2+pw)}$
[011], any $\perp$H	(81)	$\frac{\langle \epsilon \Pi_p \rangle \langle \epsilon \tau \rangle}{\langle \epsilon \rangle \langle \epsilon \Pi_p \tau \rangle} \left[\frac{(2+w)(1+w+pw)}{(1+2w)(2+pw)} \right]$
[011], [100]	(81)	$\frac{\langle \epsilon \Pi_p \rangle \langle \epsilon \tau \rangle}{\langle \epsilon \rangle \langle \epsilon \Pi_p \tau \rangle} \left[\frac{5+w+p+2pw}{3(2+pw)} \right]$
[001], [01$\bar{1}$]	(81)	$\frac{\langle \epsilon \Pi_p \rangle \langle \epsilon \tau \rangle}{\langle \epsilon \rangle \langle \epsilon \Pi_p \tau \rangle} \left[\frac{(2+w)(p+2)}{3(2+pw)} \right]$
[011], [11$\bar{1}$]	(81)	$\frac{\langle \epsilon \Pi_p \rangle \langle \epsilon \tau \rangle}{\langle \epsilon \rangle \langle \epsilon \Pi_p \tau \rangle} \left[\frac{13+5w+5p+4pw}{9(2+pw)} \right]$

where $| \epsilon_b - \epsilon_f |$ is the distance of the Fermi level from the band edge, the upper sign is for electrons, the lower for holes, the angular brackets denote Maxwellian averages, and, for the present case of energy-independent anisotropies, τ may be taken as either $\tau_\parallel$ or $\tau_\perp$ (only the energy dependence matters). When $\mathbf{H}$ and $\mathbf{j}$ are perpendicular, the energy distribution of the current is the same as it would be for $H = 0$, $\tau =$ constant. So, for $\mathbf{H} \perp \nabla T$,

$$Q_e(\infty) = \mp \left[\frac{5}{2} \left(\frac{k}{e} \right) + \frac{| \epsilon_b - \epsilon_f |}{eT} \right]. \tag{15}$$

Table III gives the formulas for $Q_p(\infty)$, the saturation value of the phonon-drag part of the thermoelectric power, again for [111] valleys and energy-independent anisotropies. The ratio $Q_p(\infty)/Q_p(0)$ is the product of a factor dependent on the energy variations of $\mathbf{\Pi}_{pq}$ and $\mathrm{m}^* \cdot \boldsymbol{\tau}^{-1}$ by a factor dependent on their anisotropies. Figs. 3 and 4 show how these anisotropy factors depend on $\Pi_{p\parallel}/\Pi_{p\perp}$, again for different assumptions

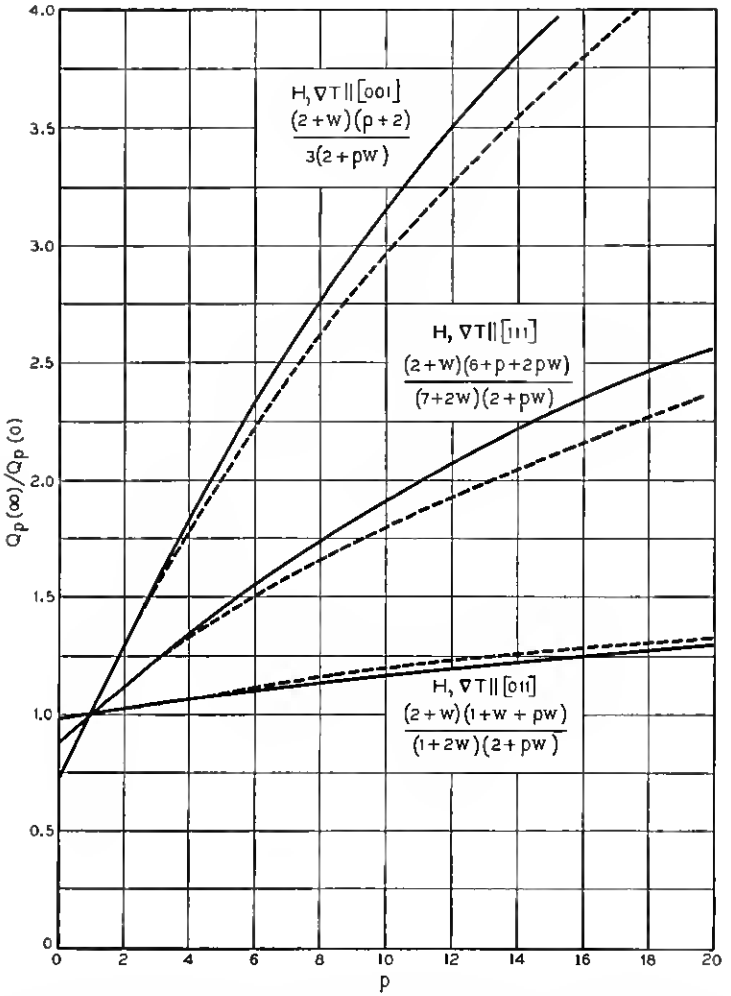

Fig. 3 — Dependence on $p = \Pi_{p\parallel}/\Pi_{p\perp}$ of the expressions of Table III for $Q_p(\infty)/Q_p(0)$, for **H** parallel to ∇T in various directions of a cubic crystal with [111] valleys. The full curves apply for $w = m^*_\perp \tau_\parallel / m^*_\parallel \tau_\perp = 0.06$, the dashed curves for $w = 0.08$.

on the anisotropy of τ. For longitudinal effects ($\nabla T \parallel \mathbf{H}$) the energy factor is unity; thus the ratio for these cases gives information on the anisotropy of $\mathbf{\Pi}_{pq}$ independently of its energy variation. For the transverse effects the energy factor goes to unity if either $\mathbf{\Pi}_{pq}$ or τ is independent of energy.

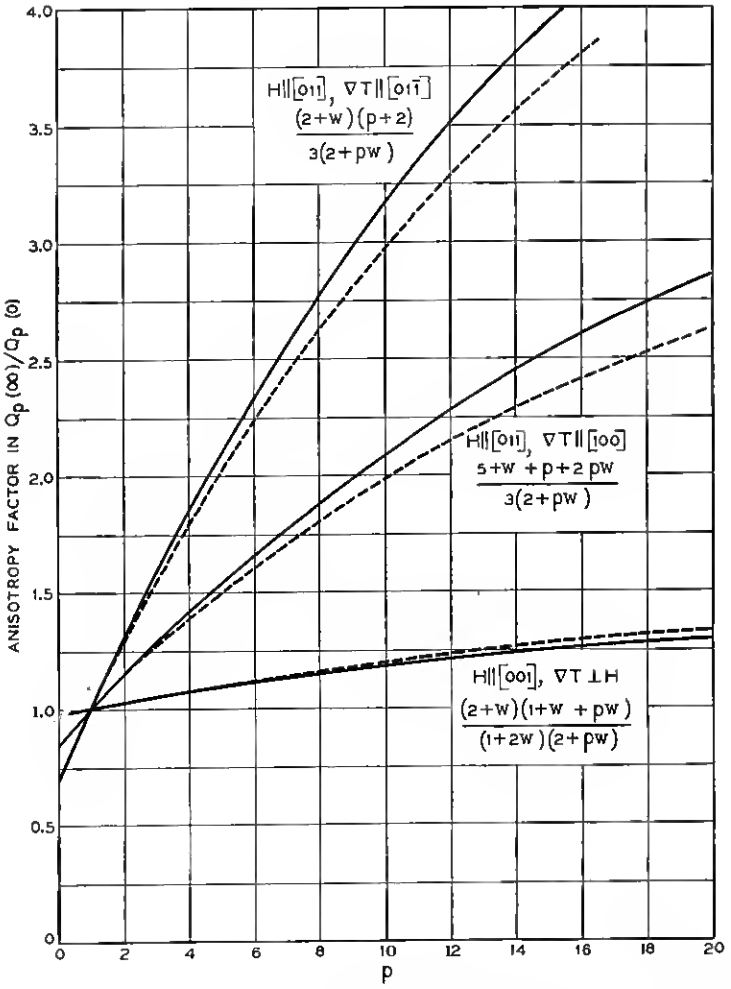

Fig. 4 — Dependence on $p = \Pi_{p\parallel}/\Pi_{p\perp}$ of the anisotropy factors in the expressions of Table III for $Q_p(\infty)/Q_p(0)$, for various orientations of a cubic crystal with [111] valleys, when H is normal to ∇T. The full curves apply for $w = m^*_{\perp}\tau_{\parallel}/m^*_{\parallel}\tau_{\perp} = 0.06$, the dashed curves for $w = 0.08$. Note two of the factors are the same as for Fig. 3. No curves are given for H ∥ [011], ∇T ∥ [01$\bar{1}$], as this case is just one-third the way toward [011][100] from [011][01$\bar{1}$].

Table IV, finally, gives the expressions for the low-field limits of $\Delta Q_e/H^2$, $\Delta Q_p/H^2$. These have a less simple behavior than the high-field limits. However, it is noteworthy that, when **H** is in the [001] direction and ∇T in the [100], the expression for $\Delta Q_p/Q_p$ involves the anisotropy of $\mathbf{\Pi}_p$ only through the same coefficient ζ_p as occurs in the expression (13) for B_p. The reason for this has been elucidated in our previous paper.[1]

V. DATA AND CORRECTIONS

5.1 *Measurements and Extrapolations*

Measurements of electrical and thermomagnetic properties were made on a number of samples of n-type germanium having various orientations and dopings, at a number of temperatures from the liquid-hydrogen range to room temperature, and for magnetic fields up to 18,000 gauss. The samples were of the usual shape with three pairs of side-arms. Heat or electric current was fed in at the ends, the potential drop was measured between a side-arm of the first pair and one of the last pair, and the Hall or Nernst voltage was measured between the two middle side-arms. A full description of the experimental procedures has been given in our earlier paper.[1]

Table V gives all the thermomagnetic quantities measured, as functions of magnetic field, for temperatures above 60°K; measurements were also made at a number of fields intermediate between those listed. Such data may be useful for comparison with future theoretical expressions for the various quantities in the intermediate-field range. In this paper, however, we have developed the theory only for the limiting cases of high and low fields, and so the most appropriate quantities for comparison with theory are the high- and low-field limits; these are given in Table VI. The limits of the various quantities as $H \to 0$ were obtained, since the quantities are even functions of H, by plotting the quantity in question against H^2, fitting the low-field part of the plot to a parabola, and noting its intercept. The average size of the random errors involved in this procedure can be gauged from the sample plots given in Fig. 5. It will be noted that, at low fields, ΔQ is a little less accurately determinable than $\Delta\rho$, because of the smaller signals involved; similarly, the errors in B are larger than those in R. For the same reason, the random errors in the thermomagnetic quantities become larger, percentagewise, at higher temperatures. The extrapolations to $H = \infty$ were made in the same way, by plotting the quantities against $1/H^2$ and fitting with parab-

TABLE IV

Limiting low-field behavior of ΔQ_e, ΔQ_p, for various directions of **H** and ∇T. Assumptions and notation are the same as for Table I, except that the expressions apply only for [111] valleys. The upper sign is for electrons, the lower for holes, and $\Delta\rho/\rho$ is the magnetoresistance.

Quantity	H, ∇T	Reference, Appendix B	Value if $\tau \propto \epsilon^{-1/2}$, $\Pi_p \propto \epsilon^{-1/2}$	Value if $\tau \propto \epsilon^{-1/2}$, Π_p independent of ϵ	Value if τ independent of ϵ, any $\Pi_p(\epsilon)$
$\frac{(e/k)\Delta Q_e}{(\mu_H H/c)^2}$	Parallel	(62)	$\mp \frac{\Delta\rho/\rho}{(\mu_H H/c)^2}$	same	0
	Perpendicular	(63)	$\mp\left[\frac{\Delta\rho/\rho}{(\mu_H H/c)^2} + \frac{1}{2}\right]$	same	0
$\frac{\Delta Q_p}{Q_p(\mu_H H/c)^2}$	[001], [001]	(67)	$\frac{8}{3\pi}\frac{(2+w)(1-w)(pw^2+5pw-4w-2)}{(1+2w)^2}$	$\frac{8}{\pi}\frac{w(2+w)(1-w)(p-1)}{(1+2w)^2}$	$\frac{2w(2+w)(1-w)(p-1)}{(1+2w)^2}$
	[001], any $\perp H$	(66)	$\zeta_p - \frac{4}{3\pi}\frac{(2+w)^2}{(1+2w)}$	ζ_p	ζ_p

For any model the value of ΔQ in the direction of the unit vector **u** is, to order H^2

$$\Delta Q = q_b H^2 + q_c(\mathbf{H}\cdot\mathbf{u})^2 + q_d(H_x^2 u_x^2 + H_y^2 u_y^2 + H_z^2 u_z^2),$$

where the coordinate axes are assumed oriented along cube-edge directions. For [111] valleys and low carrier concentration the additional relation $q_b = -q_c$ must hold whenever the electron-group approximation is valid (Ref. 1, Appendix C). Therefore, the values of ΔQ_p for any orientations can be expressed in terms of the two given above. For example,

$$\Delta Q_p\Big]_{001}^{001} = 2\Delta Q_p\Big]_{011}^{011} = 3\Delta Q_p\Big]_{111}^{111}, \qquad \Delta Q_p\Big]_{0\bar{1}1}^{011} = \Delta Q_p\Big]_{100}^{001} + \tfrac{1}{2}\Delta Q_p\Big]_{001}^{001}, \qquad \text{etc.}$$

olas, as shown in Fig. 6. The legitimacy of assuming that ΔQ and $\Delta\rho$ are representable by power series in $1/H^2$ is borne out by the calculations of Appendix B, within the limitations imposed by the neglect of orbital quantization, inhomogeneities, etc. However, these latter factors are known to prevent $\Delta\rho$ from saturating completely as $H \to \infty$, so the extrapolations may be slightly different from the value which it is appropriate to compare with the present theory. We shall discuss this further below. Random errors in the high-field extrapolations are, however, inconsequential, as Fig. 6 shows.

A general discussion of the sources of experimental errors and the probable accuracy of the data has been given in our previous paper,[1] and will not be repeated here. However, there are some new observations which have an important bearing on the trustworthiness of the results, and in the following paragraphs we shall discuss these and some theoretical adjustments which should be made to the data in order to make them comparable with the theory. We have tried to evaluate the more predictable of these corrections for all the table entries that we shall use in the analysis in Sections VI and VII, and we have given the sum of these corrections in parentheses after the quantity to which they apply.

5.2 *Surface Damage*

In the attempt to track down empirically the magnitude of the effect of orbital quantization (an investigation which we have summarized in Appendix A) we encountered a stumbling-block in the high value of the infinite-field extrapolation of the resistivity normal to H when H is in a [100] direction. At 77°K, for example, the originally measured $\Delta\rho/\rho_0$ for Sample 606 extrapolates to a value 0.5 unit above the value predicted by the electron-group model. This is many times larger than the expected effect of orbital quantization as deduced from other evidence. However, such an increase could occur if a partial short-circuiting of the large Hall field were effected by surface or dislocation conduction. A surface contribution to the conductance of only a few parts in a thousand would suffice. To check this, some of the measurements on this and other samples were repeated after etching off about a mil of the original sand-blasted surface with superoxol. For the case mentioned (Sample 606 at 77°), two-thirds of the original excess of observation over theory disappeared; the full excess reappeared on sand-blasting again. Thus, it is clear that reliable transverse magnetoresistance results cannot be expected with sand-blasted surfaces.

Theoretically, one would not expect most of the other tabulated quan-

TABLE V

Observed values of thermomagnetic properties of n germanium at various magnetic fields and temperatures for selected orientations and impurity concentrations. All entries refer to unetched samples, and none of the corrections discussed in Section V has been applied.

Sample No., (N_D and N_A* in 10^{13}/cm^3)	Direction		T, °K	σ, Ω^{-1} cm^{-1}	Q, μv/deg.	Q_e, μv/deg.	Magnetic Field, H, in 10^3 gauss						
	∇ T	H					0.5	1	2.5	6	10	14	18
							Increase in Seebeck voltage, ΔQ in μv/deg., as a function of magnetic field and temperature						
606													
$N_D = 1$	100	001	60	0.0723	3196	1166	25.3	78.0	214.2	337.6	383.1	401.3	409.8
$N_A \sim 0.2$	100	100	60	0.0723	3196	1166	100.1	346.5	1318	2938	3642	3936	4088
	100	001	77	0.0491	2329	1199	7.0	23.7	83.1	222.5	190.6	206.7	214
	100	100	77	0.0491	2329	1199	29.1	107.4	462.7	1265	1771	2024	2163
	100	001	94	0.0355	1904	1224	3.0	10.4	38.8	89.1	114.1	127.6	134.2
	100	100	94	0.0355	1904	1224	10.7	38.6	182.8	565.2	883.6	1074	1190
	100	001	122	0.0237	1623	1258	0.96	3.62	16.8	48.2	69.9	82.3	89.6
	100	100	122	0.0237	1623	1258	3.86	12.4	62.1	210.6	362.4	474.9	553
	100	001	148	—	1532	1282	0.47*	1.82*	9.61*	—	—	—	—
	100	100	148	—	1532	1282	1.16*	4.55*	25.2*	—	—	—	—
	100	001	163	—	1504	1294	0.29*	1.16*	6.16*	—	—	—	—
	100	100	163	—	1504	1294	0.68*	3.67*	14.8*	—	—	—	—
580													
$N_D = 3.3$	100	001	79.5	0.144	2139	1094	4.8	17.3	66.8	140.6	177.4	198.7	214
$N_A = 0.5$	100	100	79.5	0.144	2139	1094	19.1	71.2	344.9	1024	1487	1727	1863
	100	001	91	0.1174	1845	1110	2.5	8.7	39.1	—	—	—	—
	100	100	91	0.1174	1845	1110	9.5	35.9	181.0	590	922	1117	1234

601													
$N_D = 26$	100	001	94	1.143	1590	910	1.9	6.2	28.5	78.5	108.0	125.4	137.0
$N_A = 2$	100	100	94	1.151	1590	910	6.2	22.2	123.0	457	759	945	1059
	100	001	208	0.341	1152	1012	0.100[a]	0.40[a]	2.34[a]	8.4[a]	—	—	—
	100	100	208	0.341	1152	1012	0.183[a]	0.78[a]	4.75[a]	23.0[a]	—	—	—
	100	001	234	0.281	1144	1026	0.062[a]	0.248[a]	1.48[a]	7.2[a]	—	—	—
	100	100	234	0.281	1144	1026	0.132[a]	0.523[a]	3.16[a]	14.6[a]	—	—	—
	100	001	275	0.208	1142	1048	0.036[a]	0.144[a]	0.87[a]	4.1[a]	—	—	—
	100	100	275	0.208	1142	1048	0.062[a]	0.250[a]	1.53[a]	7.6[a]	—	—	—
596													
$N_D = 180$	100	001	91	4.86	1499	764	1.3	3.7	26.1	66.7	102.8	124.0	138.8
$N_A = 6$	100	100	91	4.86	1499	764	3.6	12.6	73.0	324	605	803	932
	100	001	235	1.36	1002	886	0.045[a]	0.179[a]	1.06	4.8	11.2	17.6	23.4
	100	100	235	1.36	1002	886	0.085	0.337	1.98	10.4	25.0	42.0	56.3
604													
$N_D = 2$	100	011	61	0.1125	3066	1116	18.8	70.1	318	886	1298	1531	1677
$N_A = 0.6$	100	100	61	0.1125	3066	1116	76	274	1124	2615	3319	3624	3784
	100	011	77.6	0.0815	2277	1147	6.3[a]	24.6	118.5	373.3	598.6	748.8	850.0
	100	100	77.4	0.0811	2277	1147	25.1	93.5	423	1183	1676	1923	2059
	100	011	92	0.0630	1886	1171	2.5[a]	10.4[a]	54.8	187.0	319	419	491
	100	100	92	0.0630	1886	1171	11.1[a]	42.8	196.3	611	946	1142	1256
	100	100	235	0.0135	1406	1290	0.046[a]	0.184[a]	1.11[a]	—	—	—	—
576A													
$N_D = 10$	110	001	80	0.495	2019	989	4.1[a]	15.2	65.8	136.7	174	195	212
$N_A = 1$	110	110	80	0.498	2019	989	7.1[a]	26.1	90.8	154.7	175.8	185.0	190.4
	110	110	93	0.394	1693	998	3.4	12.8	49.6	98.4	111.1	117.7	121.7
	110	001	133	0.224	1359	1054	0.44[a]	1.67	9.3	31.6	49.2	60.0	66.8
	110	110	133	0.224	1359	1054	0.77[a]	2.87	15.8	31.4	41.2	45.4	47.7

TABLE V — *Continued*

Sample No., (N_D and N_A* in 10^{13}/cm³)	Direction ∇T	Direction H	T, °K	σ, Ω^{-1} cm^{-1}	Q_i, μv/deg.	Q_s, μv/deg.	Magnetic Field, H, in 10^3 gauss: 0.5	1	2.5	6	10	14	18
							Increase in Seebeck voltage, ΔQ, in μv/deg., as a function of magnetic field and temperature						
603													
$N_D = 2$	110	1$\bar{1}$0	61	0.154	3043	1093	61.6	218	861	2060	2824	3237	3482
$N_A = 0.3$	110	110	61	0.154	3043	1093	32.8	96.7	231	316	341	351	356
	110	1$\bar{1}$0	77.4	0.1136	2254	1124	19.1	74.9	333	912	1359	1643	1831
	110	110	77.4	0.1136	2254	1124	11.0	39.0	113.7	175.6	191.2	201	205
	110	1$\bar{1}$0	94	0.0816	1830	1150	7.0	25.5	120.3	371	600	765	884
	110	110	94	0.0816	1830	1150	4.1	14.1	50.3	90.4	104.7	109.8	112.6
	110	1$\bar{1}$0	135	0.0463	1496	1196	1.44[a]	5.6[a]	28.3	—	—	—	—
	110	110	135	0.0463	1496	1196	0.84	3.18	14.4	—	—	—	—
	110	1$\bar{1}$0	155	0.0372	1443	1213	0.71[a]	2.9[a]	15.5	—	—	—	—
	110	110	155	0.0372	1443	1213	0.34[a]	1.34[a]	7.3[a]	—	—	—	—
595													
$N_D = 0.3 + A$	111	111	91	0.01201	2038	1303	3.4[a]	13.3[a]	70.9	233	369	453	499
$N_A = A$	111	111	98	0.01145	1918	1313	2.9[a]	11.3	60.0	204	330	407	456
610													
$N_D = 1.7$	111	1$\bar{1}$0	92	0.0598	1894	1179	6.4[a]	23.9	112.4	352	596	726	839
$N_A = 0.4$	111	111	92	0.0598	1894	1179	3.7[a]	14.4	75.3	248	391	477	529
							Nernst voltage, $B\Pi$, in μv/deg., as a function of magnetic field and temperature						
606													
$N_D = 1$	100	001	60	0.0723	3196	1166	123	199	234	158	107	82	66
$N_A \sim 0.2$	100	001	77.4	0.0491	2329	1199	41[a]	72	107	93	75	64	63
	100	001	94	0.0355	1904	1224	17	31	52	54	48	44	42
	100	001	122	0.0237	1623	1258	4.7	9.4	19.2	26.8	29.0	31.3	34.5
	100	001	155	0.0157	1518	1288	1.55[a]	3.88[a]	7.03[a]	—	—	—	—

580													
$N_D = 3.3$	100	001	79.5	0.144	2139	1094	31	57	94	85	64	—	42
$N_A = 0.5$	100	001	91	0.1174	1845	1110	17	32	56	—	—	—	—
	100	001	145	0.0605	1428	1168	1.8[a]	3.5	7.2	9.5	7.9[a]	6.9[a]	6.3
601													
$N_D = 26$	100	001	94	1.143	1590	910	13.8	26.4	52.3	59	47	38	32
$N_A = 2$	100	001	160	0.534	1196	976	0.65[a]	1.27[a]	2.78[a]	0.29	1.8	−0.05[a]	−0.15
	100	001	208	0.341	1152	1012	−0.39	−0.77	−1.92	−4.6	−7.3	−9.4	−10.2
	100	001	234	0.281	1144	1026	−0.54[a]	−1.08[a]	−2.65[a]	—	—	—	—
	100	001	275	0.205	1142	1048	−0.50[a]	−0.99[a]	−2.45[a]	—	—	—	—
596													
$N_D = 180$	100	001	91	0.486	1499	764	11.5	22.5	49.5	71	64	53	43
$N_A = 6$	100	001	235	0.136	1002	886	−0.35[a]	−0.68	−1.68	−4.1	−6.6	−8.4	−9.9
604													
$N_D = 2$	100	011	77.4	0.0815	2277	1147	40	81	223	485	590	590	540
$N_A = 0.6$	100	011	92	0.0630	1886	1171	17.8[a]	37.0[a]	105	252	340	360	360
576.1													
$N_D = 10$	110	001	80	0.495	2019	989	30.6[a]	57.4	97	89	67	53	45
$N_A = 1$	110	001	133	0.224	1359	1054	2.43	4.67	9.8	12.9	10.9	8.5	7.6
603													
$N_D = 2$	110	1$\bar{1}$0	61	0.153	3043	1093	104	221	602	1060	1080	980	860
$N_A = 0.3$	110	1$\bar{1}$0	77.4	0.1136	2254	1124	45	93	265	540	640	630	580
	110	1$\bar{1}$0	94	0.0826	1830	1150	16.4[a]	34.7	102	245	332	357	340
	110	1$\bar{1}$0	135	0.0463	1496	1196	2.3[a]	4.9	17	57	98	123	137
	110	1$\bar{1}$0	155	0.0373	1443	1213	1.0[a]	2.4	9	34	62	84	101
	110	1$\bar{1}$0	178	0.0290	1418	1238	−0.10[a]	−0.14	1.28[a]	—	—	—	—
610													
$N_D = 1.7$	111	1$\bar{1}$0	92	0.598	1894	1179	19.2[a]	39.7[a]	113	271	359	385	380
$N_A = 0.4$													

* From analysis of Hall coefficient–temperature curves
[a] Value from smoothed curve

TABLE VI

Low- and high-field limits of electrical and thermomagnetic quantities, for various samples and temperatures. For all the entries used in the analyses of Sections VI and VII, and for a few other cases, the sum of the corrections discussed in Section V has been evaluated and is listed in parentheses following the table entry; these corrections are the side-arm correction (Table VII), the temperature-gradient correction (only for the less pure samples — see Table XI) and the boundary-scattering correction, (16) and (17). The estimated true value is obtained by adding the correction to the tabulated value. The symbol (---) means that the correction is zero.

Sample No. (N_D and N_A ‡ in 10^{13}/cm³)	Direction		T,° K	μ_H, 10^3 cm²/vs	$\lim_{H\to 0} \frac{\Delta\rho}{\rho H^2}$ 10^{-8} gauss^{-2}	$\lim_{H\to\infty} \frac{\Delta\rho}{\rho}$	$-Q_p$, μv/deg.	$B(H=0)$, 10^{-3} v/gauss deg.	$\lim_{H\to 0} -\frac{\Delta Q}{H^2}$ 10^{-12} v/gauss² deg.	$\lim_{H\to\infty} -\Delta Q$, μv/deg.
	j or ∇T	H								
606										
$N_D = 1$	100	001	60	51.9(−1.35)	10.8(---)	1.68(---)	2030(+283)	269(+33.4)	103(+10.6)	424(+53)
$N_A \sim 0.2$	100	100	60	—	27.5(−0.1)	3.94(−0.11)	—	—	429(+62.5)	4345(+605)
	100	001	63	48.3*(−1.26)	8.2*(---)	0.68*(---)	1830	—	—	—
	100	100	63	—	23.3*(−0.1)	3.32*(−0.11)	—	—	—	—
	100	001	77.4	37.5*(−0.9)	5.4*(---)	0.61*(---)	—	—	—	—
				36.0	5.6	0.94	1130(+60)	80(+0.8)	26.3(+0.9)	225(+10)
	100	100	77.4	—	14.0*(−0.06)	3.28*(−0.12)	—	—	120 (+8)	2415(+127)
					13.9	3.45	—	—	—	—
	100	001	94	26.7(−0.7)	3.3*(---)	0.56*(---)	—	31*(+0.2)	9.9*(+0.1)	141*(+3)
					3.20	0.73	680(+17)	31	11.1	150
	100	100	94	—	8.1*(−0.03)	3.34*(−0.12)	—	—	43*(+1.4)	1450*(+35)
					8.04	3.37	—	—	42	1413
	100	001	122	18.18(−0.47)	1.58(---)	0.625(---)	365(+3)	9.8(−0.1)	3.8(---)	104
	100	100	122	—	3.76(−0.01)	3.04(−0.10)	—	—	12.8(+0.2)	721(+6)
	100	001	131	16.4*(−0.4)	1.23*(---)	0.54*(---)	315(+2)	4.2*(−0.08)	2.4*(---)	87*(+0.3)
	100	100	131	—	2.99*(−0.01)	2.98*(−0.10)	—	—	8.5*(+0.14)	597*(+4)
	100	001	148	—	0.88	—	250	—	1.89	—
	100	100	148	—	1.87	—	—	—	4.6	—
	100	001	155	12.06	—	—	230	3.1	—	—
	100	001	163	—	0.72	—	210	—	1.16	—
	100	100	163	—	1.43	—	—	—	2.7	—

580												
$N_D = 3.3$	100	001	63	39.3		—		—	1830	—	—	—
$N_A = 0.5$	100	001	77.4	31.4		—		—	1130(+60)	—	—	—
	100	100	77.4		—	10.1		3.05	—	—	—	—
	100	001	79.5		—	—		—	1045	64	22.7	241
	100	100	79.5		—	—		—	—	—	76.2	2109
	100	001	91	25.5		—		—	735	35	9.2	—
	100	100	91		—	6.45		3.11	—	—	37.9	1465
	100	001	92		—	—		—	705	—	—	159
	100	001	145		—	—		—	260	3.6	—	—
601												
$N_D = 26$	100	001	77.4	28.3*†(−0.4)		2.08*†(---)		0.82*†(---)				
$N_A = 2$				28.4(−0.8)		2.08		0.84	1130(+60)	—	—	—
	100	100	77.4		—	6.57*†(−0.01)		2.74*†(−0.04)	—	—	—	—
						6.60(−0.02)		2.79(−0.08)	—	—	—	—
	100	001	94	22.5(−0.6)		1.44(---)		0.628(---)	680(+16)	27.9(+0.2)	5.9(+0.12)	167(+5)
	100	100	94		—	4.4(−0.04)		2.89(−0.10)	—	—	22.3(+0.81)	1265(+44)
	100	001	115	17.9		—		—	425	—	—	—
	100	001	160		—	—		—	220	1.30	—	—
	100	001	208		—	—		—	140	−0.77	0.40	—
	100	100	208		—	—		—	—	—	0.78	—
	100	001	234	5.97(−0.15)		0.166(---)		—	118(≈0)	−1.06(+0.03)	0.249(---)	—
	100	100	234		—	0.396(−0.002)		—	—	—	0.53(+0.005)	—
	100	001	275	4.42		—		—	94	−0.99	0.145	—
	100	100	275		—	—		—	—	—	0.25	—
596												
$N_D = 180$	100	001	77.4	21.3		—		—	1130(+60)	—	—	—
$N_A = 6$	100	001	87	18.9		0.81		0.633	820	—	—	—
	100	100	87		—	2.6		2.32	—	—	—	—
	100	001	91		—	—		—	73.5	23.2	3.77	166
	100	100	91		—	—		—	—	—	13.0	1167
	100	001	235	5.21		0.095		0.306	116	−0.69	0.18	—
	100	100	235		—	0.27		1.07	116	—	0.34	—
	100	001	299	3.70		—		—	85	—	—	—
604												
$N_D = 2$	100	011	61		—	8.1		2.43(---)	1950	—	76.6	1911
$N_A = 0.6$	100	100	61		—	33.3		3.25(−0.11)	—	—	315	4045
	100	011	77.4	34.2*†(−0.4)		4.85*†(−0.03)		2.14*†(−0.01)	1130(+60)	—	—	—
			77.6	33.6		4.82		2.08	—	79(+0.9)	25.6(+0.3)	1031(+52)

TABLE VI — *Continued*

Sample No. (N_D and N_A† in 10^{13}/cm³)	Direction		T,° K	μH, 10^3 cm²/vs	$\lim_{H\to 0} \frac{\Delta\rho}{\rho H^2}$, 10^{-8} gauss^{-2}	$\lim_{H\to\infty} \frac{\Delta\rho}{\rho}$	$-Q_P$, μv/deg.	$B(H\doteq 0)$, 10^{-9} v/gauss deg.	$\lim_{H\to 0} -\frac{\Delta Q}{H^2}$, 10^{-12} v/gauss² deg.	$\lim_{H\to\infty} -\Delta Q$, μv/deg.
	j or $\sqrt{T}$	H								
	100	100	77.4	—	12.7*†(−0.02)	3.28*†(−0.06)	—	—	—	—
					12.4	3.24	—	—	103(+5)	2265(+120)
	100	011	92	26.4(−0.7)	3.2(−0.04)	1.94(−0.02)	715	36(+0.4)	10.7(−0.2)	638(+16)
	100	100	92	—	7.86(−0.03)	3.23(−0.11)	—	—	45(+1.5)	1502(+40)
	100	011	195	7.96	0.32	0.68	155	—	—	—
	100	100	195	—	0.747	1.72	—	—	—	—
	100	011	235	5.70(−0.15)	0.183(−0.002)	—	116	—	—	—
	100	100	235	—	0.388(−0.002)	—	—	—	0.18	—
576A										
$N_D = 10$	110	001	63	40.9	—	—	1830	—	—	—
$N_A = 1$	110	001	77.4	32.1	—	—	1130(+60)	—	—	—
	110	110	77.4	—	4.6	0.334	1130(+60)	—	—	—
	110	001	80	—	—	—	1030	62.5	16.7	252
	110	110	80	—	—	—	—	—	29.2	200
	110	110	91	—	3.1	0.319	735	—	—	—
	110	001	93	25.8	—	—	695	—	—	—
	110	110	93	—	—	—	—	—	14.4	130
	110	001	133	14.8	—	—	305	4.92	1.74	80.3
	110	110	133	—	—	—	—	—	3.13	52.2
	110	001	195	—	0.30	—	155	—	—	—
603										
$N_D = 2$	110	1$\bar{1}$0	61	47.0	—	—	1950	200	257	3960
$N_A = 0.3$	110	110	61	—	—	—	—	—	150	365
	110	1$\bar{1}$0	77.4	35.8*(−0.9)	10.4*(+0.06)	3.72*(+0.04)	1130(+60)	—	—	—
				34.6	10.3	3.59	—	87(+0.9)	79.5(+4.2)	2264(+118)
	110	110	77.4	—	6.20*(−0.22)	0.328*(−0.035)	1130(+60)	—	—	—
					5.95	0.328	—	—	47(+2.8)	214(+11)
	110	1$\bar{1}$0	94	26.0(−0.7)	5.95(+0.04)	3.32(+0.03)	680(+17)	32(+0.2)	27.9(+0.75)	1163(+28)
	110	110	94	—	3.40(−0.12)	0.313(−0.034)	—	—	15.9(+0.5)	116.5(+2.9)
	110	1$\bar{1}$0	135	15.21	2.25	—	300	4.6	5.8	—
	110	110	135	—	1.20	—	—	—	3.4	—

	110	1$\bar{1}$0	155	12.31	1.53	—	230	2.1	2.9	—
	110	110	155	—	0.82	—	—	—	1.4	—
	110	1$\bar{1}$0	178	9.38	1.02	—	180	−0.21	1.7	—
	110	110	178	—	0.50	—	—	—	0.80	—
	110	1$\bar{1}$0	200	7.77	—	—	150	—	—	—
	110	1$\bar{1}$0	204	7.49	0.565	—	146	—	0.66	—
	110	110	204	—	0.305	—	—	—	0.39	—
595										
$N_D = 0.3 + A$	111	110	77.4	30.4	—	—	1130(+60)	—	—	—
$N_A = A$	111	111	91	—	—	—	735	—	13.8	593
	111	111	98	—	—	—	605	—	11.7	546
610										
$N_D = 1.7$	111	1$\bar{1}$0	77.4	36.6*(−0.9)	8.65*(≈)	3.07*(+0.02)	1130(+60)	—	—	—
$N_A = 0.4$				35.7	8.6	3.08				
	111	111	77.4	—	4.31*(−0.15)	1.42*(−0.06)	—	—	—	—
					4.35	1.44				
	111	1$\bar{1}$0	92	28.3(−0.7)	5.5(≈0)	2.90(+0.02)	715	38(+0.3)	26.0(+0.5)	1079(+28)
	111	111	92	—	2.78(−0.09)	1.39(−0.04)	—	—	14.9(+0.5)	641(+17)

* Etched samples
† Side-arms removed
‡ From analysis of Hall coefficient–temperature curves

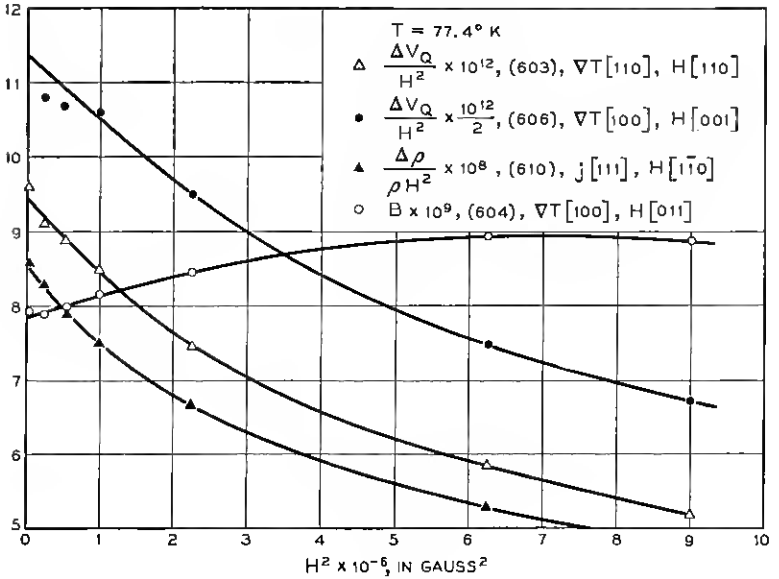

Fig. 5 — Sample plots of low-field Nernst, magnetoresistance and ΔQ data against the square of the magnetic field H showing extrapolations to zero field. Here ΔV_Q is the change in the measured thermoelectric emf in volts between the end-arms, due to H, at constant temperature gradient. The field H is measured in gauss, and B is in volts/degree gauss.

tities to be nearly as sensitive to surface effects as is the high-field transverse magnetoresistance, since only in the latter case is a large Hall field present. The high-field Nernst coefficient (see Section VIII) is the one exception, since its approach to zero makes a small Hall field due to longitudinal counter-currents amount to a large percentage error. The measurements confirm the expectation that the effects on the other quantities should be small. However, though small, the changes found in the apparent mobility, etc., were often appreciable. The effects seem to involve a complex interplay of reduced mobility in the damaged surface layer and conduction with little or no Hall effect; moreover, the latter conduction seems to be extremely anisotropic, since the large excess of magnetoresistance was found only when there were [100] surfaces normal to the magnetic field.

Table VI lists, along with the original values for sand-blasted surfaces, the values (identified by asterisks) appropriate to etched surfaces, for all cases for which the latter were measured.

5.3 *Side-Arm Corrections*

The raw data given in Tables V and VI were obtained from the measurements on the assumption that the flow of heat or electric current down the sample was purely one-dimensional and that the side-arms acted merely as infinitesimal probes with which potentials could be measured without disturbing this flow. This assumption is not quite correct, for the width of the side-arms (0.06 cm) was not negligible compared with the width (0.15 cm) of the current-carrying portion. Currents passed through such a sample must bulge out a little into the side-arms, in a way which will be altered by a magnetic field. Moreover, the anisotropy which a magnetic field introduces into the thermoelectric power can cause circulating currents to flow near the side-arms in the presence of an electric field, even though no net current flows along the specimen. These effects can become very serious when a large magnetic field is ap-

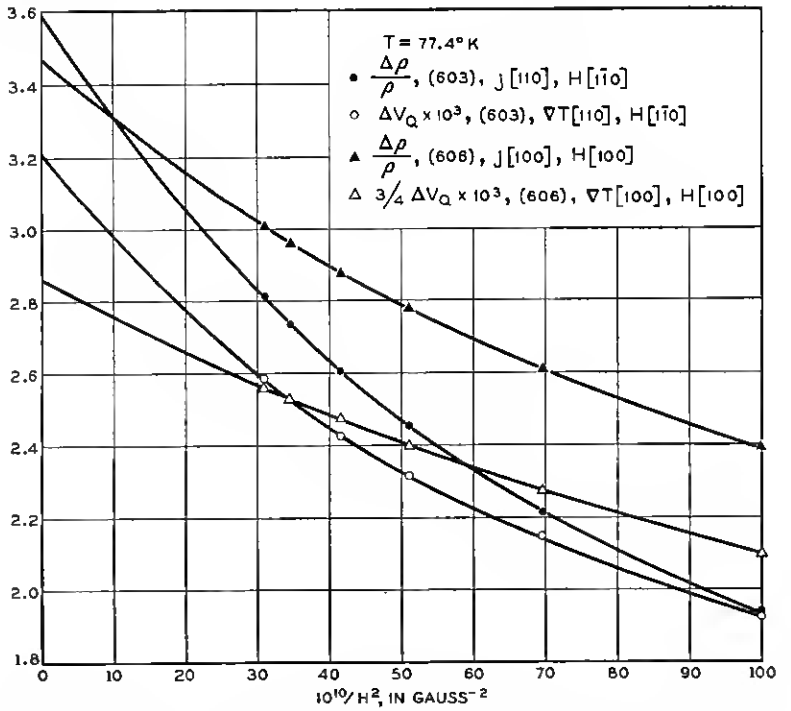

Fig. 6 — Sample plots of high-field magnetoresistance and ΔQ data against the inverse square of the magnetic field H, showing extrapolations to infinite field. Notation and units are the same as for Fig. 5.

plied in the direction of the side-arms. For example, in indium antimonide magnetoresistances of several times the ideal value have been observed for this geometry.[16] For this reason, all the transverse measurements reported here were made with the magnetic field normal to the plane of the arms, and we shall show that, for this case and for all longitudinal and zero-field cases, the side-arm errors are small and can be approximately corrected for.

A number of statements about the effects of the side-arms can be made from simple theoretical considerations. For example, it is obvious that the current distortions have no effect on the measured values of the zero-field thermoelectric power or of the Hall coefficient. The conductance of the sample is, of course, higher with the side-arms than without; measurements on scaled cutouts of stainless-steel sheet showed the difference of true and apparent resistivities in the absence of a magnetic field to be about 2.6 per cent for our geometry. However, it can be shown fairly easily that the measured transverse magnetoresistance $\Delta\rho/\rho$, and likewise the transverse ΔQ, are unaffected by the presence of the side-arms when **H** is in a [100] direction; this invariance arises from the two-dimensional nature of the potential distribution and the isotropy of ρ and Q in the plane normal to **H**. When **H** is in a [110] direction the anisotropies of $\Delta\rho$ and ΔQ cause a difference between the apparent and true $\Delta\rho/\rho$ and ΔQ, which for transverse cases can be expressed in terms of the anisotropies and the correction to the zero-field resistivity. When **H** is longitudinal, more complicated effects arise, due to the Hall fields where the current lines depart from longitudinality at the bases of the side-arms. However, for almost all the cases listed in Table VI there exist scaling relations which allow the side-arm corrections to be expressed, at least approximately, in terms of the correction to the apparent conductivity at $H = 0$.

Several experiments were performed to verify that these effects were small and to evaluate the corrections for the two cases (high-field transverse ΔQ with **H** in a [110] direction) for which the scaling relations do not suffice for a theoretical prediction. These experiments consisted in removing the middle pair of side-arms of some of the specimens and noting the changes in the apparent values of $\Delta\rho/\rho$ and ΔQ. The changes due to removal of all side-arms would, of course, be twice as great. Table VII summarizes the theoretical and experimental results for the corrections to be added to the entires of Table VI. In no case are these greater than about 4 per cent.

5.4 *Gross Inhomogeneities*

Gradients of impurity concentrations can greatly falsify the results. For example, the apparent Hall constant depends on the carrier concen-

TABLE VII

Approximate correction factors by which the entries of Table VI should be multiplied to give the "true" quantities as they would be measured on a specimen without side-arms. Except for the ΔQ's, the factors are independent of temperature, or nearly so. In the last two rows, the factors given apply in the neighborhood of liquid-air temperature.

Direction of j or ∇T Direction of **H**	[100] [001]	[100] [011]	[110] [1$\bar{1}$0]	[110] [110]	[100] [100]	[111] [111]
Quantity:						
μ_H	1.026	1.026	1.026	---	---	---
$\lim_{H\to 0}\left(\frac{\Delta\rho}{\rho H^2}\right)$	1.000	0.987	1.006	0.965	0.996	---
$\lim_{H\to\infty}\frac{\rho(H)}{\rho(0)}$	1.000	0.994	1.008	0.974	0.974	0.974
$B(0)$	0.974	0.974	0.974	---	---	---
$\lim_{H\to 0}\frac{\Delta Q}{H^2}$	1.000	0.975	1.009	1.014	1.013	---
$\lim_{H\to\infty}\Delta Q$	$\approx$1.000	$\approx$1.000	$\approx$1.000	1.000	1.000	1.000

tration between the middle side-arms, while the apparent conductivity depends on the carrier concentration over the whole length; if the concentration varies, the apparent Hall mobility will be incorrect. Most of the samples were checked for homogeneity by measuring Hall constant on the end arms as well as on the middle pair. All three measurements usually agreed to within 1 per cent. Inhomogeneities can also cause measurements designed to give quantities even in the magnetic field ($\Delta\rho$, ΔQ) to contain contributions from effects odd in the field (R, B), and vice versa. This effect occasionally showed up as an asymmetry in the measured values when the direction of **H** was reversed. This asymmetry was small for all cases listed in the tables and was consistent with the present interpretation, e.g., the magnetoresistance asymmetry could be calculated from the Hall inhomogeneity. The entries represent averages of measurements for **H** and $-$**H**.

5.5 *Value of the Temperature Gradient*

The measurements tabulated in Tables V and VI were all taken with the special-purpose apparatus described in our earlier paper.[1] With this

apparatus the temperature gradient used for the thermomagnetic effects was not measured directly, but was computed from the thermoelectric voltage developed between the potential leads at $H = 0$, together with the thermoelectric power Q of the specimen. The latter was computed on the assumption that, for a given temperature, the only source of variation of Q from specimen to specimen is the variation in the height of the Fermi level associated with the different carrier concentrations. In other words, the Q for any sample was computed from values previously measured on other samples by adding a term equal to 86 μv/degree times the logarithm of the ratio of carrier concentrations. This will not be correct if impurity scattering affects Q appreciably.

Previous empirical evidence suggested that, for fairly pure material, Q is almost unaffected by impurity scattering. The same conclusion follows from a theoretical analysis which we shall carry out in Section VII. When $T \geqq 77°$K, it turns out that no correction is needed to the data for Samples 603, 604, 606 and 610, on which most of the analysis of the next two sections will be based, nor for Sample 595. The corrections should be small for these samples at $T \approx 60°$K, and for Samples 576A and 580 at $T \geqq 77°$. For Sample 601 the correction begins to be perceptible at 94°, and for Sample 596 at 87° it amounts to about 8 per cent of the quantities tabulated.

5.6 *Boundary Scattering*

The final—and largest—correction we shall consider has to do with the scattering of phonons from the boundary of the specimen. We wish to interpret the data in terms of a theory of conduction in an infinite homogeneous medium. The side-arm correction has eliminated effects of the shape of the sample, but we have yet to correct for the finiteness of its dimensions.

We may start from the observation that phonon-drag effects are due to the anisotropy of the low-frequency part of the phonon distribution. This anisotropy, due to the temperature gradient, has a certain value at depths below the surface that are large compared with the mean free path of a phonon. However, immediately below the surface the anisotropy is only about half as great, since that half of the phonons that comes from the surface has no tangential anisotropy if the surface scatters diffusely. Thus, one may say, approximately, that the tensor $\mathbf{Q}_p$ has one value at depths greater than some value Δ, of the order of a phonon mean free path, and has half this value at depths less than Δ. The effect of this alteration is easily seen to be to make the effective $\mathbf{Q}_p(\mathbf{H})$ less than the in-

terior value by the ratio

$$\frac{Q_p}{Q_p \text{ (ideal)}} = 1 - \frac{2\Delta}{A^{\frac{1}{2}}}, \tag{16}$$

independently of H, where A is the cross-sectional area of the sample. The effect on the low-field Nernst coefficient can be calculated similarly; it is

$$\frac{B_p}{B_p \text{ (ideal)}} = 1 - \frac{\Delta}{t}, \tag{17}$$

where t is the thickness of the sample normal to its plane. We shall take Δ as roughly independent of the orientation of the surface and equal, in millimeters, to $0.037\ (77°/T)^{3.9}$, the best value currently available from experiments on the variation of Q_p with diameter near liquid-air temperature.[2]

In parentheses after each entry in Table VI we have given the sum of the side-arm correction calculated from Table VII and (for the thermoelectric quantities) the temperature-gradient correction and the boundary-scattering correction computed from (16) or (17). This total correction is to be added to the table entry to get the ideal value appropriate for the comparison with theory.

VI. ANALYSIS

At each temperature and for each impurity content we have 10 or 11 measured quantities which depend on the partial Peltier coefficients $\Pi_\parallel(\epsilon)$, $\Pi_\perp(\epsilon)$ of the energy shells, and among which no relations derivable from phenomenological theory exist. These are: Q and B at $H = 0$, $\Delta Q(H = \infty)$ for [100], [110] and [111] longitudinal orientations, one transverse $\Delta Q(H = \infty)$ for $\mathbf{H} \parallel [100]$ and two such for $\mathbf{H} \parallel [110]$, and two (or three) constants describing the low-field ΔQ behavior. (There are three phenomenologically independent constants of the latter type, but there is one relation between them which follows merely from the band structure and the electron-group approximation.[1]) We shall now derive what information we can about $\Pi_{p\parallel}(\epsilon)$ and $\Pi_{p\perp}(\epsilon)$ by fitting the theory of Section IV and Appendix B to the data.

We shall first note briefly that all these data can be approximately fitted by the specialized formulas of Tables I, III and IV, with three adjustable constants $A_\parallel$, $A_\perp$ and n, where

$$\Pi_{p\parallel,\perp} = A_{\parallel,\perp}\left(\frac{\epsilon}{kT}\right)^n$$

TABLE VIII

Comparison of thermomagnetic data observed at 94°K with values computed from the formulas of Tables I and III and from the mean moment curves of Fig. 7. For the former calculation $w = 0.061$ and the approximately optimum values $p \equiv \Pi_{p\parallel}/\Pi_{p\perp} = 9.5$, $Q_p = 697$, $\Pi_p \propto \epsilon^{-0.25}$ were used. The corrections in parentheses in Table VI have been included in the observed values, and the data for Samples 603 and 610 have been corrected to 94°. The data for Sample 606 are starred to indicate that this sample had been etched. The units of the ΔQ's are μv/degree, those of $B(0)$ are 10^{-9}v/gauss degree. Acoustic scattering has been assumed; correction for impurity scattering would lower the computed $B(0)$ slightly. In the first row, $Q(0) - Q^*$ is T^{-1} times the Peltier heat relative to the band edge, i.e., the sum $Q_p + 172\mu$v/degree.

Quantity	Sample No.	Directions		Value Computed from Tables I and III	Observed Value	Value Computed from Fig. 7
		H	∇T			
$Q^* - Q(0)$				869	869	863
$-\Delta Q(\infty)$		[001]	[001]	1440		1459
	606				1484*	
	604				1460	
	610	[111]	[111]	605	621	615
	603	[011]	[011]	118	119	124
	606	[001]	[100]	91	144*	93
	603	[011]	[01$\bar{1}$]	1325	1191	1187
	604	[011]	[100]	655	613	610
$B(0)$				22		34
	606				31*	
	603				32	
	604				36	

and with the value of $w = m^*_\perp \tau_\parallel / m^*_\parallel \tau_\perp$ given by, say, the high-field magnetoresistance measurements. Table VIII gives, in its fifth and sixth columns, a sample comparison of observed values with the predictions of this simplified theory; low-field ΔQ values have been omitted from the table because, as we shall see in detail in Section VII, they need to be corrected for impurity scattering. The extent of the agreement is a fairly good measure of the adequacy of the assumed behavior of $\mathbf{\Pi}_p$, since for most of the quantities listed the electron-diffusion contribution is small enough so that uncertainties in its value are unimportant. The observations are fitted well enough to engender some confidence in the theory, but there are systematic discrepancies which suggest that $\Pi_{p\parallel}$ and $\Pi_{p\perp}$ may have different energy dependences that a less restrictive analysis could reveal.

6.1 *Analysis in Terms of Moments*

As we have mentioned in Section III, the most general formulas of the electron-group theory, as derived in Appendix B, give Q or ΔQ and B as linear combinations of Maxwellian averages of quantities of the form $\epsilon\Pi_{\parallel,\perp}f^{(n)}(\tau_\parallel, \tau_\perp)$, where $f^{(n)}$ is homogeneous of degree n. The coefficients contain in their denominators linear combinations of similar Maxwellian averages, without the Π's. Now when n is 0 or 1, corresponding respectively to the high-field transverse Q and to $Q(0)$, or the high-field longitudinal Q, it should be quite a good approximation to take $\tau_\parallel$ and $\tau_\perp$ both proportional to $\epsilon^{-\frac{1}{2}}$ in the purest of our samples (ideal acoustic scattering). The value of $w = m^*_\perp\tau_\parallel/m^*_\parallel\tau_\perp$ appropriate to these cases can be determined from the high-field longitudinal magnetoresistance. However, for $n = 2$ and especially for $n = 3$ (low-field effects), the Maxwellian averages in question become very sensitive to small amounts of impurity scattering, and one might question the legitimacy of taking the ratio $\tau_\parallel/\tau_\perp$ independent of energy. But since the term containing ${\tau_\parallel}^m{\tau_\perp}^{n-m}$ also contains ${m^*_\parallel}^{-m}{m^*_\perp}^{m-n}$, and since $\Pi_{\parallel,\perp}$ vary only slowly with energy, it will always be a good approximation to assume that, with angular brackets as usual denoting Maxwellian averages,

$$\left\langle \epsilon\Pi_{\parallel,\perp}\left(\frac{\tau_\parallel}{m^*_\parallel}\right)^m\left(\frac{\tau_\perp}{m^*_\perp}\right)^{n-m}\right\rangle \approx {w_n}^m\left\langle \epsilon\Pi_{\parallel,\perp}\left(\frac{\tau_\perp}{m^*_\perp}\right)^n\right\rangle, \tag{18}$$

$$\left\langle \epsilon\left(\frac{\tau_\parallel}{m^*_\parallel}\right)^m\left(\frac{\tau_\perp}{m^*_\perp}\right)^{n-m}\right\rangle \approx {w_n}^m\left\langle \epsilon\left(\frac{\tau_\perp}{m^*_\perp}\right)^n\right\rangle, \tag{19}$$

where, for $n = 1, 2, 3$, w_n is determined from purely electrical data. Specifically, we can define w_n so that (19) is exact for $m = 1$; (18) will also then be nearly exact for $m = 1$. For $m > 1$, (19) and (18) may be less accurate, but this inaccuracy will have very little effect on any electrical or thermomagnetic quantity, because the terms with $m > 1$, being of order ${w_n}^m$, will be very small.

We shall use the approximations (18) and (19) to express the various thermomagnetic quantities in terms of "moments" $\Pi_\parallel^{(n)}$ and $\Pi_\perp^{(n)}$, where, for $n = 0, 1, 2, 3$,

$$\Pi_{\parallel,\perp}^{(n)} \equiv \frac{\langle\epsilon{\tau_\perp}^n\Pi_{\parallel,\perp}\rangle}{\langle\epsilon{\tau_\perp}^n\rangle}. \tag{20}$$

From the formulas of Appendix B we obtain the expressions listed in Table IX. Since the low-field Nernst coefficient involves $\Pi_{\parallel,\perp}^{(1)}$ and $\Pi_{\parallel,\perp}^{(2)}$, we have listed as the second entry in the first column that combination of B and Q which involves only the $\Pi_{\parallel,\perp}^{(2)}$. Similarly, we have

TABLE IX

Thermomagnetic quantities in terms of the moments $\Pi_{\parallel,\perp}^{(n)}$ defined by (20), as obtained from the formulas of Appendix B using the approximations (18) and (19) and the assumption of n-type material and [111] valleys.

Quantity	Directions of H and ∇T		Expression	Reference, Appendix B
$TQ(\infty)$	[011]	[100]	$\frac{1}{3}\frac{1+2w}{2+w}\Pi_{\parallel}^{(0)}+\frac{1}{3}\frac{(5+w)}{(2+w)}\Pi_{\perp}^{(0)}$	(81)
	[011]	[01$\bar{1}$]	$\frac{1}{3}\Pi_{\parallel}^{(0)}+\frac{2}{3}\Pi_{\perp}^{(0)}$	(81)
	[001]	any $\perp$H	$\frac{w}{1+2w}\Pi_{\parallel}^{(0)}+\frac{1+w}{1+2w}\Pi_{\perp}^{(0)}$	(81)
	[001]	[001]	$\frac{1}{3}\Pi_{\parallel}^{(1)}+\frac{2}{3}\Pi_{\perp}^{(1)}$	(78)
	[111]	[111]	$\frac{1+2w}{7+2w}\Pi_{\parallel}^{(1)}+\frac{6}{7+2w}\Pi_{\perp}^{(1)}$	(80)
	[011]	[011]	$\frac{w}{1+2w}\Pi_{\parallel}^{(1)}+\frac{1+w}{1+2w}\Pi_{\perp}^{(1)}$	(79)
$TQ(0)$	—	—	$\frac{w}{2+w}\Pi_{\parallel}^{(1)}+\frac{2}{2+w}\Pi_{\perp}^{(1)}$	(50)
$-T\left[\frac{B(0)}{(\mu_H/c)}+\lvert Q\rvert\right]$	—	—	$\frac{w_2}{1+2w_2}\Pi_{\parallel}^{(2)}+\frac{1+w_2}{1+2w_2}\Pi_{\perp}^{(2)}$	(57)
$T\left[-\lim_{H\to 0}\frac{\Delta Q+(B\mu_H H^2/c)}{(\Delta\rho/\rho)+(\mu_H H/c)^2}+Q\right]$	[001]	[100]	$\frac{w_3}{2+w_3}\Pi_{\parallel}^{(3)}+\frac{2}{2+w_3}\Pi_{\perp}^{(3)}$	(58), (65)
$T\left[-\lim_{H\to 0}\frac{\Delta Q}{(\Delta\rho/\rho)}+Q\right]$	[001]	[001]	$-\frac{w_3}{1-w_3}\Pi_{\parallel}^{(3)}+\frac{1}{1-w_3}\Pi_{\perp}^{(3)}$	(58), modified (65)

listed in the last two rows those combinations of the low-field ΔQ, B, and Q which involve only the $\Pi_{\parallel,\perp}^{(3)}$. These equations can in most cases be inverted to give the $\Pi_{\parallel,\perp}^{(n)}$ in terms of the observed quantities. Thus, the first two rows just suffice to determine $\Pi_{\parallel,\perp}^{(0)}$, the next four rows overdetermine $\Pi_{\parallel,\perp}^{(1)}$, the next row gives one relation between $\Pi_{\parallel}^{(2)}$ and $\Pi_{\perp}^{(2)}$, and the last two rows just determine $\Pi_{\parallel,\perp}^{(3)}$.

Our procedure will now be to determine the moments $\Pi_{\parallel,\perp}^{(n)}$ from these equations and the observational data, and then to discuss the separation of each such empirically determined $\Pi_{\parallel,\perp}^{(n)}$ into electron-diffusion and phonon-drag contributions and to interpret the variation of the latter part with n in terms of the energy dependence of $\Pi_{p\parallel,\perp}$.

TABLE X

Values of w_1, w_2 and w_3 used in the moment analysis. The values of w_1 were obtained independently for each case by fitting the electron-group theory to the observed high-field limit of the longitudinal magnetoresistance. The side-arm corrections of Table VI have been included and, whenever possible, data obtained after etching have been used. The latter cases are identified by asterisks. The values of w_3 were estimated from these w_1's (assumed for the first four samples equal to 0.061) and the approximate dependence of w_3 on impurity concentration found by Goldberg.[17] The values of w_2 were interpolated between w_1 and w_3.

Sample	T, °K	Empirical w_1	Assumed w_2	Assumed w_3
606	60°		0.0625	0.064
	63°	0.061*		
	77.4°	0.0615*	0.0615	0.062
	94°	0.061*	0.061	0.061
604	63°	0.062		
	77.4°	0.061*	0.0625	0.064
	92°	0.0625	0.0615	0.062
610	77.4°	0.061*	0.0625	0.064
	92°	0.061	0.0615	0.062
603	77.4°		0.0625	0.064
	94°		0.0615	0.062
Value adopted for all above cases		0.0610		
601	94°	0.069	0.076	0.084
596	87°	0.081		
606	131°	0.067* (0.0595 adopted, see text)	0.0595	0.0595

6.2 *Choice of the w_n*

To begin with, we need values of w, w_2 and w_3. Magnetoresistance evidence on w ($\equiv w_1$) for the present samples is summarized in the column labeled "Empirical w_1" of Table X. The good agreement of the w_1 values from Samples 606 and 604 with that from Sample 610 speaks well for the validity of the electron-group model. There seems to be no significant change of w_1 with temperature in the range 60° to 94°K. No reliable value of w_1 can be obtained from Sample 603, since in this orientation a change of w_1 from 0.04 to 0.08 only changes the theoretical high-field resistance by 0.05 of the zero-field value. The data for 603 do, however, agree fairly well with the theory, in that the $\Delta\rho/\rho_0$ predicted from the w_1 of the other specimens is within 0.02 or 0.03 of the value in Table VI.

The empirical w_1 value for Sample 606 at 131°, though listed, is not to be trusted, as a field of 18,000 gauss does not give a very good approach to saturation. We have preferred to rely on the value 0.061 found at the lower temperatures, decreasing it to 0.0595 to allow for the gradual decrease of w with temperature found by Goldberg,[17,18] a decrease which also shows up, though less clearly, in our own low-field data at higher temperatures.

The estimation of w_3 is somewhat less satisfactory. In principle w_3 can be estimated from the longitudinal and transverse low-field magnetoresistances, since, as we noted at the start of this section, two independent phenomenological constants should suffice for the complete description of the low-field magnetoresistance in reasonably pure material. However, the w_3 values computed in this way for Samples 603, 604 and 610 turn out to be quite different — ranging, for example, from 0.056 to 0.073 at 77°K, all for etched samples — whereas the similarity in impurity content between these three samples would lead one to expect similar w_3's. This sort of discrepancy might have been anticipated from the fact (Ref. 1, Fig. 13) that the four data for 603 and 604 depart perceptibly from the predictions of the phenomenological theory with two adjustable constants. The trouble can arise from any of several causes. To compute w_3 from the data, one needs the longitudinal and transverse magnetoconductances, and the second of these equals the corresponding magnetoresistance plus $(\mu_H/c)^2$. Now the empirical value of μ_H, unlike magnetoresistance and ΔQ values, depends on the measured thickness of the sample and is affected by errors in this measurement. Also, it can be falsified if the carrier concentration between the Hall arms differs slightly from the average over the length of the sample. Since a change of μ_H by 1 per cent affects w_3 by 0.003, this source of scatter from specimen to specimen could well be serious. Moreover, our random errors are large enough to affect w_3 perceptibly, and comparison of etched and unetched samples has shown that the surface damage effect can alter the empirical w_3 by 0.007 or so.

Fortunately, a study of the fomulas of Table IX, which we shall describe below, shows that, once w_3 is specified, the $\Pi_{\parallel,\perp}^{(3)}$ computed from the measured quantities is not nearly so sensitive to small errors in the latter as we have just found the empirical w_3 to be. This suggests that one can get a fairly reliable analysis by disregarding the apparent w_3's of the specimens and estimating the true w_3 for each temperature and impurity concentration in some other way. Now for pure acoustic scattering w_3 should be practically the same as w_1, for which we have obtained the presumably trustworthy value 0.061 (Table X). Several studies of the effect of impurity scattering on magnetoresistance have

been published,[17,18,19] and, while the absolute values of w_3 obtained in these studies may possibly have been affected by various kinds of systematic errors, their picture of the variation with impurity content and temperature is undoubtedly correct. From the work of Goldberg[17] and of Goldberg and Howard,[18] it appears that, at 77°K, a sample with impurity concentration 7×10^{13} cm^{-3} has a w_3 differing from that of an ideally pure sample by only about 10 per cent, or at the very most 20 per cent.† Thus it is a reasonable guess to say that the corresponding deviation at a concentration of 2×10^{13} cm^{-3} is perhaps 5 per cent, i.e., 0.003 in w_3. While the error in this estimate may be as large as the estimate itself, it is surely much smaller than the scatter mentioned in the preceding paragraph, and we shall see that this accuracy suffices for our present purpose. The last column of Table X gives the values we shall adopt for our analysis, obtained by adding an estimate of this sort to our w_1. The next to the last column gives the corresponding w_2's, obtained by interpolating between w_1 and w_3.

6.3 *Results for* $\Pi_{\parallel}^{(n)}$ *and* $\Pi_{\perp}^{(n)}$

It is now a straightforward matter to insert the w_n of Table X into the formulas of Table IX, equate to the empirical quantities of Table VI (with the corrections included), and solve for the moments $\Pi_{\parallel,\perp}^{(n)}$ defined by (20). To make a comparison of the values for different specimens more meaningful, it is best to compare not the $\Pi_{\parallel,\perp}^{(n)}$, which depend on the location of the Fermi level through Π_e, but the quantities $\Pi^* - \Pi_{\parallel,\perp}^{(n)}$, where

$$\Pi^* = \frac{\epsilon_F - \epsilon_b}{e} \tag{21}$$

represents the part of Π_e due to the difference between the Fermi level ϵ_F and the band edge ϵ_b. The quantities $\Pi^* - \Pi_{\parallel,\perp}^{(n)}$ thus are positive for n-type material and measure moments of the Peltier heat relative to the band edge.

Fig. 7 shows the results for $\Pi^* - \Pi_{\perp}^{(n)}$ and $\Pi^* - \Pi_{\parallel}^{(n)}$, respectively, for a number of the purest samples at several temperatures from 60° to 131°K. Here the moments for $n = 1$ were calculated from Q and the high-field limit of ΔQ for H longitudinal. Those for $n = 3$ were calculated from the longitudinal and transverse values of

$$\lim_{H \to 0} \frac{\Delta Q}{H^2},$$

† We are indebted to C. Goldberg for having informed us of some of these results prior to publication.

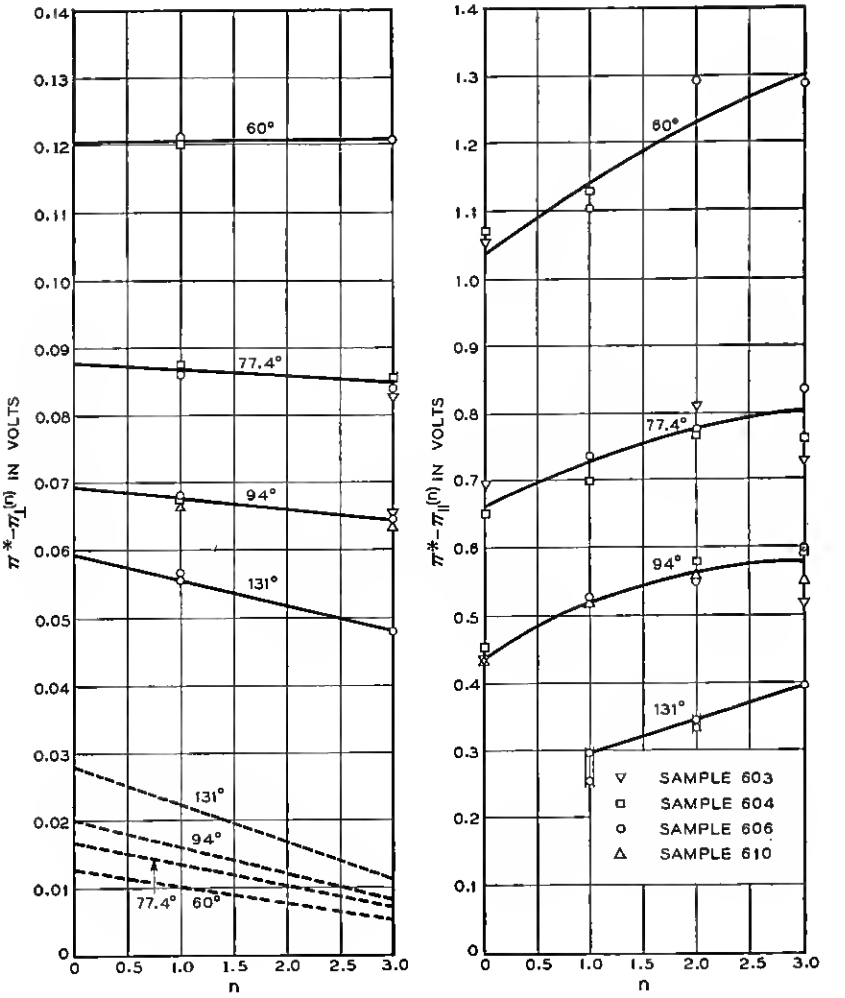

Fig. 7 — Empirical values of the moments $\Pi_\perp^{(n)}$ (left) and $\Pi_\parallel^{(n)}$ (right) defined by (20), as obtained from the method of analysis described in the text. Note that the two scales differ by a factor of ten. The dashed curves at the bottom of the chart for $\Pi_\perp^{(n)}$ show the contributions which Π_s would make to $\Pi_\parallel^{(n)}$ or $\Pi_\perp^{(n)}$ at the various temperatures, if the scattering were purely acoustic. The full curves are reference means which we shall use in Figs. 11 and 12.

using, if necessary, the phenomenological identities mentioned at the bottom of Table IV to relate the ΔQ values for the directions going with a particular sample to those for the directions listed in Table IX. For $n = 2$, only one moment can be determined; since $\Pi_\perp^{(n)}$ is very reproducible and varies very little with n, we have chosen to determine $\Pi_\perp^{(2)}$ by linear interpolation between $\Pi_\perp^{(1)}$ and $\Pi_\perp^{(3)}$, and then to determine $\Pi_\parallel^{(2)}$ for each specimen by the equation specified in Table IX. For $n = 0$, a similar procedure was followed, using a linearly extrapolated value of $\Pi_\perp^{(0)}$; the alternative procedure of combining transverse ΔQ data on two different samples would lead to larger random errors.

For the 131° data the method just described for determining the moments for $n = 1$ starts to break down, since, as we noted above, the high-field limit is not reliable. However, it is probably safe to say that $\Delta Q(\infty)$ lies in between the extrapolated value of Table VI and a value increased from this in the ratio of the $\Delta\rho(\infty)$ calculated for the assumed w_1 to the $\Delta\rho(\infty)$ of the table. The first moments obtained from both these limits are plotted in Fig. 7 and connected by vertical lines to emphasize the uncertainty. A corresponding though smaller ambiguity results for the second moment $(\Pi^* - \Pi_\parallel^{(2)})$. The second and probably more nearly correct assumption gives the higher $(\Pi^* - \Pi_\parallel^{(1)})$ and the lower $(\Pi^* - \Pi_\perp^{(1)})$.

Fig. 7 also shows, for comparison, the electronic contribution

$$\Pi^* - \Pi_e^{(n)},$$

as given by an equation analogous to (20) on the assumption $\tau_\perp \propto \epsilon^{-\frac{1}{2}}$, i.e., without correction for impurity scattering. The latter correction should be very small for these specimens; some estimates of it will be given in Section VII. It will be seen that, with our neglect of impurity scattering, the electronic contribution is linear in n, and that it accounts for the major part of the variation of $\Pi_\perp^{(n)}$ with n; this makes our use of linear interpolations and extrapolations seem reasonable. Subtraction of the electronic and total moments shows that $|\Pi_{p\perp}|$ is almost independent of energy, decreasing slightly with increasing energy, and that $|\Pi_{p\parallel}|$ has a more rapid, though still modest, decrease. This is a refinement of the conclusion of our first paper to the effect that some average of $|\Pi_{p\parallel}|$ and $|\Pi_{p\perp}|$ decreases with increasing energy. Since an accurate quantitative estimate of the energy dependences of $\Pi_{p\parallel}$ and $\Pi_{p\perp}$ requires a correction for impurity scattering, we shall postpone this topic to Section VII.

The last two columns of Table VIII give a sample comparison of the measured thermomagnetic quantities with values predicted from the mean moment curves of Fig. 7. The fit is, indeed, significantly better

than was obtained in the middle column on the assumption of energy-independent anisotropies.

6.4 *Accuracy of the Results*

A few words are in order regarding the sensitivity of these results to random or possible systematic errors in the inputs. As one might infer from the consistency of the values of $\Pi_\perp^{(1)}$ and $\Pi_\perp^{(3)}$ for different samples and from their regular trend with temperature, these quantities are rather insensitive. For germanium with its small w, Table IX shows that the quantity $\Pi_\perp^{(1)}$ equals $TQ(0)$ minus a small fraction of the longitudinal high-field limit of ΔQ; since the latter term is only about one-fifth of $TQ_p(0)$, errors in it have little effect. This term is almost proportional to w. Thus, for example, it turns out that, at 77°K, an alteration of even as much as 10 per cent in the assumed w, or in the high-field ΔQ, would affect the plotted quantity $\Pi^* - \Pi_\perp^{(1)}$ by only 2 per cent of its value. The makeup of $\Pi_\perp^{(3)}$ is similar. It equals $TQ(0)$ plus a number of terms involving the Hall mobility and the low-field $\Delta\rho$'s and ΔQ's; the latter terms are again only a small fraction of $Q_p(0)$, and they depend hardly at all on w_3. For example, for Sample 606 at 77°K, a change of the assumed w_3 by 10 per cent would alter $\Pi^* - \Pi_\perp^{(3)}$ by only one-third of 1 per cent; changes of 10 per cent in any one of the quantities B, μ_H or the transverse $\Delta\rho/\rho H^2$ or $\Delta Q/H^2$ would affect $\Pi^* - \Pi_\perp^{(3)}$ by 1 per cent or less; a 10 per cent change in the longitudinal $\Delta\rho/\rho H^2$ or $\Delta Q/H^2$ would have a 3 per cent effect. The sensitivity for the other cases is similar. Thus, the values of $\Pi_\perp^{(3)}$ should be quite reliable.

Turning to the $\Pi_\parallel^{(n)}$, we find these quantities to be much more sensitive. The values of $\Pi_\parallel^{(1)}$, which depend primarily on the longitudinal high-field limit of ΔQ, should be more reliable than those for other values of n. Thus, for example, for Sample 606 at 77°K an error of 5 per cent in the high-field ΔQ would affect $\Pi^* - \Pi_\parallel^{(1)}$ by a little over 4 per cent. A 10 per cent change in the assumed w would affect this quantity by only about one-half of 1 per cent. On the other hand, $\Pi_\parallel^{(3)}$ is much more sensitive to w_3, being in fact very nearly proportional to w_3^{-1}. It is also fairly sensitive to the [100] longitudinal $\Delta Q/H^2$ and $\Delta\rho/\rho H^2$. For example, at 77°K a 10 per cent change in either of the latter quantities would change $\Pi^* - \Pi_\parallel^{(3)}$ by about 9 per cent. However, the sensitivity to the other inputs mentioned in the preceding paragraph is small; a 10 per cent change in any one of them at 77°K would affect $\Pi^* - \Pi_\parallel^{(3)}$ by no more than 2 per cent. The quantity $\Pi^* - \Pi_\parallel^{(2)}$ behaves very similarly. It is very nearly proportional to w_2^{-1}; however, the uncertainties in w_2

should be rather less than those in w_3. Changes of 10 per cent in B or μ_H would affect $\Pi^* - \Pi_\parallel^{(2)}$ at 77° by about 5 per cent, and a change of 3 per cent in the interpolated $\Pi_\perp^{(2)}$ would affect it by 6 per cent. The values of $\Pi^* - \Pi_\parallel^{(0)}$, finally, are insensitive to w when derived from measurements with H in a [110] direction. The sensitivity to the assumed high-field transverse ΔQ is moderate; for Sample 603 at 77°, for example, a 10 per cent change in the latter quantity would change $\Pi^* - \Pi_\parallel^{(0)}$ by perhaps 9 per cent.

6.5 *Other Orientations*

Several conceivable calculations have been omitted from the list used in the construction of Fig. 7; these correspond to cases where the observed quantity is very insensitive to the moment which one might wish to calculate from it. Thus, as Fig. 3 shows, the longitudinal ΔQ in the [011] direction is very small and insensitive to p (i.e., to $\Pi_\parallel^{(1)}$). Similarly, Fig. 4 shows that the transverse ΔQ with H in an [001] direction is small and very insensitive to p (or $\Pi_\parallel^{(0)}$). Although no reliable points for Fig. 7 can be computed from these data, the entries in the last two columns of Table VIII show that the ΔQ's for these orientations are in fair agreement with the predictions of the theory. (It is more significant to compare values of $Q(\infty) = Q(0) + \Delta Q$ than values of ΔQ itself, since the latter quantity could conceivably be of either sign.) The small discrepancies remaining are of the order of magnitude of the expected effect of orbital quantization.

VII. DEPENDENCE OF $\Pi_{p\parallel,\perp}$ ON ENERGY

The obvious next step is to convert the empirical moments of $\Pi^* - \Pi_{\parallel,\perp}$ plotted in Fig. 7 into moments of $-\Pi_{p\parallel,\perp}$ by subtracting the theoretical moments of $\Pi^* - \Pi_e$. One may then hope to determine the rate of variation of $\Pi_{p\parallel,\perp}$ with energy ϵ by comparing the way in which these moments vary with n with the n-variation to be expected for, say, $\Pi_{p\parallel,\perp} \propto \epsilon^t$. For a specimen completely free of impurity scattering, all this could be done very simply indeed. However, as we shall see, the second and third moments, i.e., those with weight factors $\tau_\perp^2$ and $\tau_\perp^3$ in (20), are extremely sensitive to impurity scattering, since this modifies $\tau_\perp$ greatly in the low-energy region, where it is large, and since $\Pi_{p\parallel,\perp}$ also tend to be largest at low energies. Thus, in spite of our efforts to avoid the morass of impurity-scattering theory by using very pure specimens, we must still resort to it if we are to make a complete analysis of our data. However, the smallness of the impurity scattering in the sam-

ples used for Fig. 7 will turn out to simplify greatly the task of correcting for it. We shall therefore digress for a moment to discuss the nature of impurity scattering and to establish the validity of the procedure we wish to use to take account of it.

7.1 *Impurity Scattering*

The Conwell-Weisskopf theory of ionized-impurity scattering,[20] combined with various modifications,[21,22,23,24] has had some success in correlating mobility data and other properties of semiconductors.[25,26]* However, a theory of this form can be rigorously justified only in the limit of carrier and ion densities rather lower than those normally encountered in semiconductors; even for this case, a rigorous treatment requires inclusion of the effects of electron-electron collisions,[27] a refinement which has usually been ignored in the semiconductor literature. Under conditions such as those of our experiments, there are several aspects of the theory which become rather dubious, e.g., use of the Born approximation in scattering,[23,24] the justification for treating the screened coulomb potential of an ion as a static scattering potential, etc. Thus, about all one can safely say about ionized-impurity scattering in this range is that it is something which modifies the distribution function more and more as the energy becomes lower. Fortunately, this fact seems to be about all one needs to know in order to correlate the various effects of impurity scattering with one another, in the range where impurity scattering is slight. We shall now try to demonstrate this empirically.

Although the fact of electron-electron scattering prevents a relaxation-time model from being strictly valid for impurity scattering, we shall follow custom and assume that, in the range of interest, the effects of impurity scattering can be adequately allowed for by modifying the form of the functions $\tau_{\parallel}(\epsilon)$, $\tau_{\perp}(\epsilon)$. The usual assumption takes the form

$$\tau^{-1} = a\epsilon^{\frac{1}{2}} + b\epsilon^{-\frac{1}{2}}, \tag{22}$$

where the first term represents acoustic scattering, and the second impurity scattering. This leads to difficult integrals in the various transport expressions. Since no real justification can be given for the exact form of (22) — except at densities far below ours — we shall try using instead another expression, which has the same property of reducing τ at low

* For a general review with further references, see Ref. 26.

energies but leads to more tractable integrals, namely,

$$\tau \propto \epsilon^{-\frac{1}{2}} \left[1 - \exp\left(\frac{-\epsilon}{k\theta} \right) \right]. \tag{23}$$

Here θ is a parameter which measures the amount of impurity scattering.

7.2 *Legitimacy of (23)*

Our argument that (23) is justified will consist of two parts. The first will be to show that (23) gives practically the same results as (22) for a variety of problems, i.e., that when impurity scattering is just beginning to be appreciable the exact form of the impurity-scattering law is of less consequence that the mere fact that the τ's of low-energy electrons are greatly reduced. The second argument will be empirical and will consist in a rough quantitative correlation of magnetoresistance, Hall, and mobility data, based on (23).

The curves of Fig. 8 show the first of the comparisons just mentioned. The abscissas are values of the ratio μ_H/μ_{Ha}, where μ_H is the Hall mobility computed with (22) or (23) for a simple-model semiconductor, and μ_{Ha} is the corresponding quantity for pure acoustic scattering ($b = 0$ or $\theta = 0$). The upper two sets of curves show the values of the ratio of Hall to drift mobility and of the electronic Peltier heat relative to the band edge. The full curves were computed from (23), while the dashed ones were taken from the literature[28,29,30] based on (22).* Note that the agreement is very good near $\mu_H/\mu_{Ha} = 1$, but that, as one must expect, it becomes poor for $\mu_H/\mu_{Ha} < \frac{1}{2}$. For the magnetoconductivity (bottom curve) the agreement with the dashed curve, calculated from (22) by means of the tables of Beer, Armstrong and Greenberg,[30] is even better. It is worth noting, incidentally, that Mansfield[31] has also found μ_H/μ to be insensitive to the form of the impurity-scattering law for $\mu_H/\mu_{Ha} > 0.7$ or so.

Although it is encouraging to find such insensitivty of the predictions of impurity-scattering theory to the exact form of the scattering law, a comparison of the predictions of (23) with experiment is desirable as a test of its reliability. In applying (23) to n germanium we must, of course, take account of the anisotropy of the valleys, and of possible anisotropy in the impurity scattering. We shall do this in the same way as was described for the moment analysis of Section VI. Thus, we shall describe

* Ref. 28 gives a general review and references to the earlier literature, Ref. 29 an accurate table of integrals and Ref. 30 the most complete tables of Hall and magnetoresistance integrals.

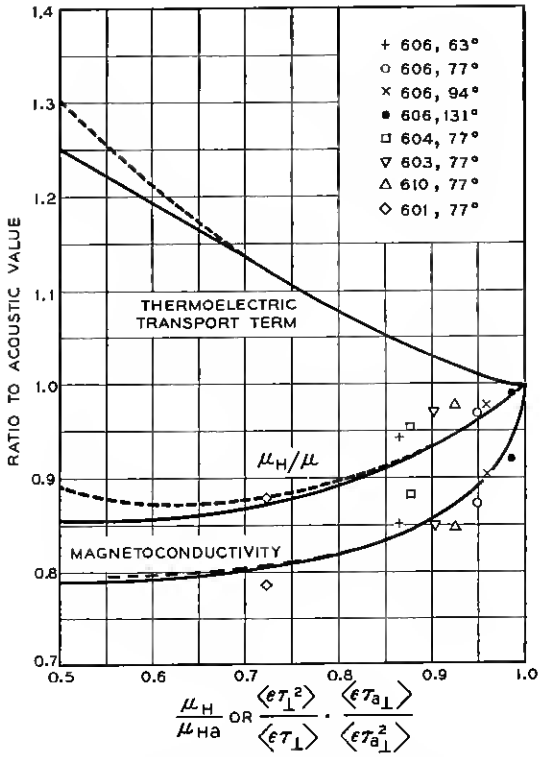

Fig. 8 — Tests of the predictions of the impurity-scattering assumption (23). The full curves represent the predictions of (23), the dashed curves those of (22), for a semiconductor with isotropic effective mass. Abscissas are ratios of Hall mobility to its value for pure acoustic scattering. Ordinates are the ratios of the values computed for the designated quantities with impurity scattering to the values with pure acoustic scattering. The top curves pertain to $\Pi^* - \Pi_\epsilon = \langle \epsilon^2\tau \rangle / e\langle \epsilon\tau \rangle$, where Π^* is defined by (21); the acoustic value of $\Pi^* - \Pi_\epsilon$ is $2kT/e$. The middle curves pertain to $\mu_H/\mu = \langle \epsilon\tau^2 \rangle \langle \epsilon \rangle / \langle \epsilon\tau \rangle^2$; the acoustic value is $3\pi/8$. The bottom curves pertain to the low-field transverse magnetoconductivity ratio $(c/\mu_H H)^2(\Delta\sigma/\sigma_0) = \langle \epsilon\tau^3 \rangle \langle \epsilon\tau \rangle / \langle \epsilon\tau^2 \rangle^2$; the acoustic value is $4/\pi$. The points represent empirical values for the various etched specimens as obtained from the observed μ_H/μ and the magnetoresistance constant $b = (\Delta\rho/\rho H^2)_{100}^{001}$ with abscissas based on the assumption; $\mu_{Ha} = 54.3$, 38.6, 28.0, and 16.2×10^3 cm^2/vs at 63°, 77°, 94°, and 131°K, respectively; both ordinates and abscissas represent ratios of observed quantities to values which would obtain if the w_1, w_2 and w_3 of Table X were combined with the acoustic value of $\tau_\perp$. The ratios of μ_H/μ and of b to their ideal values are rather insensitive to the anisotropy of m^*/τ when this is allowed for in this manner.

the anisotropy by the w_3, w_2 and w_1 values given in Table X, and shall take the transverse magnetoconductivity of a [100] specimen to be given by

$$-\frac{\Delta\sigma}{\sigma(\mu_H H/c)^2} = \frac{\Delta\rho}{\rho(\mu_H H/c)^2} + 1 \approx \left[\frac{(2 + w_3)(1 + 2w_3)(2 + w_1)}{3(1 + 2w_2)^2}\right]\left[\frac{\langle\epsilon\tau_\perp{}^3\rangle\langle\epsilon\tau_\perp\rangle}{\langle\epsilon\tau_\perp{}^2\rangle^2}\right], \tag{24}$$

an expression which follows from the known[3] forms for $\Delta\sigma$, σ and μ_H in the electron-group approximation, and the further assumption (19). Similarly, we shall take for the Hall and drift mobilities

$$\mu_H \propto \left[\frac{(1 + 2w_2)}{(2 + w_1)}\right]\left[\frac{\langle\epsilon\tau_\perp{}^2\rangle}{\langle\epsilon\tau_\perp\rangle}\right], \tag{25}$$

$$\mu \propto (2 + w_1)\left[\frac{\langle\epsilon\tau_\perp\rangle}{\langle\epsilon\rangle}\right], \tag{26}$$

so that the ratio of μ_H to its ideal acoustic-scattering value μ_{Ha} can be obtained from the ratio of the right of (25) to its ideal value. If now we assume (23) for $\tau_\perp$, and the w_n's of Table X, we can use the curves of Fig. 8, since the ratio of the magnetoconductivity or the Hall mobility to the factor involving w_n's in (24) or (25) is just the value for the isotropic-mass case.

As we have no direct measurement of μ_{Ha} from which to compare (25) with (24) for a single specimen, we have adjusted this one parameter to fit the average behavior of the magnetoresistance of the purer specimens at 77.4°K. The μ_{Ha} values for other temperatures were determined from the assumption $\mu_{Ha} \propto T^{-1.65}$, this exponent having been chosen to make the fractional departure of μ_H from μ_{Ha} scale a little more slowly than T^{-3}, as one expects from the Conwell-Weisskopf law. Using the ratio of the observed μ_H to this μ_{Ha} and the w_1 and w_2 of Table X, we can determine the ratio $\langle\epsilon\tau_\perp{}^2\rangle\langle\epsilon\tau_{a\perp}\rangle/\langle\epsilon\tau_\perp\rangle\langle\epsilon\tau_{a\perp}{}^2\rangle$ of the last factor in (25) to the value it has when $\tau_\perp = \tau_{a\perp}$, the value for pure acoustic scattering. With this ratio as abscissa, we have plotted, on the graphs of Fig. 8, the ratios of empirical value to acoustic value for the last factor in (24) and for the ratio of the last factors in (25) and (26), as obtained from the ratio of the low- and high-field Hall constants. Only data from etched specimens have been used, as extreme accuracy is required for a significant comparison; even so, there is a fair amount of scatter in the points. Much of this may be due to errors in μ_H resulting from errors — perhaps 1 per cent — in the assumed dimensions, or from the fluctuations in impurity

density; such errors will displace the μ_H/μ points horizontally and the magnetoconductivity points along a line sloping at about 45° from upper left to lower right. However, the curves account at least roughly for the at first sight surprisingly low magnetoconductivity of the pure specimens, and for the further reduction of magnetoconductivity and μ_H/μ found for the less pure specimen (Sample 601).

In concluding this digression, a few words are in order regarding the validity of the assumption that nothing except ionized-impurity scattering interferes appreciably with the ideal acoustic scattering law $\tau \propto \epsilon^{-\frac{1}{2}}$. Optical-mode or intervalley scattering has sometimes been suggested as one of several possible causes of the departure of the mobility from a $T^{-\frac{3}{2}}$ law. Though such scattering freezes out at low temperatures, it is easily verified[13] that the amount of it which would be needed to account entirely for the mobility exponent could raise μ_H/μ by 3 per cent or so at 131°K, depress it by perhaps 1 per cent at 77°, and lower the absolute value of the magnetoconductivity by 1 per cent or so. The fact that, for Sample 606 at 131°, the ratio μ_H/μ is 0.992 of the acoustic-scattering value suggests that this and other departures from ideal acoustic-scattering behavior are small.

7.3 *Behavior of the Moments of* $\Pi_{p\parallel,\perp}$

Fig. 9 shows the way in which the various moments of $\mathbf{\Pi}_p$, as defined by (20) for either component, would be affected by impurity scattering of the type (23), if Π_p were $\propto \epsilon^{-\frac{1}{2}}$ or $\epsilon^{-\frac{3}{2}}$. Impurity scattering, of course, does not affect the zeroth moment, and if $\mathbf{\Pi}_p$ is independent of energy it does not affect any moment. We have chosen as abscissa the same ratio of Hall mobility to ideal acoustic mobility which was used in Fig. 8. Fig. 10 shows, analogously, the effect of impurity scattering on the second and third moments of the quantity $(\Pi^* - \Pi_e) \propto \epsilon$; the effect on the first moment has already been shown in Fig. 8. Comparison of Figs. 9 and 10 with Fig. 8 shows that, for even our purest samples at 77°K, the effects of impurity scattering on the moments with $n = 2$ and 3 can be considerable if Π_p varies as rapidly as $\epsilon^{-\frac{3}{2}}$. This is why we have undertaken such an elaborate discussion of these effects.

The first step in analyzing the data of Fig. 7 is to correct $\Pi^* - \Pi_e$ for the effects of impurity scattering and subtract it from the curves of Fig. 7 to get curves representing the moments of $\Pi_{p\parallel}$ and $\Pi_{p\perp}$, averaged over the purer specimens. To describe the average behavior of the purer specimens, we have chosen the values $\langle \epsilon\tau_\perp^2 \rangle \langle \epsilon\tau_{a\perp} \rangle / \langle \epsilon\tau_\perp \rangle \langle \epsilon\tau_{a\perp}^2 \rangle = 0.89$ at 60°, 0.93 at 77.4°, 0.96 at 94° and 0.98 at 131°. These choices, though

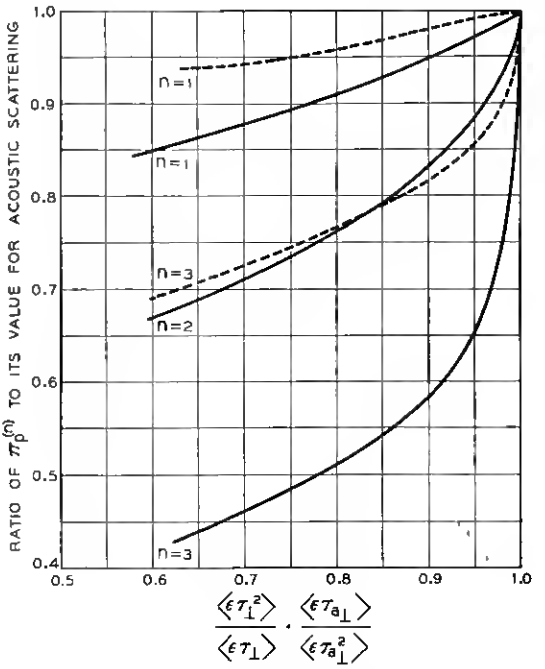

Fig. 9 — Effect of impurity scattering on the moments $\Pi_p^{(n)}$ if Π_p is assumed $\propto \epsilon^{-1/2}$ (full curves) or $\propto \epsilon^{-1/4}$ (dashed curves). Abscissas are the ratio of Hall mobility to its value for same anisotropy parameters w_1 and w_2, but $\tau_\perp \propto \epsilon^{-1/2}$.

reasonable enough, differ slightly from other equally reasonable choices which one might make from Fig. 8; we shall discuss the sensitivity of the results to the choice in the next paragraph. From these abscissas in Fig. 10 and the top curve of Fig. 8 we have determined the corrections to $\Pi^* - \Pi_e^{(n)}$. The resulting values of $\Pi_{p\perp}^{(n)}$ and $\Pi_{p\parallel}^{(n)}$ are shown in Fig. 11 as full curves. The dashed curves are the moments to be expected for $\Pi_{p\parallel,\perp} \propto \epsilon^0$, $\epsilon^{-1/4}$, or $\epsilon^{-1/2}$, as determined from the values of μ_H/μ_{Ha} just given and the curves of Fig. 9; the dashed curves have been fitted to the full curves at $n = 1$.

A word about the sensitivity of the results to the choice of abscissas in Figs. 8 to 10 is in order. Shifting the abscissa 0.01 unit at 77° has a negligible effect on the moments with $n = 0$ or 1. It shifts the full and dashed curves of Fig. 11 in the same direction for $n > 1$, the dashed curves being shifted much the greater amount; for $n = 3$, it shifts the $\epsilon^{-\frac{1}{2}}$ dashed curves by about 0.02 volt for $\Pi_{p\parallel}$, or 0.002 volt for $\Pi_{p\perp}$. At 131°K, the effect is more serious: a decrease of the assumed abscissa from 0.98 to 0.97, though affecting the $n = 1$ moments and $\Pi_{p\parallel}^{(3)}$ very

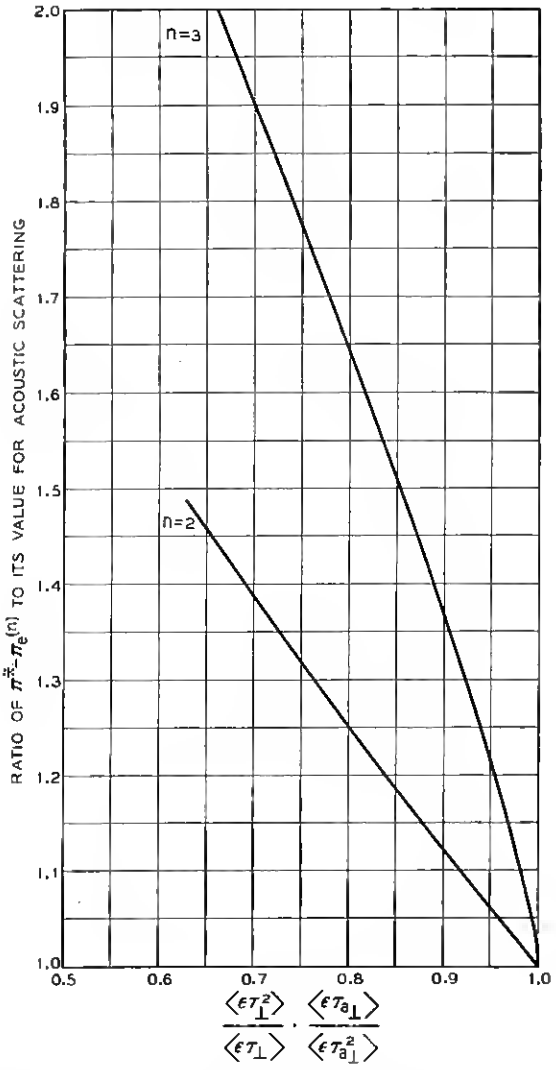

Fig. 10 — Effect of impurity scattering on the moments $\Pi^* - \Pi_e^{(n)}$. Abscissas are the ratio of Hall mobility to its ideal acoustic value for the same anisotropy parameters w_1 and w_2, but $\tau_\perp \propto \epsilon^{-1/2}$.

little, would lower the empirical $-\Pi_{p\perp}^{(3)}$ by about 0.001 volt, and would lower the corresponding ordinate of the $\epsilon^{-\frac{1}{2}}$ curve for $-\Pi_{p\parallel}^{(3)}$ by 0.09 volt.

As is to be expected from our experience in constructing Fig. 7, the results for $\Pi_{p\perp}^{(n)}$ are the more consistent. At all four temperatures the

empirical $\Pi_{p\perp}$ curves lie between those for $\Pi_{p\perp} \propto \epsilon^{0}$ and $\epsilon^{-\frac{1}{4}}$, and nearer to the former. By interpolation we estimate $\Pi_{p\perp} \propto \epsilon^{-0.08}$, the exponent being within 0.02 or so of this value at all four temperatures. The curves for $\Pi_{p\parallel}^{(n)}$ have, for $n > 1$, roughly the behavior to be expected for $\Pi_{p\parallel} \propto \epsilon^{-0.25}$ (77° and 94°K), $\epsilon^{-0.35}$ (60°) and $\epsilon^{-0.50}$ (131°K); between $n = 0$ and $n = 1$ the slope is steeper, corresponding on the average to,

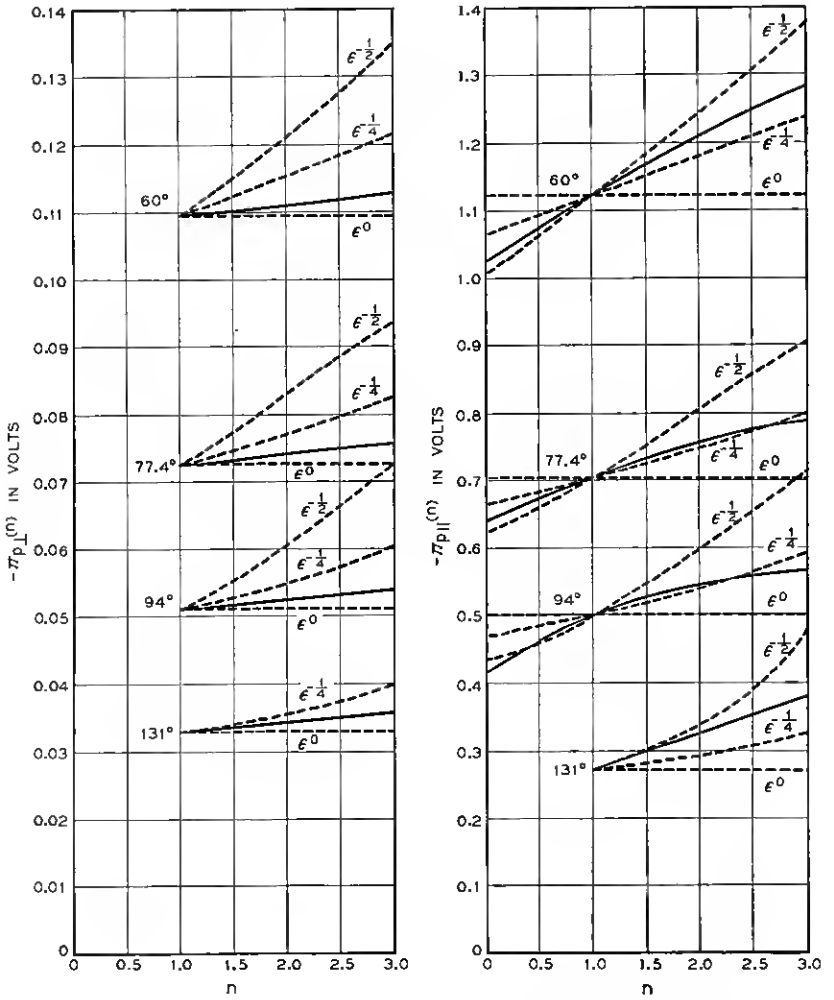

Fig. 11 — Moments of $\Pi_{p\perp}$ and $\Pi_{p\parallel}$ (full curves), as determined from Fig. 7 and the values of $\Pi^* - \Pi_e$ corrected for impurity scattering. The dashed curves show the behavior which would be expected if $\Pi_{p\parallel,\perp}$ were $\propto \epsilon^{0}$, $\epsilon^{-1/4}$ or $\epsilon^{-1/2}$, with allowance for impurity scattering.

TABLE XI

Computed fractional errors in the assumption that Q is the sum of the ideal Q_e and Q_p values which would occur in the absence of impurity scattering. Here $\delta \mid Q \mid = \mid Q \mid_{\text{true}} - \mid Q \mid_{\text{ideal}} = \delta \mid Q_e \mid + \delta \mid Q_p \mid$ and $\delta \mid Q_p \mid = \delta_w \mid Q_p \mid + \delta_1 \mid Q_p \mid$, where $\delta_w \mid Q_p \mid$ arises from the departure of $w_1 = m^*_\perp \langle \epsilon \tau_\parallel \rangle / m^*_\parallel \langle \epsilon \tau_\perp \rangle$ from its acoustic-scattering value, and $\delta_1 \mid Q_p \mid$ arises from the corresponding departures of the $\Pi_{p\parallel}^{(1)}$, $\Pi_{p\perp}^{(1)}$ defined by (20).

Sample	Estimated Abscissa for Figs. 8 & 9	T, °K	$\delta \mid Q_e \mid$, μv/deg.	$\delta_w \mid Q_p \mid$, μv/deg.	$\delta_1 \mid Q_p \mid$, μv/deg.	$\frac{\delta \mid Q \mid}{\mid Q \mid}$
606	0.91	60°	+5	$\leqq$+5	−25	$\approx$−0.005
	0.99	122°	0	0	0	0.000
603	0.93	77°	+3	$\leqq$+5	−4	$\leqq$+0.002
601	0.75	94°	+18	+16	−17	+0.010
596	0.56	87°	+38	+57	−30	+0.041

say, $\epsilon^{-0.4}$ at the three lower temperatures. Considering these variations and the random scatter of the points in Fig. 7, we can state as our best estimate that $\Pi_{p\parallel} \propto \epsilon^{-0.3 \pm 0.05}$ at low energies and that its energy dependence probably becomes more rapid at higher energies. There is no reliable evidence that the energy dependence of either component changes appreciably in the temperature range 60° to 131°K, although the accuracy of the determination of energy dependence is not very good for $\Pi_{p\parallel}$. The ratio $\Pi_{p\parallel}^{(1)}/\Pi_{p\perp}^{(1)}$ seems to be decreasing slightly with increasing temperature, although here again it is hard to be sure that the effect is real.

7.4 *Effect of Impurity Scattering on the Assumed Q*

As we have mentioned in Section V, all our thermomagnetic quantities were measured relative to the value of Q at $H = 0$, and the values originally tabulated for them were based on the value of Q characteristic of the observed carrier concentration and pure acoustic scattering. If impurity scattering causes the total Q to depart appreciably from this assumed value, these values will require correction. The results obtained in this section allow us to estimate how much effect impurity scattering has on Q_e and Q_p, and so to check this point.

According to Tahle IX, impurity scattering can affect Q_p in two ways: through changing the anisotropy $w(=w_1)$ of $\mathbf{m}^* \cdot \boldsymbol{\tau}^{-1}$, and through its effect on the moments $\Pi_{p\parallel}^{(1)}$, $\Pi_{p\perp}^{(1)}$. The effect on Q_e is, of course, simply obtained from the top curve of Fig. 8. Table XI shows some sample eval-

uations of the two kinds of effects on Q_p and of the effect on Q_e, computed from Figs. 8 and 9, the w's of Table X, and the assumptions $\Pi_{p\parallel} \propto \epsilon^{-0.30}$, $\Pi_{p\perp} \propto \epsilon^{-.08}$. It will be noted that the change in w largely compensates the changes in $\Pi_{p\parallel,\perp}{}^{(1)}$; this explains the previously puzzling lack of sensitivity of Q_p to impurity scattering. The fractional errors $\delta Q/Q$ in our assumed Q values are seen to be at most a fraction of a per cent for the purer specimens; this implies errors in the ordinate of Fig. 7 of rather less than a per cent. For Samples 601 and 596, however, at the temperatures shown, $\delta Q/Q$ is 1 per cent and 4 per cent, respectively, and $\delta\Pi/(\Pi^* - \Pi)$ is about twice as great.

7.5 *Confirmation of Impurity-Scattering Theory on Sample 601*

We have based our corrections for impurity scattering in the purer samples on plausible theoretical reasoning and on favorable though not ideally consistent evidence from isothermal electrical measurements. It is therefore of some interest to see if the thermomagnetic measurements on a sample with a sizable amount of impurity scattering differ from those on the pure samples, in the way in which we would predict on the basis of (23) and Figs. 8 to 10, assuming the energy dependences of $\Pi_{p\parallel}$ and $\Pi_{p\perp}$ which we inferred from Fig. 11.

Fig. 12 shows the comparison just mentioned for Sample 601 at 94°K. This sample was chosen for the comparison because good isothermal data were available for it and because it had about the maximum amount of impurity scattering for which the predictions of (23) are likely to be reliable. (For some of the other samples, the electrical and thermomagnetic data were at different temperatures, and for 596 at 87° the divergence between the full and dashed curves of Fig. 7 is beginning to be appreciable.) The dashed curves in Fig. 12 are the curves of Fig. 7, and represent the mean moments of the total $\Pi^* - \Pi_{\parallel,\perp}$ for the purer samples. The plotted points represent the empirical moments for Sample 601, computed from the data of Table VI in the same way as for the pure samples of Fig. 7. The small temperature-gradient correction just discussed is, of course, included in the corrections of Table VI. These points are to be compared with the full curves, which were constructed by computing the differences $\Pi_{\parallel,\perp}{}^{(n)}$ (601) $- \Pi_{\parallel,\perp}{}^{(n)}$ (ideal) theoretically and combining them with the dashed curves. The differences in question were computed by the following steps: (a) From (25), the observed μ_H of 601, the empirical w_1 and w_2 of Table X, and the assumed acoustic value μ_{Ha} (94°) = 28,200 cm^2/vs (probably good to within a few per cent), we computed the abscissa appropriate to Sample 601 in Figs. 8 to

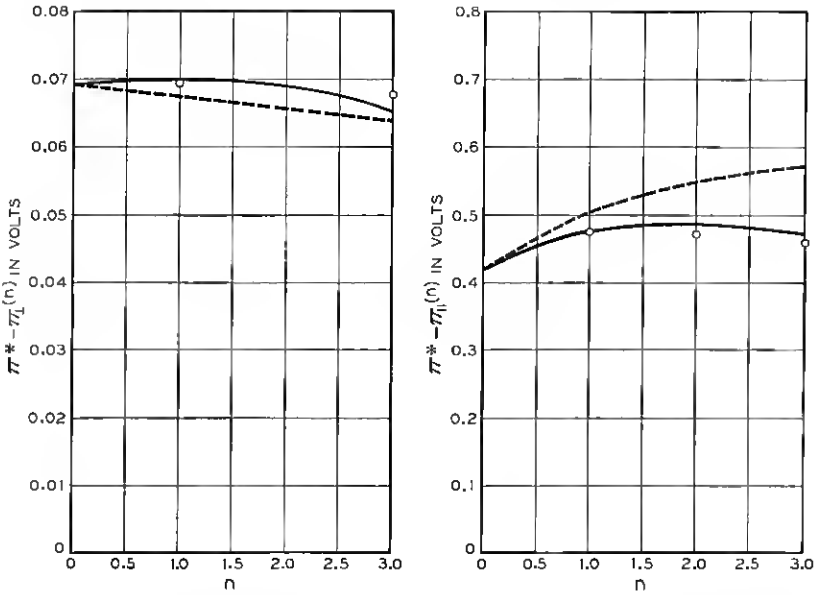

Fig. 12 — Comparison of the empirical moments $\Pi^* - \Pi_{\parallel,\perp}^{(n)}$ for Sample 601 (points) with those of the purer samples of Fig. 7 (dashed curves) at 94°K. The full curves are moments computed from the latter, with allowance for the amount of impurity scattering present for Sample 601.

10. (b) From these figures and the assumptions $\Pi_{p\parallel} \propto \epsilon^{-0.30}$, $\Pi_{p\perp} \propto \epsilon^{-0.08}$, the ratios of $\Pi_{p\parallel,\perp}^{(n)}$ (601) to $\Pi_{p\parallel,\perp}^{(n)}$ (ideal) were obtained. (c) The same ratios were obtained for the average of the pure specimens, assuming an abscissa of 0.97 in the figures. (This is larger than corresponds to the above μ_{Ha} and the mobilities measured on the unetched samples, but is more reasonable in the light of the 77° data and the effect of etching at that temperature.) (d) From steps (b) and (c) and the empirical $\Pi_{p\parallel,\perp}^{(n)}$ of Fig. 11 the $\Pi_{p\parallel,\perp}^{(n)}$ to be expected for Sample 601 were calculated. (e) The theoretical $\Pi^* - \Pi_e^{(n)}$ were calculated for Sample 601 from Figs. 8 and 10, and combined with the $\Pi_{p\parallel,\perp}^{(n)}$ just obtained.

It will be seen that, for $\Pi_\parallel^{(n)}$ especially, the empirical points fall much closer to the curve computed with allowance for impurity scattering than to the curve for the pure samples. Since the theoretical difference between the two curves is proportional to the rate of variation of $\Pi_\parallel$ with energy and to the departures of the ordinates of Figs. 8 to 10 from unity, the agreement is a significant bulwark for the analysis of this section. However, it is of more qualitative than quantitative significance, for the inputs to the calculation were numerous and some of them a little

uncertain. The discrepancy for $\Pi_{p\perp}^{(3)}$ may well be due to the great sensitivity of the $\Pi^* - \Pi_e^{(3)}$ curve of Fig. 10 to the abscissa chosen.

VIII. FURTHER OBSERVATIONS SUBSTANTIATING AND EXTENDING THE PRESENT MODEL

In this section we shall discuss several parts of our data which are not adapted to as precise an analysis as that of Sections VI and VII, but which can still be semiquantitatively explained and give indications of how well our conclusions can be extended to higher energies and higher temperatures.

8.1 *The High-Field Asymptote of BH*

So far, we have made no use of our observations of the Nernst coefficient at large magnetic fields. If the asymptotic high-field behavior were accurately known, it could provide a valuable extension of the moment analysis of Section VI. For, as (86) of Appendix B shows, this asymptotic behavior involves the moments (20) for $n = 0$ and -1, so that measurements in two orientations could be used to determine $\Pi_{\parallel}^{(-1)}$ and $\Pi_{\perp}^{(-1)}$. In practice, however, the accuracy of such a determination would be very questionable, as it would depend on the already rather uncertain zeroth moments and on accurate knowledge of the asymptotic BH, which, as we shall presently see, is rather uncertain for various experimental reasons. We have therefore chosen merely to compare the high-field behavior of BH with the asymptotic behavior predicted by the special-case formulas of Table II, with the object of showing that there is at least fair agreement with the model previously deduced.

As we have noted in Section V, the small value of the Nernst constant at high fields makes it very sensitive to falsification by the Hall fields of the longitudinal counter-currents which will be set up if surface conduction partially short-circuits the thermoelectric field; a surface conductance of a fraction of one per cent can be serious. We did not realize this soon enough to carry out extensive Nernst measurements on etched specimens. The lowest temperature at which such measurements were made was 94°K. At this temperature the difference between the behavior of Sample 606 etched and unetched was profound, the unetched having about twice the Nernst field of the etched at 18 kilogauss. At higher temperatures, the surface effect gets even worse, because the counter-currents are driven by the full Q, including the term proportional to the distance of the Fermi level below the band edge, whereas the Nernst effect arises only from Q_p and the small transport term in Q_e.

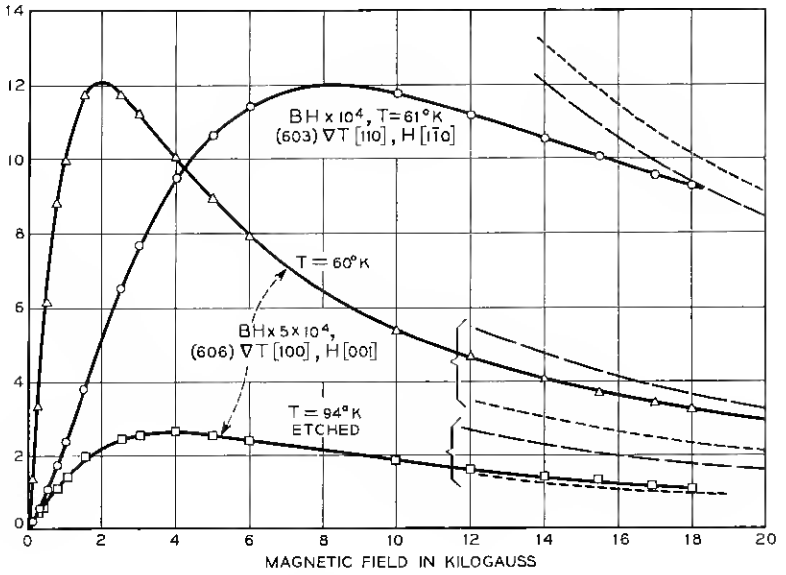

Fig. 13 — Comparison of the asymptotic behavior of the Nernst field constant, BH, at high fields with the predicted $(B_s + B_p)H$ of the simplified asymptotic formulas of Table II. The three experimental curves are for two samples of different orientations; note that the two scales are different. The short-dashed curves are computed from the formulas of Table III for Π_p independent of energy, the long-dashed curves for $\Pi_p \propto \epsilon^{-1/2}$. For both sets, the values $w = 0.061$, $p = 9.8$ were assumed. The unit of BH is volts/degree.

Fig. 13 shows a comparison of three observed curves of BH against H with the leading (H^{-1}) term in the asymptotic expression calculable from Table II. The data for Sample 606 at 94°K are the most reliable, since this sample has been etched; however, these data do not extend to as high a value of $\mu H/c$ as is obtainable at lower temperatures, so there may be some doubt as to how well they approach asymptotic behavior at 18 kilogauss. The data for Sample 606 at 60°, though on an unetched specimen, appear not to have been very seriously falsified by surface conduction, since they match the 94° data pretty well — as far as they go — if ordinates are scaled proportionally to Q_p and abscissas to μ, and if a little allowance is made for the electronic contribution. However, at the high-field end, the 60° data lie closer to the theoretical asymptote for $\Pi_p \propto \epsilon^{-\frac{1}{2}}$ than to that for Π_p independent of energy, whereas the reverse is the case for the 94° data; this may be due to a slight raising of the experimental curve by surface conduction.

The data for Sample 603 — with H in a [110] direction — show the

vastly slower saturation which is to be expected from the fact that, for this orientation, half the valleys have a very large cyclotron mass. Since the curves for the two samples are plotted on different scales, the values of BH at 18 kilogauss and 60°–61°K actually differ by a factor of 14 in the two orientations, roughly the factor predicted by the theory. As nearly as one can estimate from the range available, the experimental curve seems to be heading for an asymptote closer to that for Π_p independent of energy than to that for $\Pi_p \propto \epsilon^{-\frac{1}{2}}$ — perhaps even the other side of it. This is a slight discrepancy with theory which might again be due to the presence of a little surface conduction.

Thus, it appears that the qualitative features of the high-field Nernst curves are accounted for by the theory. The curves also give some information on the value of the anisotropy $p = \Pi_{p\parallel}/\Pi_{p\perp}$. Since the entries in the next to the last column of Table II are almost proportional to $(p - 1)$, it is probably safe to say that the present curves indicate a p within 20 per cent or so of the value derived in the last section. Regarding the variation of the weighted average of $\Pi_{p\parallel}$ and $\Pi_{p\perp}$ with energy, about all that can be said is that this variation again appears not to be as rapid a decrease as $\epsilon^{-\frac{1}{2}}$.

8.2 *Reversal of the Sign of B with H*

All our analysis so far has been based on data at temperatures in the range 60° to 131°K. No comparably accurate analysis can be made at higher temperatures, partly because the limits of the various quantities as $H \to \infty$ can no longer be determined, and partly because the value of Q_p is much less accurately known than in the lower range. What evidence there is, however, suggests that, at temperatures in the range 150° to 235°K, the anisotropy and energy dependence of Π_p are similar to those which we have found in the liquid-air range. This evidence is provided partly by the magnitudes of the low-field B and $\Delta Q/H^2$, which we shall discuss presently, and partly by an interesting reversal of the sign of B with increasing magnetic field. The latter effect occurs at temperatures at which the negative $B_e(0)$ and the positive $B_p(0)$ almost cancel each other. This cancellation occurs near 175°K, $B(0)$ being greater than zero below this temperature, less than zero above it[1] (although easily falsified by surface conduction). Fig. 14 shows some curves of B versus H at temperatures in this range, taken on etched samples. The data previously reported[1] on 606 and 604 unetched showed no region of negative $B(0)$, but now both show sign reversals at 171° to 174°. What we wish to discuss now, however, is the fact that, as H increases,

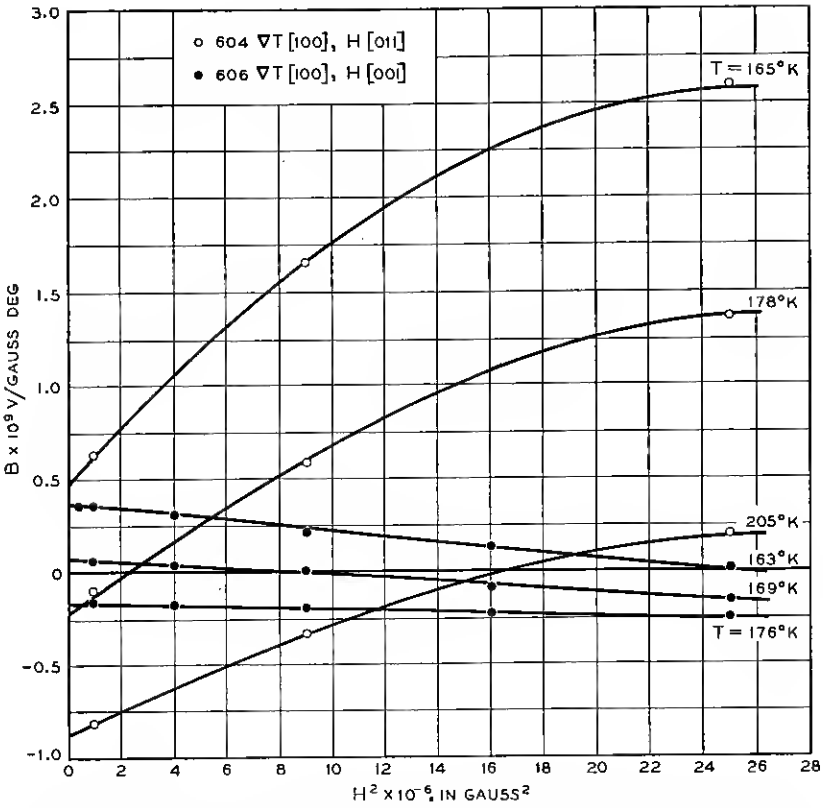

Fig. 14 — Variation of the Nernst coefficient B with magnetic field H, for two orientations, showing the sign reversal which takes place at temperatures near where B_e and B_p compensate each other. For comparison, the computed $B_e(178°)$ is -4.0×10^{-9}v/deg gauss.

the B of Sample 604 goes from negative to positive, and that of 606 from positive to negative.

Although we have not elaborated the theory of B at intermediate fields, it is doubtless safe to assume that, for all field strengths, $B_p > 0$ and $B_e < 0$. We can get a fair idea how the ratio of B_p to B_e varies with H by comparing the low- and high-field limits of $| B_p/B_e |$ as given by the formulas of Tables I and II. Table XII gives the comparison, for several sets of assumptions about the anisotropy and energy dependence of $\mathbf{\Pi}_p$. We have constructed schematic curves of B_e and B_p against H, shown in Fig. 15, from this information and the knowledge[1] that B_p decreases monotonically with H for $\mathbf{H} \parallel [001]$, while it has an initial

TABLE XII

Comparison of high- and low-field ratios of B_p (positive) to B_e (negative), for several orientations and for different assumptions regarding the anisotropy $p = \Pi_{p\parallel}/\Pi_{p\perp}$ and the dependence of Π_p on energy ϵ. The numerical values given are for $w = m^*_{\perp}\tau_{\parallel}/m^*\tau_{\parallel\perp} = 0.06$.

Direction of		Ratio of $\left\lvert \frac{B_p(\infty)}{B_e(\infty)} \right\rvert$ to $\left\lvert \frac{B_p(0)}{B_e(0)} \right\rvert$, for			
H	∇T	Π_p independent of ϵ, any p	$\Pi_p \propto \epsilon^{-1/2}$		
			$p = 5$	$p = 10$	$p = 20$
[001]	$\perp$ H	1	0.45	0.50	0.54
[011]	[100]	$\frac{1 + 2w}{3w} = 6.2$	1.46	2.06	2.58
[011]	[01$\bar{1}$]	$\frac{(2 + w)(1 + 2w^2)}{3w(1 + 7w + w^2)} = 8.1$	2.27	3.31	4.17

rise for **H** $\parallel$ [011], if $p = \Pi_{p\parallel}/\Pi_{p\perp}$ is large. From these curves it is clear that, if the anisotropy and energy dependence of $\mathbf{\Pi}_p$ are similar at the temperatures of Fig. 14 to what we found in Fig. 11, then B should become more negative with increasing H for Sample 606, more positive for 604. This is exactly what is observed.

Only the crudest sort of quantitative limits can be derived, from this comparison, for p and the rate of variation of $\mathbf{\Pi}_p$ with energy. From an inspection of Table XII, Fig. 15 and the curves of Fig. 9 of Ref. 1, it seems clear that the sizes of the shifts of B with field in Fig. 14 are eminently consistent with the previously found anisotropy and energy dependence, and that they would be hard to reconcile with a $\mathbf{\Pi}_p$ that increased with increasing energy, or with a p close to unity. Specifically, Table XII suggests that the theoretical curve for 606 is nearly independent of p, so that the downward slopes in Fig. 14 must arise from an inverse energy dependence of $\mathbf{\Pi}_p$. The swing in B between zero and 5000 gauss is of the order of a twentieth of $\lvert B_e(0) \rvert$; this would not be unreasonable for $\mathbf{\Pi}_p \propto \epsilon^{-\frac{1}{2}}$. The swing for 603, on the other hand, is probably due to the fact that B_p rises with H while B_e falls; if so, it should be of the order of one or two times the rise in B_p, a rise due mainly to the anisotropy of $\Pi_p (p \gg 1)$. For the observed anisotropy at liquid-air temperature ($p \approx 10$) this rise (see Fig. 9 of Ref. 1), at the $\mu_H H/c$ corresponding to 5000 gauss at 178°, is perhaps 15 per cent of $B_p(0)$. The observed swing is about twice this.

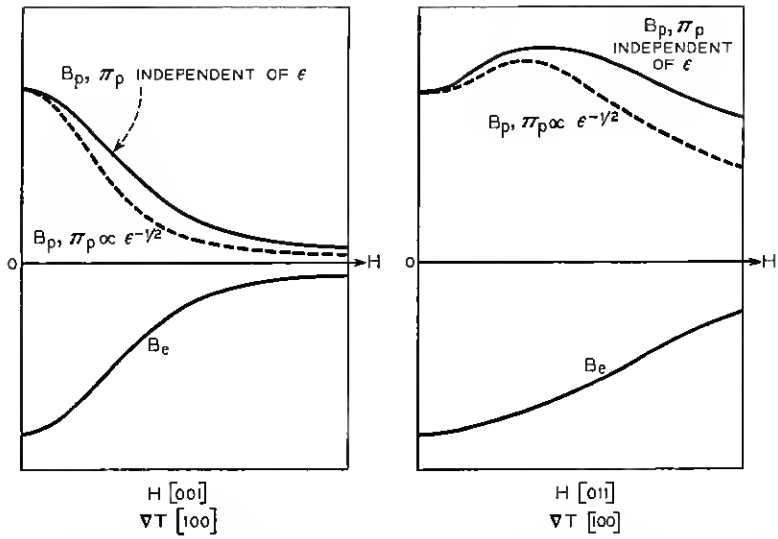

Fig. 15 — Schematic variation of B_e and B_p with magnetic field, for two orientations, assuming the temperature such that $B_e(0) = -B_p(0)$. Two B_p curves are shown for each case, corresponding to $\Pi_p \propto \epsilon^0$ and $\epsilon^{-1/2}$, respectively. It is assumed that $\Pi_{p\parallel}/\Pi_{p\perp} \gg 1$.

8.3 *Analysis of High-Temperature Data*

The sort of moment analysis which we made in Figs. 7 and 11 gets increasingly difficult as T increases, for several reasons: high-field limits become unavailable; the phonon-drag effects become a much smaller part of the total; because of this, it is easier for such things as surface inversion layers to falsify measurements of bulk thermomagnetic effects. We shall nevertheless try to draw what inferences we can from the temperature at which $B(0)$ changes sign, and from the totality of measurements on Sample 601 at 234°K, a sample pure enough to be fairly free of impurity scattering at this temperature, yet sufficiently highly conducting to be insensitive to surface conduction.

As Fig. 14 shows, $B(0)$ reverses sign in the pure, etched specimens at 174°K (603) or 172°K (606). From the average of these and interpolations of the Q_p values of Table VI we can deduce a value for the ζ_p of (13). With the acoustic-scattering value of B_e, we obtain $\zeta_p = 0.226$, a value close to the average ζ_p of 0.229 found for the pure specimens at 77°K, corrected for the effect of impurity scattering on B_e. This suggests either that the anisotropy and energy variation of $\mathbf{\Pi}_p$ are very similar at 173° and 77° or that the difference in anisotropy just happens to be such as to compensate for the difference in energy dependence. The 131°

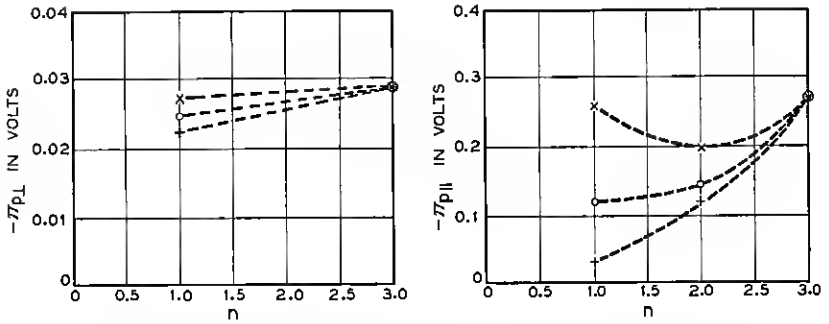

Fig. 16 — Results of an attempt to determine empirically the moments $\Pi_{p\parallel,\perp}^{(n)}$ defined by (20) for Sample 601 at 234°K. The points ○, + and × correspond respectively to three choices of the assumed $\Pi_{p\perp}^{(1)}$; it will be seen that the ○ choice gives the most nearly plausible behavior for $\Pi_{p\parallel}^{(n)}$.

data of Fig. 11 suggested a possible decrease of the anisotropy with increasing temperature, and a possible increase in the rapidity of variation of $\Pi_{p\parallel}$ with energy. These factors would affect ζ_p in opposite ways, so they could cancel.

We have attempted a moment analysis like that of Sections VI and VII for Sample 601 at 234°K. We adopted the plausible anisotropy $w_1 = w_2 = w_3 = 0.056$, (see Table X and the discussion of Section VI, especially the remarks about change of w with temperature). This is a value which happens to fit the anisotropy of the magnetoresistance. The data give $\Pi^* - \Pi_\perp^{(3)} = 0.0507$ volt, $\Pi^* - \Pi_\parallel^{(3)} = 0.298$ volt. The only additional knowledge obtainable, however, is one relation between $\Pi_\parallel^{(1)}$ and $\Pi_\perp^{(1)}$ (to fit Q) and one relation between $\Pi_\parallel^{(2)}$ and $\Pi_\perp^{(2)}$ (to fit B). If, as before, we assume $\Pi_\perp^{(n)}$ to be linear in n, we can adjust $\Pi_\perp^{(1)}$ until the curve of $\Pi_\parallel^{(n)}$ against n is reasonably smooth. Fig. 16 shows the results for $\Pi_{p\parallel,\perp}^{(n)}$ after subtracting off the values of $\Pi^* - \Pi_e^{(n)}$, slightly corrected for impurity scattering. Several choices of $\Pi_{p\perp}^{(1)}$ have been made, and their consequences are shown in the figure. There are strong suggestions that $\Pi_{p\parallel}^{(1)}/\Pi_{p\perp}^{(1)}$ is still smaller than at 131°K, that $\Pi_{p\parallel}$ varies more rapidly with energy than at 77° and that $\Pi_{p\perp}$ continues to vary slowly. However, the data are so limited that only the last of these points can be considered reasonably established.

IX. SUMMARY AND IMPLICATIONS OF THE RESULTS

9.1 *Evidence on* $\Pi_{p\parallel}(\epsilon)$ *and* $\Pi_{p\perp}(\epsilon)$

We have concluded that, near liquid-air temperature, the dependence of the phonon-drag Peltier tensor of an energy shell on the energy ϵ of

the shell is given, at least roughly, by $\Pi_{p\parallel}(\epsilon) \propto \epsilon^{-0.3}$, $\Pi_{p\perp}(\epsilon) \propto \epsilon^{-0.08}$, while the first-moment ratio $\langle \epsilon^{\frac{1}{2}}\Pi_{p\parallel}\rangle/\langle \epsilon^{\frac{1}{2}}\Pi_{p\perp}\rangle$ is about 9.6. These conclusions were based primarily on the analysis of high- and low-field ΔQ data and low-field Nernst data on the several purest samples, with auxiliary use of mobility and magnetoresistance data. The use made of the low-field data depended to some extent on corrections for impurity scattering, the method of making the corrections having been roughly checked both against purely electrical measurements and against alternative theoretical assumptions. The data for Sample 601, which showed a sizable effect of impurity scattering, were consistent with the assumed characteristics of $\mathbf{\Pi}_p(\epsilon)$ combined with the assumed impurity-scattering law. The conclusions regarding $\Pi_{p\perp}(\epsilon)$ were very insensitive to the more uncertain of the inputs and were consistent from sample to sample and from one temperature to another. Those regarding $\Pi_{p\parallel}(\epsilon)$ were more sensitive and showed more fluctuation, but always showed roughly the same behavior. High-field Nernst data, though less suited to accurate analysis, independently indicated the ratio of $\Pi_{p\parallel}$ to $\Pi_{p\perp}$ to be of the order of 10, and also indicated a decrease of the weighted average of these quantities with ϵ, slower than $\epsilon^{-\frac{1}{2}}$.

The high-field limit of the transverse ΔQ's gave strong but not entirely certain indications that the decrease of $\Pi_{p\parallel}$ with increasing energy becomes more rapid than the above-mentioned $\epsilon^{-0.3}$ at high energies. The variation of the anisotropy and energy dependence of $\mathbf{\Pi}_p$ with temperature was too small to be detected over the range 60° to 94°K. However, we found some rather uncertain indications that $\Pi_{p\parallel}/\Pi_{p\perp}$ decreases slowly with increasing T, and that the energy dependence of $\Pi_{p\parallel}$ becomes steeper. These conclusions came from a comparison of 131° thermomagnetic data with data at lower temperatures, and from studies of low-field thermomagnetic data at 234°. The low- and intermediate-field behavior of the Nernst coefficient near 175°K was found to be consistent with the anisotropy and energy dependences found from the previous sources, but did not suffice to check the temperature variation of these two factors individually. The data at all temperatures are clearly inconsistent with a law $\Pi_{p\parallel} \propto \epsilon^{\frac{1}{2}}$, such as would result (see below) if the relaxation times of the phonons were independent of frequency.

9.2 *Implications for Phonon-Phonon Scattering*

The energy dependence of $\mathbf{\Pi}_p(\epsilon)$ reflects the dependence of the relaxation times τ_{ph} of the different phonon modes on their frequency ω. For example, if all branches of the phonon spectrum had

$$\tau_{ph} = \omega^t \times (\text{function of direction}), \tag{27}$$

then, since the wave numbers, or frequencies, of the modes coupled to electrons of energy ϵ scale proportionally to $\epsilon^{\frac{1}{2}}$, we would have, as ϵ varies

$$\begin{aligned} \Pi_p &\propto \tau^{-1} \times (\text{a mean } \tau_{ph}) \\ &\propto \epsilon^{\frac{1}{2}+\frac{1}{2}t}. \end{aligned} \tag{28}$$

If the longitudinal and transverse branches were to obey (27) individually, but with different exponents t_l and t_t, then the effective energy exponents for $\Pi_{p\parallel}$ and $\Pi_{p\perp}$ would be intermediate between $\frac{1}{2} + \frac{1}{2}t_l$ and $\frac{1}{2} + \frac{1}{2}t_t$, and the exponents would in general be different for $\Pi_{p\parallel}$ and $\Pi_{p\perp}$.

Our liquid-air-temperature result is thus that the phonons interacting with a current parallel to the valley axis have an average relaxation time $\tau_{ph} \propto \omega^{-1.6}$, while those interacting with a current in the perpendicular direction have an average $\tau_{ph} \propto \omega^{-1.15}$. These are to be compared with the "ideal" phonon-phonon scattering laws[2,32]

$$\text{longitudinal branch:} \quad \tau_{ph} \propto \omega^{-2}, \tag{29}$$

$$\text{transverse branch:} \quad \tau_{ph} \propto \omega^{-1}, \tag{30}$$

valid if $\omega \ll$ the frequency of the average thermal phonon and if only three-phonon noncollinear collisions contribute to the relaxation of the modes concerned. Estimates[32] of the frequency at which appreciable departures from (29) or (30) set in have suggested that, for germanium at liquid-air temperature, these laws should be approximately obeyed, but that departures from them may well be appreciable. As it can be shown that τ_{ph} goes as a higher power of ω when ω gets large, it seems likely that the finiteness of ω will lead to higher, rather than lower, negative exponents. Thus, at present a more plausible explanation of the observed exponents is that the longitudinal and transverse branches contribute comparably to the phonon-drag phenomenon. Since it is known[3] that the longitudinal and transverse branches contribute comparable amounts to the scattering of the electrons, this would require that, in the frequency range most important for the scattering of electrons, the relaxation times of the transverse modes be comparable with or rather larger than those of the longitudinal modes. This is contrary to what one would anticipate from (29) and (30), but cannot yet be considered unreasonable, in view of our present ignorance about scattering matrix elements, etc.

There are two further possibilities which would lead to departures from the asymptotic laws (29) and (30). One of these is three-phonon collisions in which the three phonons belong to the same branch and have

almost collinear wave vectors. If such collisions are possible, they will change (29) into the same form as (30). For this to occur for a low-frequency longitudinal mode, it is necessary that some higher-frequency mode with the same direction of propagation have a higher group velocity than a mode of infinitesimal frequency.[32] This could happen, for example, if the curve of frequency against wave number in the longitudinal branch curved upward instead of downward. Although this does not seem impossible *a priori*, no real crystal or mathematical model has to our knowledge been found with this property. Moreover, by now our knowledge of the elastic spectrum of germanium[33] is good enough to make it fairly certain that this does not occur for the present material.

More intriguing is the possibility of higher-order processes, i.e., collisions involving four or more phonons,[34] or possibly even processes more appropriately describable as relaxation effects.[35] From the standpoint of collision theory, a calculation of, say, three-phonon collisions becomes invalid when the frequeucy of one of the modes involved becomes less than the natural widths τ_{ph}^{-1} of the other modes, or when the failure of energy conservation in an "energetically impossible" process gets less than some relevant $\hbar\tau_{ph}^{-1}$. Moreover, even when neither of these catastrophies occurs, and the three-phonon process that is being considered is perfectly meaningful, it may happen that the number of such possible three-phonon processes is so small that the relaxation of the low-frequency mode involved occurs predominantly by higher-order processes.

However, the rates of four-phonon processes vary much more rapidly with temperature than do those of three-phonon processes.[34] At the frequencies of the phonon-drag modes, which are high compared to the reciprocal thermal relaxation time of the majority modes, relaxation can be described as due to some, though not all, of the collisions involving four or more protons. Since the temperature dependence of Q_p in the range 60° to 90°K is not far from that to be expected for three-phonon processes,[2] we must conclude that higher-order processes are at most a small correction in this range. But if they are at all appreciable at one temperature, they must become completely dominant at a higher temperature. The changeover from dominance of three-phonon processes to dominance of higher-order processes would almost certainly change the anisotropy or the energy dependence of $\mathbf{\Pi}_p(\epsilon)$. In particular, if the relaxation time of the phonon-drag modes became independent of frequency — as it would for the simplest type of higher-order processes — $\mathbf{\Pi}_p$ would go as $\epsilon^{\frac{1}{2}}$, in violent disagreement with our observations at all temperatures. The absence of any abrupt change of the energy dependence or anisotropy of $\mathbf{\Pi}_p$ with temperature thus shows that, for the phonon-drag

modes, three-phonon processes are more important than higher-order processes, up to at least 234°K, and that over most of this range the dominance of the former must be extreme.

It is not possible to follow the phonon-phonon scattering to temperatures much below 60°K without a theory that takes account of boundary scattering, an effect which spoils the crystalline symmetry of the problem. In fact, some of the apparent changes which Fig. 11 shows in the behavior of $\Pi_{p\parallel}$ at 60° may well be due to the fact that boundary scattering is beginning to be too large to he corrected for by the crude method of Section V.

9.3 *Transport Theory and Deformation-Potential Theory*

Although the study of the purely electrical properties of n-type germanium was only an incidental feature of the present work, our results have led to a number of new conclusions in this field, which we shall summarize here.

To begin with, we have found considerable evidence (presented in Appendix A and summarized in Section II) that in a magnetic field one need not abandon conventional transport theory in crystal-momentum space in favor of a quantum treatment until the cyclotron spacing $\hbar\omega_c$ has become close to kT. Specifically, we found that, at $\hbar\omega_c/kT \approx \frac{1}{3}$ and for acoustic scattering, the longitudinal and transverse resistivities are correctly given by conventional theory to within 5 per cent or so, and in most cases probably rather closer than this. Even at $\hbar\omega_c/kT \approx 1$ our ΔQ evidence suggests, again for predominantly acoustic scattering, that the errors may be only of the order of 10 per cent or so.

We have found the magnetoresistance and Hall data at high and low magnetic fields to be fairly consistent with the predictions of the electron-group theory, i.e., with the picture which approximates the effect of the scattering processes by relaxation times $\tau_\parallel(\epsilon)$ and $\tau_\perp(\epsilon)$. For the most accurately measured cases (etched samples at 77.4°K), the accuracy of the fit can be described as follows: The single parameter $w_1 = m_\perp{}^*\langle\epsilon\tau_\parallel\rangle / m_\parallel{}^*\langle\epsilon\tau_\perp\rangle$ can be chosen to reproduce the longitudinal high-field magnetoresistance limits $\rho(\infty)/\rho(0)$ for the four purest samples in [100], [110] and [111] orientations to within the reproducibility of measurements from sample to sample (2 per cent or so). The values of $\rho(\infty)/\rho(0)$ for three transverse orientations also agree with predictions based on this anisotropy and the assumption $\tau_{\parallel,\perp} \propto \epsilon^{-\frac{1}{2}}$, to within a somewhat larger uncertainty (worst discrepancy 13 per cent), due in part to surface conduction, etc., and in part to quantization. The low-field magneto-

resistance constants obey the symmetry relation characteristic of the electron-group approximation (the relations at the bottom of Table IV with $\Delta\rho$ substituted for ΔQ_p) about as accurately as they obey the requirements of macroscopic symmetry (consistency to a few per cent).

Concerning the energy dependence of $\tau_\parallel$ and $\tau_\perp$, the most accurate evidence we have is that from the ratio of low- to high-field Hall constant, i.e., the ratio of Hall to drift mobility. As was shown in Section VII and Fig. 8, this ratio, when measured on etched samples, gets closer and closer to the value predicted for $\tau_{\parallel,\perp} \propto \epsilon^{-\frac{1}{2}}$ as the importance of impurity scattering is reduced. We were able to conclude that only a very small amount of optical-mode or intervalley scattering, or of any other departure from the law $\tau_{\parallel,\perp} \propto \epsilon^{-\frac{1}{2}}$, can be present at temperatures in the range 77° to 131°K.

In the calculation of the absolute value of the acoustic mobility, μ_a, of n-type germanium from deformation-potential theory,[3] two deformation-potential constants are required. One of these can be obtained with some accuracy from piezoresistance measurements, and the other can be inferred if magnetoresistance or other data give a reliable value of the acoustic-scattering anisotropy $\tau_\parallel/\tau_\perp$. Our present measurements have yielded much better values, both for μ_a and for $w = m_\perp{}^*\tau_\parallel/m_\parallel{}^*\tau_\perp$, than were available when Ref. 3 was written, so it is of interest to see how well the deformation-potential calculation of μ_a now works out.

The first step is to obtain $\tau_\parallel/\tau_\perp$ from the cyclotron masses[36] $m_\perp{}^* = 0.082m$, $m_\parallel{}^* = 1.58m$ (assumed for the moment to be valid near liquid-air temperature) and the high-purity limit $w = 0.061_0$, presumably characteristic of acoustic scattering. The result is $\tau_\parallel/\tau_\perp = 1.18$. From this and Equations (52) and (53) or Fig. 5 of Ref. 3 (also based on the masses mentioned), we get the value -0.40 for the ratio Ξ_d/Ξ_u of the deformation-potential constant for stretch along a direction normal to the valley axis to that for the combination of a compression along such a direction with an equal stretch along the valley axis. From this value of Ξ_d/Ξ_u and the piezoresistance constant[3,37]

$$m_{44}{}^{(P)} = \frac{1}{3}\frac{\Xi_u}{kT}\frac{w-1}{w+2} = 30{,}400/T \tag{31}$$

we obtain Ξ_d, Ξ_u, and thence the acoustic mobility. The value predicted in this way for 77.4°K is

$$\mu_a\ (77.4°) = 45{,}100\ \text{cm}^2/\text{vs}. \tag{32}$$

The empirical value is obtained by dividing the ideal value $\mu_{Ha}/\mu_a = 0.933$ into the observed Hall mobility, after correction for impurity

scattering by the estimates described in Section VII. With the value 38,600 cm^2/vs there adopted for μ_{Ha} (see Fig. 8), we get

$$\mu_a\ (77.4°) = 41{,}400\ cm^2/vs. \tag{33}$$

The agreement between (32) and (33) is gratifying. Although the 8 or 9 per cent discrepancy between them is larger than the uncertainty in either due to uncertainties in the experimental inputs (perhaps 2 or 3 per cent), it is of the right sort to be attributable to departures of the masses or deformation-potential constants at 77° from the low-temperature values we have assumed; moreover, the inherent inaccuracy of the deformation-potential method could conceivably be of this same order. As regards the former point, we may notice that the difference between mobilities varying as $T^{-1.50}$ and as $T^{-1.65}$ amounts to 8 per cent between 46° and 77°K. If the latter variation, which we found to be closer to the truth over the range 60° to 94°K, were due to something like a temperature variation of the masses which disappeared below 40° or so, the discrepancy would be eliminated.

Regarding impurity scattering, finally, we have found in Section VII that it is possible to correlate with each other the effects of ionized-impurity scattering on mobility, Hall-to-drift-mobility ratio, magnetoresistance, etc. — at least in the range where impurity scattering is small to moderate. In this correlation the anisotropy of the impurity scattering was treated as an empirical parameter; beyond this, no specific assumption was necessary about the mechanism of impurity scattering, except that it affected low-energy carriers much more than high-energy ones. The correlations we were able to make in Fig. 8 and Fig. 12 seem to be quantitatively significant, but still leave something to be desired.

All these items deserve more careful study. Our Table XV (Appendix B), incidentally, which gives Maxwellian averages of powers of the energy, may prove handy for various types of calculations.

9.4 *Surface Effects*

We have encountered serious effects of surface conduction in a number of places in the present study. Our experience justifies the statement that, at all temperatures, one must eliminate or allow for surface effects before one can get really accurate measurements of any bulk electrical property of high-purity material. For some properties, even the qualitative behavior can be completely falsified by surface effects. Specifically, we have found that a surface contribution of less than one per cent to the conductance can greatly affect the apparent high-field transverse magneto-

resistance and the high-field Nernst coefficient near liquid-air temperature and below, and that it can change the sign of the low-field Nernst coefficient in the range 175° to 250°K. Near liquid-air temperature, changes in surface treatment can alter the apparent conductivity and Hall coefficient by amounts ranging up to several per cent.

X. ACKNOWLEDGMENTS

We are indebted to G. W. Hull for his skill in preparing the samples and in mounting them in the various pieces of apparatus used. A large amount of careful observation was required in order to obtain the data presented here. Much of this work was entrusted to J. J. Byrnes, G. W. Hull and P. A. Liberti, and we are indebted to them for their most helpful and sustained efforts. R. G. Treuting and J. N. Hobstetter provided us with a useful program that enabled much of the data to be processed on the I.B.M. 704 computer. Thanks are also due T. T. Wu for discussions of current flow near side-arms.

APPENDIX A. ORBITAL QUANTIZATION

We give here the reasoning behind a number of statements which one can make, including those made in the text. We shall take up first some quantitative statements about the relation of the magnetoresistance of a multivalley semiconductor to that of the simple model assumed in the existing theoretical literature (items 2 and 3 below). Next we shall present empirical and theoretical evidence on the smallness of the effect of quantization on longitudinal magnetoresistance (item 4). Finally, in items 5, 6 and 7, we shall discuss the relation of the effect of quantization on ΔQ to that on magnetoresistance, and shall present evidence that these effects are fairly small even for transverse orientations. As the basis of the whole treatment we shall take the fairly obvious statement:

1. *For the region* $\mu H/c \gg 1$, *the orbital-quantization correction functions for* $\rho(\mathbf{H})/\rho(0)$ *and* $Q_p(\mathbf{H})/Q_p(0)$ *are practically the same functions of* H *as they would be if the electron-phonon coupling were allowed to approach zero.*

In other words, the difference between the true $\rho(\mathbf{H})/\rho(0)$ or $Q_p(\mathbf{H})/Q_p(0)$ and the value calculated without quantization is a function of the cyclotron spacing $\hbar\omega_c$ (primarily of $\hbar\omega_c/kT$), which depends, of course, on the anisotropy of the electron-phonon interaction, but which depends on the magnitude of the latter (i.e., on $\mu H/c$) in such a way as to approach a limit uniformly as the scattering goes to zero ($\mu H/c \to \infty$). This is, of course, what one expects intuitively; it follows from any trans-

port theory in which $\rho(0)$, $\rho(H)$, etc. are representable by expansions in powers of the strength of the scattering.

We shall show first that, if the scattering processes are energy-conserving collisions with a squared matrix element that is the same for all transitions within a valley, the following statement holds:

2. *In the approximation of isotropic scattering over an energy shell (i.e.,* $\tau_\parallel = \tau_\perp$*), the longitudinal magnetoresistance ratio* $\rho(\mathbf{H})/\rho(0)$ *for any multivalley case equals the product of the value calculated in the absence of quantization by a weighted average of the values calculated for isotropic* m^**'s equal to the cyclotron masses of the various valleys for the given direction of* $\mathbf{H}$*, provided* $\mu H/c \gg$ *a value which for germanium is of the order of a fraction of* $m_\parallel^*/m_\perp^*$.

Thus, for longitudinal magnetoresistance, the orbital-quantization correction can be deduced from the simple-model calculations in the literature.[5,6,7,8]

For the proof we note first that when $\mathbf{E} \parallel \mathbf{H}$ in, say, the z direction, $\rho_{zz} = 1/\sigma_{zz}$; this is exact for all $\mathbf{H}$ in symmetry directions, and asymptotically exact as $H \to \infty$ in any direction. Therefore we need consider only σ_{zz} , which is a sum of contributions $\sigma_{zz}^{(i)}$ from the different valleys i. For any such valley we can reduce the transport problem to that for the simple model by means of a transformation which projects the energy surfaces into spheres.[3] In considering this transformation we must remember that it is not an orthogonal one, and that it therefore carries with it a need to distinguish between covariant and contravariant vectors. For covariant vectors, $\mathbf{F}$, the transformed vector, $\bar{\mathbf{F}}$, is related to the original vector $\mathbf{F}$ by

$$\bar{\mathbf{F}}_\parallel = r^{\frac{1}{2}}\mathbf{F}_\parallel , \qquad \bar{\mathbf{F}}_\perp = \mathbf{F}_\perp , \tag{34}$$

where $\parallel$ and $\perp$ refer to the valley axis and $r = m_\perp^*/m_\parallel^*$. For contravariant vectors $\mathbf{G}$ the relation is

$$\bar{\mathbf{G}}_\parallel = r^{-\frac{1}{2}}\mathbf{G}_\parallel , \qquad \bar{\mathbf{G}}_\perp = \mathbf{G}. \tag{35}$$

The scalar product of a covariant and a contravariant vector is unchanged by the transformation. It is easily verified that, if we regard $\mathbf{E}$, the crystal momentum $\mathbf{P}$, and the vector-potential $\mathbf{A}$ as covariant vectors, while regarding velocity (or $\mathbf{j}$) and $\mathbf{H}$ as contravariant vectors, all the usual relations involved in the Schrödinger equation and the transport equation are the same for the transformed and original vectors, except that in the transformed space the effective-mass tensor becomes isotropic.

Now let $\bar{\sigma}_l(\bar{\mathbf{H}})$ be the conductivity in the transformed system when

$\bar{\mathbf{E}} \parallel \bar{\mathbf{H}}$, and $\bar{\sigma}_t(\bar{H})$ be that for $\bar{\mathbf{E}} \perp \bar{\mathbf{H}}$. These conductivities will be independent of the orientation of $\bar{\mathbf{H}}$ or of the azimuth of $\bar{\mathbf{E}}$ about $\bar{\mathbf{H}}$, if the scattering for $H = 0$ is isotropic over each energy shell, as is known to be very nearly the case for acoustic scattering in n-type germanium, and if at the same time any effects associated with finiteness of phonon energies are also isotropic. Since it is known that the latter effects are important for incipient quantization effects in longitudinal magnetoresistance,[8] this last assumption deserves further investigation; however, we shall make it and proceed. Then, for the conductivity along H of all the valleys i in parallel, we have

$$\sigma_{zz}(\mathbf{H}) = \sum_i [\lambda_l^{(i)} \bar{\sigma}_l(\bar{H}^{(i)}) + \lambda_t^{(i)} \bar{\sigma}_t(\bar{H}^{(i)})], \tag{36}$$

where the coefficients $\lambda_l^{(i)}$, $\lambda_t^{(i)}$ depend only on the orientation of $\mathbf{H}$ with respect to the axis of valley i. Therefore, since $\bar{\sigma}_l = \bar{\sigma}_t = \bar{\sigma}_0$ at $\mathbf{H} = 0$,

$$\frac{\sigma_{zz}(\mathbf{H})}{\sigma(0)} = \sum_i \left[\frac{\sigma_l(\bar{H}^{(i)})}{\bar{\sigma}_0} \frac{\lambda_l^{(i)}}{\sum_i (\lambda_l^{(i)} + \lambda_t^{(i)})} + \frac{\bar{\sigma}_t(\bar{H}^{(i)})}{\bar{\sigma}_0} \frac{\lambda_t^{(i)}}{\sum_i (\lambda_l^{(i)} + \lambda_t^{(i)})} \right]. \tag{37}$$

Now, in the absence of quantization, $\bar{\sigma}_t$ is of order $\bar{H}^{-2}$ or less as $\bar{H} \to \infty$, while $\bar{\sigma}_l$ remains finite; when quantization is just starting to be important and $\mu H/c \gg 1$, $\bar{\sigma}_t$ will still be $\ll \bar{\sigma}_l$. Under our assumptions, the dependence of both these quantities on $\bar{H}$ is given by the theory for the simple model with isotropic effective mass. If we keep only the first term of (37), we have the result italicized above. For some orientations, however, the coefficient involving λ's in the second term of (37) is larger than that in the first term by a factor of the order of a fraction of $m_\parallel^*/m_\perp^*$. This explains the qualification in the statement of the theorem.

3. *In the approximation of isotropic scattering over an energy shell (i.e., $\tau_\parallel = \tau_\perp$), any contribution to the transverse magnetoresistance ratio $\rho(\mathbf{H})/\rho(0)$ which goes as H^2 must for a cubic crystal be independent of the orientations of* $\mathbf{E}$ *and* $\mathbf{H}$, *in the range $\mu H/c \gg 1$, and any contribution which goes as H has only the modest orientation dependence shown in Table XIII.*

We interpret our assumption in the same way as for item 2 above, and with the same degree of risk. The proof is again quite simple if we use the transformations (34) and (35). Since $\mathbf{E}$ is covariant, $\mathbf{H}$ contravariant, $\mathbf{E} \cdot \mathbf{H} = 0$ implies $\bar{\mathbf{E}} \cdot \bar{\mathbf{H}} = 0$ in every valley. When $\mu H/c \gg 1$,

TABLE XIII

Orientation dependence of a hypothetical orbital-quantization term in the transverse magnetoresistance which is proportional to H. The value $r = m^*_\perp/m^*_\parallel = 0.052$ has been assumed.

Direction of		Value of (40) = relative value of b in $\rho(H)/\rho(0) = a + bH$
H	**j**	
[001]	$\perp$**H**	1.03
[011]	[100]	1.74
[011]	[01$\bar{1}$]	1.28

$E \sim RHj$, and so, with **j** along x and **H** along z,

$$\rho_{xx}(H) = j^{-2}\sigma_{yy}E^2 = R^2H^2\sigma_{yy} = R^2H^2\sum_i \frac{\bar{\sigma}_i(\bar{H}^{(i)})\bar{E}^{(i)2}}{E^2}, \qquad (38)$$

where, as before, $\bar{\sigma}_i(\bar{H})$ is the conductivity of the simple-model spherical-ized valley transverse to a magnetic field $\bar{\mathbf{H}}$, and the summation is over the different valleys. In the absence of orbital quantization, $\bar{\sigma}_i$ would go as $\bar{H}^{-2}$, and so (38) would be independent of the magnitude of H. A term in ρ_{xx} going as H^2 can arise only from a term in $\bar{\sigma}_i$ independent of $\bar{H}$. If $\delta\bar{\sigma}_i$ is such a term, the corresponding increment in ρ_{xx} is

$$\delta\rho_{xx}(\mathbf{H}) = R^2H^2\delta\bar{\sigma}_i\sum_i \frac{\bar{E}^{(i)2}}{E^2}. \qquad (39)$$

But the summation is a quadratic function of the components of **E** with the symmetry of the crystal, hence it is isotropic for any cubic case. This proves the first statement. A term in ρ_{xx} going as H must come from a term in $\bar{\sigma}_i$ going as $\bar{H}^{-1}$, so the relative magnitudes of this term in various orientations must be proportional to the values of the quantity

$$\sum_i \left(\frac{H}{\bar{H}^{(i)}}\right)\left(\frac{\bar{E}^{(i)}}{E}\right)^2. \qquad (40)$$

These values are shown in Table XIII.

4. *Theory and experiment agree that the effect of orbital quantization on longitudinal magnetoresistance in pure germanium is very small as long as* $\hbar\omega_c/kT \lesssim 1$ *or so.*

Calculations[8] based on the simple-model theory of Argyres[7] give $\rho(H)$ actually about 15 per cent below $\rho(0)$ for $\hbar\omega_c/kT = 1$, rising to $\rho(0)$ for $\hbar\omega_c/kT \approx 2$ and increasing linearly at high fields. The initial depression, however, is due to the fact that, in this theory, the scattering is

describable by a relaxation time $\tau(\epsilon)$ which goes to zero when $\epsilon = (n + \frac{1}{2})\hbar\omega_c$. Since τ^{-1} is proportional to the density of states in energy, the mean value of τ^{-1} in an energy range several times $\hbar\omega_c$ in width is close to the value calculated without quantization. Because of the fluctuations, the mean value of τ over such a range is greater than the reciprocal of the mean of τ^{-1}; hence the conductivity is greater than in the absence of quantization, the current being carried preferentially in the energy ranges with the highest τ's. Now these fluctuations in τ will be considerably smoothed out if the energies of the phonons responsible for the scattering are even a fraction of $\hbar\omega_c$, and crude numerical calculations[8] show that a reasonable amount of such smoothing will change the maximum reduction of ρ from 15 per cent to a few per cent. Thus, we expect theoretically that the effect of quantization will be small for at least the range $\hbar\omega_c/kT \lesssim 1$.

The highest values of $\hbar\omega_c/kT$ which have so far been obtained experimentally for material with essentially acoustic scattering have been those of Furth and Waniek[12] for germanium in pulsed fields at room temperature. Their maximum field of 460,000 gauss corresponds to $\hbar\omega_c/kT = 2.1$. Up to this field, their $\rho(H)$ shows nice saturation, agreeing fairly well with the predictions of the theory ignoring quantization. By contrast, a combination of the latter curve with the quantization correction computed for zero phonon energies gives a curve which is rising conspicuously at the highest fields, and this is in marked disagreement with the observations. Moreover, the saturation values of longitudinal magnetoresistance in both the [100] and the [111] directions agree with the predictions of the unquantized theory with $w = m_\perp{}^*\tau_\parallel/m_\parallel{}^*\tau_\perp$ equal to about 0.057, a fairly reasonable value.

5. *In the region $\mu H/c \gg 1$, $\hbar\omega_c/kT < 1$ and, for acoustic scattering, the fractional changes in $Q_p(\mathbf{H})$ and in $\rho(\mathbf{H})$ attributable to orbital quantization either should both be $\ll 1$, or else should be roughly equal.*

Since the contribution of a phonon mode $\mathbf{q}$ to the Peltier flux is proportional to $[c(\mathbf{q})]^2\tau_{ph}(\mathbf{q})$, where $c(\mathbf{q})$ is its velocity and $\tau_{ph}(\mathbf{q})$ is its relaxation time, the statement just made will be valid if we can show that the crystal momentum lost by a current to the phonons is distributed in nearly the same manner among the different modes, regardless of whether quantization is assumed or ignored.

It is easy to see qualitatively that, as $\hbar\omega_c/kT$ becomes $\gg 1$, the scattering of the electrons must involve phonons whose wave-vector components $\perp\mathbf{H}$ become very large. This will undoubtedly cause the mean relaxation time of the phonons to become much shorter. Also, the change in the average direction of the wave vectors of the contributing phonons

will alter their mean relaxation time if the individual $\tau_{ph}(\mathbf{q})$ are anisotropic. Finally, if quantization changes the relative contributions of transverse and longitudinal branches, the average $[c(\mathbf{q})]^2\tau_{ph}(\mathbf{q})$ will be changed. We shall try to show, however, that all these effects are rather small when $\hbar\omega_c/kT < 1$.

Since the theory of quantum magnetoresistance is rather complicated when $\hbar\omega_c/kT < 1$, we shall base our estimates on calculations of the distribution of crystal momentum among the different phonon modes for the case $\hbar\omega_c/kT \gg 1$. These calculations give the asymptote of the curve of $(c^2\tau_{ph})_{Av}$ against $\hbar\omega_c/kT$, an asymptote which should be very nearly valid for $\hbar\omega_c/kT \approx 3$. Since the curve almost certainly is monotonic and comes in to its low-field limit with a horizontal tangent, one can estimate the order of magnitude of its deviation from the low-field value for $\hbar\omega_c/kT < 1$, or at least a rough upper bound to this. It will suffice for our purposes to give the argument for a semiconductor with isotropic effective mass, since we have shown above that, when the scattering is nearly isotropic over an energy shell, the transport problem for an anisotropic valley can be reduced to that for the isotropic case.

For **E** parallel to **H** the appropriate quantum transport theory is well understood. A brief inspection of the formulas given by Argyres[7] shows that, for $\hbar\omega_c/kT \gg 1$, the crystal momentum in the direction of the current which is delivered to the phonon modes of various wave numbers $\mathbf{q}$ is proportional to

$$q_z^2 \exp\left(\frac{-\hbar^2 q_z^2}{8m^*kT}\right) \exp\left[\frac{-\hbar(q_x^2 + q_y^2)}{4m^*\omega_c}\right], \tag{41}$$

where we have taken the z direction to be that of **E** and **H**. From this, one can derive any kind of average which may be desired. Although our main interest is in an average τ_{ph}, hence in an average of something like q^{-2} or q^{-1} with the weight (41), it will suffice to compute the more easily evaluated averages of q_x^2, q_y^2, q_z^2, noting that the average of q^{-2} will differ by a somewhat smaller percentage from its zero-field value than will that of q^2. It is clear from (41) that the averages of q_x^2 and q_y^2 will go proportionally to ω_c, while that of q_z^2 will be independent of ω_c. The most convenient quantities to tabulate are the ratios of these averages to the corresponding averages for $H = 0$; such ratios are given for $\hbar\omega_c/kT = 3$ in the first row of Table XIV. They differ by so little from unity that it seems safe to assume that, for $\hbar\omega_c/kT < 1$, the average $c^2\tau_{ph}$ is very close indeed to the value at $H = 0$.

It is worth remarking that the decrease of longitudinal resistance below the zero-field value, which the theory predicts[7,8] in the region

TABLE XIV

Ratios of the average q_x^2, q_y^2, q_z^2 of the phonon modes, weighted in proportion to the crystal momentum they receive in the current direction, to the corresponding averages in the absence of a magnetic field. The ratios were evaluated from the high-field asymptotes for the value $\hbar\omega_c/kT = 3$. For the transverse case the predictions of two rival theories are given. Acoustic scattering has been assumed.

Direction		Theory	$\frac{(q_x^2)\text{Av. at } H}{(q_x^2)\text{Av. at } 0}$	$\frac{(q_y^2)\text{Av. at } H}{(q_y^2)\text{Av. at } 0}$	$\frac{(q_z^2)\text{Av. at } H}{(q_z^2)\text{Av. at } 0}$
E	H		(linear in H)	(linear in H)	(constant)
z	z	Argyres[7]	1.12	1.12	1.29
x	z	Argyres[10]	1.12	1.12	$\to 0$
x	z	Klinger-Voronyuk[9]	1.77	3.37	$\to 0$

$\hbar\omega_c/kT \lesssim 2$, probably has no very noticeable counterpart in the behavior of the $(q_x^2)_{\text{Av}}$ etc. This decrease arises from the current being carried preferentially in the regions of energy just below the values $(n + \frac{1}{2})\hbar\omega_c$, where the relaxation time is longer than average. But the changes in the average q_x^2 etc., for transitions at energy ϵ as ϵ passes through $(n + \frac{1}{2})\hbar\omega_c$ are much less pronounced than those in the relaxation time.

Similar calculations can be made from the theory of transverse quantum magnetoresistance, except that the correct form of the theory is still in dispute.[9,10] The alternative versions agree in predicting that for $\hbar\omega_c/kT \gg 1$ the current should be carried predominantly in states of low k_z, hence should involve transitions of low q_z. If the levels had zero natural width and the phonons had zero energy, the integral for the current in the **E**-direction would diverge. In the last two rows of Table XIV, where we have tabulated the predictions of the two types of theory, we have therefore used the entry "$\to 0$" in the last column. The distribution of crystal momentum in the current direction among the various modes turns out to be proportional, as far as q_z and q_y are concerned, to the last factor of (41) in the Argyres theory,[10] and to q_y^2 times this factor in the theory of Klinger and Voronyuk.[9] While the latter theory spreads the q_y-distribution rapidly as H increases, the over-all average $c^2\tau_{ph}$ reflects the combined behavior of all three components of $\mathbf{q}$, and it seems likely that, for $\hbar\omega_c/kT < 1$, the average $c^2\tau_{ph}$ will not deviate from its zero-field value by more than a small fraction of the latter.

By contrast, the values which these theories predict for the resistance $\rho(\mathbf{H})$ are at least several times $\rho(0)$ for $\hbar\omega_c/kT = 3$, for a substance like germanium.

6. *The high-field transverse magnetoresistance is so sensitive to inhomogeneities, surface conduction and other perturbing influences that it cannot serve as a reliable indicator of the size of the orbital-quantization effect.*

At least, before it can be so used, many auxiliary investigations will have to be made to ensure the elimination of such perturbing influences. For the present purpose it will suffice to consider the case where the normal bulk conduction is in parallel with conduction by some other mechanism (e.g., surface conduction) which has a widely different Hall effect, say zero. Slight inhomogeneities in the bulk conduction itself can be shown to have a similar effect,[4] though they are probably not of major importance for our specimens.

Let the x-axis be along the length of the specimen, and let the magnetic field $\mathbf{H}$ be in the z-direction. Let ρ_b and ρ_s be the effective resistivities due respectively to normal bulk conduction alone and to the perturbing conduction alone, and let R_b , $R_s = 0$ be the corresponding Hall constants. Then we have, assuming for simplicity that ρ_b and ρ_s are isotropic,

$$j_{sy} = -j_{by} , \tag{42}$$

$$E_y = \rho_b j_{by} - R_b H j_{bx} = -\rho_s j_{by} , \tag{43}$$

$$E_x = \rho_b j_{bx} + R_b H j_{by} = \rho_s j_{sx} . \tag{44}$$

From (43) and (44) we get the effective resistivity

$$\begin{aligned} \rho_{\text{eff}} = \frac{E_x}{(j_{bx} + j_{sx})} &= \frac{\rho_s[\rho_b(\rho_b + \rho_s) + (R_b H)^2]}{(\rho_b + \rho_s)^2 + (R_b H)^2} \\ &\approx \rho_b \left[1 + \frac{(R_b H)^2}{\rho_b \rho_s} \right] \end{aligned} \tag{45}$$

if $\rho_s \gg R_b H \gg \rho_b$. The physical meaning of (45) is that the Hall field due to the b-conduction is partially shorted by the s-conduction, with consequent increase of the total dissipation. If ρ_s is, say, 200 ρ_b but $R_b H/\rho_b$ is 7, the second term in the bracket in (45) will be 0.25, and the effect on a parabolic extrapolation to infinite field, such as we have made in Fig. 6, will be between two and three times this.

The etching experiments described in Section V have shown that surface treatment can alter the observed transverse magnetoresistance by a very sizable amount at liquid-air temperature, especially for $\mathbf{H} \parallel [001]$, $\mathbf{j} \parallel [100]$. The subject merits a much more thorough investigation. However, it should be emphasized that the high-field ΔQ effect is not com-

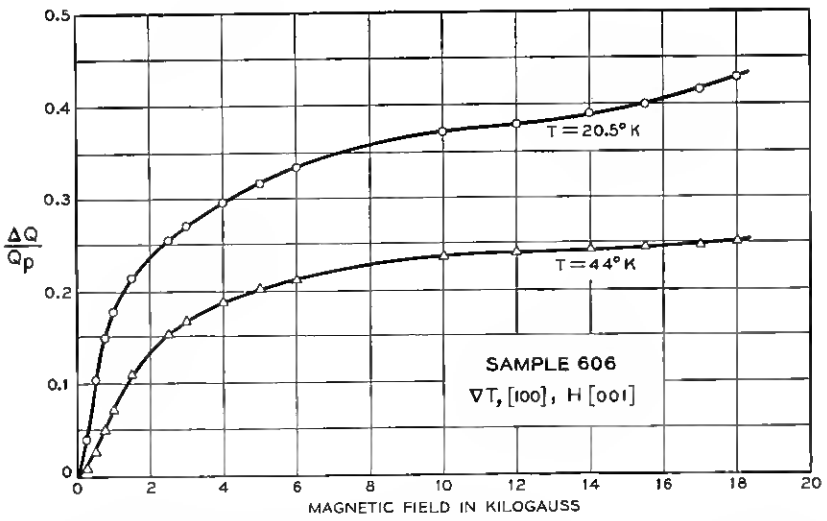

Fig. 17 — Values of the ratio of the transverse $\Delta Q(H)$ to $Q_p(0)$ for Sample 606 at 20.5° and 44°K, showing the presumed effect of orbital quantization. The values of $|Q_p(0)|$ are 8600 μv/deg at 20.5° and 3730 at 44°.

parably sensitive, either experimentally or theoretically; this is, of course, because there is no large Hall field in the ΔQ experiment.

7. *At 20° and 44°K the effect of orbital quantization on the transverse Q_p can be identified in the data, and it is small. Since the mechanisms of scattering of phonons are quite different at these two temperatures, these small values can hardly be due to an accidental cancellation of effects of quantization on $\rho(\mathbf{H})$ and on $e^2\tau_{ph}$, and it is probably safe to conclude that at liquid-air temperature quantization modifies ρ and Q_p by only a few per cent.*

Fig. 17 shows the ΔQ data for Sample 606 at these two temperatures. Both curves start to saturate as H increases, then turn upward again. These upturns are undoubtedly due to orbital quantization; one may also suspect the presence of a quantization term varying less rapidly with H than the conspicuous part of the upturn, say linearly. One would like to separate ΔQ into a nonquantization part that saturates when $\mu H/c \gg 1$ and a quantization correction dependent on $\hbar\omega_c/kT$. If, as the data suggest, a curve of the quantization correction alone against H would be concave upward, then we must surely underestimate the infinite-field limit without quantization if we assume it to equal the intercept on the $H = 0$ axis of the tangent to the $Q(H)$ curve at its most nearly horizontal portion. Thus, the difference between this intercept and the or-

dinate of the curve at 18,000 gauss ought to be an overestimate of the quantization correction. In this way we estimate that at 20.5°K, the orbital quantization correction is $\lesssim$10 per cent of $Q_p(0)$, and that at 44° it is $\lesssim$3 per cent. The reasonableness of our partition of ΔQ into its two parts is attested by the values obtained for what $\Delta Q/Q_p$ would be in the absence of quantization. Our intercept at 44° corresponds (if $|\Delta Q_e| \approx 43\mu$v/deg) to a $\Delta Q_p/Q_p$ of 0.21, only slightly larger than the values found in the liquid-air range. The intercept at 20.5° corresponds to a $\Delta Q_p/Q_p$ of about 0.33; this exceeds the high-temperature value by about the right amount to be attributed to the alteration of the phonon-phonon scattering law (see next paragraph).

Now, at 20.5°K, the scattering of the phonons involved in Q_p is almost entirely due to the boundaries of the specimen, while at 44° the phonon-phonon scattering exceeds the boundary scattering. Since these two types of scattering have quite different dependences on frequency and direction, it would not he reasonable to postulate that the effect of quantization on the average relaxation time of the participating phonons at both temperatures happens to be such as almost to cancel the effect of quantization on the magnetoresistance. The scattering of the electrons, incidentally, can be taken as approximately acoustic at both temperatures, since at 20.5° the observed Hall mobility, 215,000 cm^2/vs, is about 0.8 of the estimated ideal value. We therefore conclude that, with acoustic scattering, the effect of quantization on the transverse $\rho(H)/\rho(0)$ is probably no more than 10 per cent or possibly 20 per cent at 20.5°K. This conclusion is in violent contrast to the result of direct magnetoresistance measurements at this temperature, which for this sample (unetched!) gave $\rho(\mathbf{H})/\rho(0) = 4.8$ at 18,000 gauss. We believe the discrepancy is to be attributed to the great sensitivity of high-field transverse magnetoresistance to perturbing influences, especially surface conduction, as discussed in the Section V of the text.

From the figures given above and the plausible assumption that above 44°K the orbital-quantization term decreases at least as fast as T^{-1}, we conclude that, at liquid-air temperature and 18,000 gauss, this term is probably no more than a few per cent of the resistivity $\rho(H)$, and almost certainly is no more than this for the thermoelectric power $Q(H)$ or for $Q_p(H)$. It should be remembered, of course, that the effect of the quantization term on the extrapolation of ρ or Q to infinite field, made on a plot such as those of Fig. 6, will be proportionally larger than the effect at the field at which the extrapolation commences; for our parabolic extrapolation procedure, the factor is a little under 2 for a term proportional to H and a little over 2 for a term proportional to H^2.

APPENDIX B. DERIVATION OF FORMULAS

In this appendix we shall give some of the intermediate steps involved in applying the procedure outlined in Section III for the calculation of B and ΔQ at low and high magnetic fields. Our objective in doing so is partly to clarify the procedure used, but primarily to list a number of intermediate formulas which are especially useful or illuminating, and to give the final formulas in a form sufficiently general to be applied to other cubic many-valley structures (e.g., silicon), and to cases where the anisotropies are energy-dependent.

Our starting point is the electron-group picture, with each ellipsoidal energy shell constituting a group g. The quantities we wish to calculate are the components of the Peltier tensor $\mathbf{\Pi}$, or, rather, the terms of order 1, H, H^2 in $\mathbf{\Pi}$ at low H, and those of order 1, H^{-1} at high H. For both cases we shall base our calculations on (6) or (9), which relate $\mathbf{\Pi}$ to the partial conductivity tensors $\mathfrak{d}_g$ of the groups. These $\mathfrak{d}_g$, functions of $\mathbf{H}$, are derivable from the transport equation (10) for group g, namely,

$$\boldsymbol{\tau}^{-1}\cdot\mathbf{m}^*\cdot d\mathbf{j} \pm \left(\frac{e}{c}\right) d\mathbf{j} \times \mathbf{H} = e^2 \left(\frac{\epsilon}{\langle\epsilon\rangle}\right) \mathbf{E}\, dn\,, \tag{46}$$

where the upper and lower signs, it will be remembered, are for electrons and holes, respectively.

B.1 *Small H, Basic Formulas*

The conductivity tensor $d\mathfrak{d}(\equiv \mathfrak{d}_g)$ of an energy shell is the coefficient of $\mathbf{E}$ in the solution of (46) for $d\mathbf{j}$. For $H \to 0$ the usual way to expand $d\mathfrak{d}$ in powers of H is by iteration. In a coordinate system oriented along the principal axes of the valley we find for the parts containing H^0, H^1, H^2 respectively:

$$d\sigma_{\alpha\alpha}{}^{(0)} = e^2 \left(\frac{\epsilon}{\langle\epsilon\rangle}\right)\left(\frac{\tau_\alpha}{m_\alpha{}^*}\right) dn, \qquad d\sigma_{\alpha\beta}{}^{(0)} = 0 \qquad \text{if } \beta \neq \alpha\,; \tag{47}$$

$$d\sigma_{\alpha\beta}{}^{(1)} = \mp \left(\frac{e^3}{c}\right)\left(\frac{\epsilon}{\langle\epsilon\rangle}\right)\left(\frac{\tau_\alpha\tau_\beta}{m_\alpha{}^* m_\beta{}^*}\right) \sum_\gamma \delta_{\alpha\beta\gamma} H_\gamma\, dn\,, \tag{48}$$

where $\delta_{\alpha\beta\gamma}$ is ± 1 when α, β, γ are even (odd) permutations of 123, and is 0 otherwise; and

$$d\sigma_{\alpha\beta}{}^{(2)} = -\left(\frac{e^4}{c^2}\right)\left(\frac{\epsilon}{\langle\epsilon\rangle}\right) \sum_{\lambda\gamma\delta} \left(\frac{\tau_\alpha\tau_\beta\tau_\lambda}{m_\alpha{}^* m_\beta{}^* m_\lambda{}^*}\right) \delta_{\alpha\lambda\gamma}\delta_{\beta\lambda\delta} H_\lambda H_\delta\,. \tag{49}$$

B.2 *Value of Q at H = 0*

Let us start by computing Q for $H = 0$ in terms of the principal components $\Pi_\parallel(\epsilon)$, $\Pi_\perp(\epsilon)$ of $\mathbf{\Pi}_\beta$. From (6), (1) and (47) we have, for a cubic crystal with axially symmetrical valleys,

$$TQ(0) = \frac{1}{3}\sum_\alpha \Pi_{\alpha\alpha} = \frac{\frac{1}{3}\sum_\alpha \int \Pi_{\beta\alpha\alpha} d\sigma_{\alpha\alpha}^{(0)}}{\frac{1}{3}\sum_\alpha \int d\sigma_{\alpha\alpha}^{(0)}} = \frac{\langle \epsilon \Pi_\parallel \tau_\parallel / m_\parallel^* \rangle + 2\langle \epsilon \Pi_\perp \tau_\perp / m_\perp^* \rangle}{\langle \epsilon \tau_\parallel / m_\parallel^* \rangle + 2\langle \epsilon \tau_\perp / m_\perp^* \rangle}, \tag{50}$$

where, as always, the angular brackets denote Maxwellian averages. This equation, of course, also holds for Q_e and Q_p separately, with $\Pi_{\parallel,\perp} \to \Pi_e$ or $\Pi_{p\parallel,\perp}$. When the anisotropies $p = \Pi_{p\parallel}/\Pi_{p\perp}$ and $w = m_\perp^* \tau_\parallel / m_\parallel^* \tau_\perp$ are energy-independent, the expression for Q_p reduces to

$$TQ_p(0) = \frac{\langle \epsilon \Pi_\perp \tau_\perp \rangle}{\langle \epsilon \tau_\perp \rangle} \frac{(2 + pw)}{(2 + w)}. \tag{51}$$

When $\mathbf{\Pi}_p$ and τ depend on energy according to simple power laws, the Maxwellian averages occurring in these and subsequent expressions can be evaluated from Table XV at the end of this appendix.

B.3 *The Low-Field Value of B*

From (1), (5) and (6) we have, if $\mathbf{H}$ is in the z direction

$$TBH = \Pi_{xy}^{(1)} = \Big[\sum_\beta \Pi_\beta \cdot \sigma_\beta^{(1)}\Big]_{xy} \rho^{(0)} + \frac{\Pi^{(0)} \rho_{xy}^{(1)}}{\rho^{(0)}}. \tag{52}$$

If the crystal has over-all cubic symmetry, the evaluation of the first term on the right of (52) can be greatly simplified by noting that it is isotropic and may therefore be replaced by its average over all permutations of the directions of x, y and z (keeping the system right-handed, of course). If this averaging is done before the summing on valleys, the result will be the same for all valleys. For a single valley it can be evaluated by taking the coordinate axes along the principal axes of the valley. We find in this way, using (48),

$$\Big[\sum_\beta \mathbf{\Pi}_\beta \cdot \mathfrak{d}_\beta^{(1)}\Big]_{xy} = \mp \frac{ne^3 \rho^{(0)} H}{3c\langle \epsilon \rangle} \left[\frac{\langle \epsilon \tau_\perp^2 \Pi_\perp \rangle}{m_\perp^{*2}} + \frac{\langle \epsilon \tau_\parallel \tau_\perp \Pi_\perp \rangle}{m_\parallel^* m_\perp^*} + \frac{\langle \epsilon \tau_\parallel \tau_\perp \Pi_\parallel \rangle}{m_\parallel^* m_\perp^*}\right], \tag{53}$$

where n is the total carrier density and, as usual, the angular brackets

represent Maxwellian averages. In the last term of (52) we have, from (11),

$$\frac{\rho_{xy}^{(1)}}{\rho^{(0)}} = \pm \frac{\mu_H H}{c}, \tag{54}$$

where μ_H is the low-field Hall mobility. We may use these and the expressions of Ref. 3 — also obtainable from (47) and (48) —

$$\sigma^{(0)} = \rho^{(0)-1} = \frac{ne^2}{3\langle\epsilon\rangle}\left[\frac{2\langle\epsilon\tau_\perp\rangle}{m_\perp^*} + \frac{\langle\epsilon\tau_\parallel\rangle}{m_\parallel^*}\right], \tag{55}$$

$$\mu_H = c\left[\frac{\langle\epsilon\tau_\perp^2\rangle}{m_\perp^{*2}} + \frac{2\langle\epsilon\tau_\parallel\tau_\perp\rangle}{m_\parallel^* m_\perp^*}\right]\left[\frac{2\langle\epsilon\tau_\perp\rangle}{m_\perp^*} + \frac{\langle\epsilon\tau_\parallel\rangle}{m_\parallel^*}\right]^{-1}, \tag{56}$$

to obtain finally

$$TB = \left\{\mp\left[\frac{\langle\epsilon\tau_\perp^2\Pi_\perp\rangle}{m_\perp^{*2}} + \frac{\langle\epsilon\tau_\parallel\tau_\perp\Pi_\perp\rangle}{m_\parallel^* m_\perp^*} + \frac{\langle\epsilon\tau_\parallel\tau_\perp\Pi_\parallel\rangle}{m_\parallel^* m_\perp^*}\right] \cdot \left[\frac{\langle\epsilon\tau_\perp^2\rangle}{m_\perp^{*2}} + \frac{2\langle\epsilon\tau_\parallel\tau_\perp\rangle}{m_\parallel^* m_\perp^*}\right]^{-1} \pm TQ\right\}\frac{\mu_H}{c}. \tag{57}$$

This again applies to B_p and B_e separately, as well as to their sum, if $\Pi_{\parallel,\perp}$ and Q are given the appropriate subscript. When the anisotropies are independent of energy the formulas of Table I are easily derived from this with the use of (51). Note that the sign of B is independent of the sign of the carriers, since for electrons the upper sign is to be used in (57) with negative Π's and Q, while the reverse obtains for holes.

All the formulas we have written thus far apply to any cubic material with axially symmetrical valleys.

B.4 *General Formulas for ΔQ at Small H*

For the low-field ΔQ we must take the second-order part of (9) and use (48) and (49). Alternatively, we can eliminate the $d\mathfrak{d}^{(1)}$'s in favor of B. For the second-order part of the thermoelectric power in the α direction we find, for extrinsic material,

$$Q_{\alpha\alpha}^{(2)} = \left(\frac{\rho^{(0)}}{T}\right)\sum_g [\Pi_g \cdot \sigma_g^{(2)}]_{\alpha\alpha} + Q^{(0)}\left[\frac{\rho_{\alpha\alpha}^{(2)}}{\rho^{(0)}}\right] + \left[Q^{(0)}\left(\frac{\mu_H}{c}\right)^2 \mp B\left(\frac{\mu_H}{c}\right)\right](H^2 - H_\alpha^2), \tag{58}$$

with the usual convention of upper sign for n type, lower sign for p. The quantity $\rho_{\alpha\alpha}^{(2)}/\rho^{(0)}$ is just the magnetoresistance. Our task is now to compute the first term of (58) for various orientations.

Since in cubic material three phenomenological constants suffice to describe $\mathbf{Q}^{(2)}$ for all possible orientations of $\mathbf{H}$ and ∇T, only three evaluations of (58) need be made. We can show further than when the valleys have [100] or [111] orientations in the Brillouin zone, their axial symmetry alone gives a further relation between the three constants, at least to the accuracy of the electron-group approximation, so that only two orientations need be computed. The argument, which is a generalization of the corresponding one for magnetoresistance, was given in Appendix C of our first paper.[1] In terms of the q_b, q_c, q_d defined under Table IV the results are

$$q_c = -q_b \quad \text{for [111] valleys,} \tag{59}$$

$$q_b + q_c + q_d = 0 \quad \text{for [100] valleys.} \tag{60}$$

The evaluation of (58) can take a variety of forms, depending on whether $\boldsymbol{\varrho}^{(2)}$ and B are expressed explicitly in terms of the τ's and $\mathbf{\Pi}$'s, or are left as themselves. These forms can be converted into one another by use of (57) etc., and of

$$\frac{\rho_{\alpha\alpha}^{(2)}}{\rho^{(0)}} = -\frac{\sum_g \sigma_{g\alpha\alpha}^{(2)}}{\sigma^{(0)}} \qquad (\alpha \parallel \mathbf{H})$$

or (61)

$$= -\left[\left(\frac{\mu_H}{c}\right)^2 + \frac{\sum_g \sigma_{g\alpha\alpha}^{(2)}}{\sigma^{(0)}}\right] \qquad (\alpha \perp \mathbf{H}).$$

The expressions for $\sum_g \sigma_{g\alpha\alpha}^{(2)}$ can be taken from the magnetoresistance literature, or (for [111] valleys) from (65) below or its longitudinal modification, by setting $\mathbf{\Pi} = \mathbf{1}$.

B.5 ΔQ_e at Small H with Energy-Independent Anisotropies

As with the Nernst coefficient, the evaluation of $Q_e^{(2)}$ for the case of an energy-independent anisotropy of τ is a little easier than that of $Q_p^{(2)}$. When $\mathbf{H}$ is parallel to the direction of measurement (the α direction), the last term of (58) drops out and, with $\mathbf{\Pi}_g$ replaced by $\mp\epsilon/e$, the ratio of the first term of (58) to the second is a function only of the energy dependence of τ. Using (61) we find easily, with $\rho^{(2)} = \Delta\rho$ and with the upper sign for electrons, the lower for holes,

$$\Delta Q_e = Q_{e\alpha\alpha}^{(2)} = \mp\frac{3}{2}\frac{k}{e}\left[\frac{\langle\epsilon^2\tau\rangle}{\langle\epsilon\tau\rangle\langle\epsilon\rangle} - \frac{\langle\epsilon^2\tau^2\rangle}{\langle\epsilon\tau^3\rangle\langle\epsilon\rangle}\right]\frac{\Delta\rho}{\rho(0)} \quad (\alpha \text{ longitudinal}). \tag{62}$$

For transverse or general orientations of $\mathbf{H}$ we must use (57) to evaluate

the last term of (58) and must modify the relation of $\mathfrak{d}_g^{(2)}$ to $\varrho^{(2)}$; a little algebra gives

$$\Delta Q_e = Q_{e\alpha\alpha}{}^{(2)} = \mp\frac{3}{2}\frac{k}{e}\left[\left(\frac{\langle\epsilon^2\tau\rangle}{\langle\epsilon\tau\rangle\langle\epsilon\rangle} - \frac{\langle\epsilon^2\tau^3\rangle}{\langle\epsilon\tau^3\rangle\langle\epsilon\rangle}\right)\frac{\Delta\rho}{\rho(0)} + \left(\frac{\langle\epsilon^2\tau^2\rangle}{\langle\epsilon\tau^2\rangle\langle\epsilon\rangle} - \frac{\langle\epsilon^2\tau^3\rangle}{\langle\epsilon\tau^3\rangle\langle\epsilon\rangle}\right)\left(\frac{\mu_H}{c}\right)^2 (H^2 - H_\alpha{}^2)\right]. \tag{63}$$

These formulas are valid for any multivalley band structure in a cubic crystal. Still more general expressions for ΔQ_e, valid for [111] valleys if the anisotropy of τ is not energy-independent, could be obtained from (65) below.

B.6 ΔQ and ΔQ_p at Small H

Because of the anisotropy of $\mathbf{\Pi}_p$, the first term of (58) is a little more difficult to evaluate for the phonon-drag contribution or for the total ΔQ. We may again eliminate the sum over different valleys by noting that ΔQ is unchanged if we apply any operation D of the cubic symmetry group both to $\mathbf{H}$ and to ∇T, the α-direction in (58). If we average the contribution of each valley over all such D, the result will be the same for all valleys. If $\mathbf{u}^{(T)}$ is the unit vector in the direction of ∇T, the result can be written, in the principal-axis system of some one valley,

$$\mathbf{u}^{(T)}\cdot\sum_g [\mathbf{\Pi}_g\cdot\mathfrak{d}_g^{(2)}]\cdot\mathbf{u}^{(T)} = -\frac{ne^4}{c^2}\sum_{\alpha\beta\lambda\gamma\delta}\frac{\langle\epsilon\Pi_\alpha\tau_\alpha\tau_\beta\tau_\lambda\rangle}{\langle\epsilon\rangle m_\alpha{}^* m_\beta{}^* m_\lambda{}^*}\delta_{\lambda\beta\gamma}\delta_{\lambda\alpha\delta} \cdot\langle H_\gamma H_\delta u_\alpha{}^{(T)} u_\beta{}^{(T)}\rangle_D, \tag{64}$$

where $\langle\ \rangle_D$ means the average of the components shown over all sets, $D\mathbf{H}$, $D\mathbf{u}^{(T)}$.

So far, the equations are valid for any cubic multivalley material. We shall now specialize to valleys along the [111] axes of the Brillouin zone. For this case and for $\mathbf{H}$ along a [100] axis, $\nabla T \perp \mathbf{H}$, (64) can be evaluated to

$$\mathbf{u}^{(T)}\cdot\sum_g [\mathbf{\Pi}_g\cdot\mathfrak{d}_g^{(2)}]\cdot\mathbf{u}^{(T)} = -\frac{ne^4H^2}{c^2}\left[\frac{2}{9}\frac{\langle\epsilon\Pi_\parallel\tau_\parallel{}^2\tau_\perp\rangle}{\langle\epsilon\rangle m_\parallel{}^{*2} m_\perp{}^*} + \frac{1}{9}\frac{\langle\epsilon\Pi_\parallel\tau_\parallel\tau_\perp{}^2\rangle}{\langle\epsilon\rangle m_\parallel{}^* m_\perp{}^{*2}} + \frac{4}{9}\frac{\langle\epsilon\Pi_\perp\tau_\parallel\tau_\perp{}^2\rangle}{\langle\epsilon\rangle m_\parallel{}^* m_\perp{}^{*2}} + \frac{2}{9}\frac{\langle\epsilon\Pi_\perp\tau_\perp{}^3\rangle}{\langle\epsilon\rangle m_\perp{}^{*3}}\right]. \tag{65}$$

When $\mathbf{H}$ and ∇T are both along a [100] axis we find an expression of similar form to (65) but with the coefficients $\frac{2}{9}$, $\frac{1}{9}$, $\frac{4}{9}$, $\frac{2}{9}$ replaced respec-

tively by $\frac{2}{3}$, $-\frac{2}{3}$, $-\frac{2}{3}$, $\frac{2}{3}$. These expressions apply, of course, to either the electron or the phonon-drag contribution, or to their sum; one need only affix the proper subscript to all Π's.

For the most general case the expression for ΔQ in terms of moments of $\Pi_{\parallel,\perp}$ is obtained by inserting (65), or its longitudinal modification, into (58); one may or may not wish to express the $Q^{(0)}$ and B occurring there by (50) and (57). The magnetoresistance can be expressed if desired by (61) and (65) with $\mathbf{\Pi} = \mathbf{1}$, and $\rho^{(0)}$ and μ_H by (55) and (56). The last entries in Table IX were obtained in this way.

If we assume that $p = \Pi_{p\parallel}/\Pi_{p\perp}$ and $w = \tau_\parallel m_\perp{}^*/\tau_\perp m_\parallel{}^*$ are energy-independent, we get, after a little reduction,

$$\Delta Q_p\Big]_{100}^{001} = Q_p\left(\frac{\mu_H H}{c}\right)^2\left[\zeta_p + \frac{(2+w)^2}{3(1+2w)}\left(\frac{\langle\epsilon\tau^3\rangle\langle\epsilon\tau\rangle}{\langle\epsilon\tau^2\rangle^2} - \frac{\langle\epsilon\tau\rangle^2\langle\epsilon\Pi\tau^3\rangle}{\langle\epsilon\Pi\tau\rangle\langle\epsilon\tau^2\rangle^2}\right)\right], \quad (66)$$

$$\begin{aligned}\Delta Q_p\Big]_{001}^{001} &= Q_p\frac{\Delta\rho}{\rho} - Q_p\left(\frac{\mu_H H}{c}\right)^2 \\ &\quad\cdot\frac{2}{3}\frac{(2+w)^2(1-w)(1-pw)}{(2+pw)(1+2w)^2}\frac{\langle\epsilon\tau\rangle^2\langle\epsilon\Pi\tau^3\rangle}{\langle\epsilon\Pi\tau\rangle\langle\epsilon\tau^2\rangle^2} \\ &= Q_p\left(\frac{\mu_H H}{c}\right)^2\frac{2}{3}\frac{(2+w)(1-w)}{(1+2w)^2}\left[\frac{(1-w)\langle\epsilon\tau\rangle\langle\epsilon\tau^3\rangle}{\langle\epsilon\tau^2\rangle^2}\right. \\ &\quad\left. - \frac{(2+w)(1-pw)}{(2+pw)}\frac{\langle\epsilon\tau\rangle^2\langle\epsilon\Pi\tau^3\rangle}{\langle\epsilon\Pi\tau\rangle\langle\epsilon\tau^2\rangle^2}\right].\end{aligned} \quad (67)$$

It is perhaps worth remarking that there exist a variety of checks which can be applied to calculations of this sort. For example, ΔQ should always vanish if all $\mathbf{\Pi}_a$ are the same multiple of the unit tensor. Again, setting $\mathbf{\Pi} \propto \mathbf{m}^*\cdot\boldsymbol{\tau}^{-1}$ should give the magnetoresistance.[1] These and other tests of the same sort are very helpful in uncovering algebraic errors.

B.7 *Large H, Basic Formulas*

The leading term in the expansion of the solution of (46) in powers of H^{-1} is especially simple when the geometry is such that $\mathbf{E}$ is either exactly parallel or exactly perpendicular to $\mathbf{H}$. As these cases include all the orientations dealt with in this paper, we shall give first some formulas based on these specializations.

When $\mathbf{E}$ and $\mathbf{H}$ are parallel, the part of $d\mathbf{j}$ normal to $\mathbf{H}$ must be of order EH^{-1}, since, if it were of lower order in H^{-1}, the term of (46) in $d\mathbf{j} \times \mathbf{H}$ could not be compensated by anything else. Therefore, only the part dj_H of $d\mathbf{j}$ parallel to $\mathbf{H}$ can be of order EH^0. It is obtained by taking

the component of (46) along **H**:

$$dj_H = e^2 \left(\frac{\epsilon}{\langle\epsilon\rangle}\right) \frac{E_H dn}{(\mathbf{m}^* \cdot \boldsymbol{\tau}^{-1})_{HH}}, \qquad \text{if } \mathbf{E} \parallel \mathbf{H}, \tag{68}$$

with neglect of terms of order H^{-1}.

When **E** and **H** are perpendicular, as they always are when **H** is perpendicular to a symmetry plane and the total **j** is in this plane, we can start the solution of (46) by taking its cross product with the unit vector $\mathbf{u}^{(H)}$ in the direction of **H**. The Hall field now dominates **E**, so all components of $d\mathbf{j}$ are of order EH^{-1}, and the component normal to **H** measures in essence the Hall velocity cEH^{-1}. We find, to the first order in H^{-1},

$$(\text{part of } d\mathbf{j} \perp \mathbf{H}) = \pm ec \left(\frac{\epsilon}{\langle\epsilon\rangle}\right) \mathbf{u}^{(H)} \times \mathbf{E} H^{-1} dn \qquad \text{if } \mathbf{E} \perp \mathbf{H}, \tag{69}$$

where the upper sign is for electrons, the lower for holes. The part of $d\mathbf{j}$ parallel to **H** is now obtained by taking the dot product of (46) with $\mathbf{u}^{(H)}$ and using (69). The result of combining the two is, to the first order,

$$d\mathbf{j} = \pm ec \left(\frac{\epsilon}{\langle\epsilon\rangle}\right) \left[\mathbf{u}^{(H\times E)} - \frac{(\mathbf{m}^* \cdot \boldsymbol{\tau}^{-1})_{H\times E, H} \mathbf{u}^{(H)}}{(\mathbf{m}^* \cdot \boldsymbol{\tau}^{-1})_{HH}}\right] \frac{E}{H} \qquad \text{if } \mathbf{E} \perp \mathbf{H}, \tag{70}$$

where now we have used the label $H \times E$ in subscripts and superscripts to designate the corresponding coordinate direction, just as we used H above; $u^{(H\times E)}$ is the unit vector in this direction.

The expressions (68) and (70) will suffice for the calculation of the high-field limit of Q; to get the high-field behavior of the Nernst effect, however, for Table II, we need the conductivity tensor to one higher order. Rather than writing this down explicitly, we shall outline the result of a systematic solution of (46) by iteration of the procedures just used. Let us write for the conductivity tensor of the shell

$$d\boldsymbol{\sigma}(\mathbf{H}) = d\boldsymbol{\sigma}^{(\infty)} + d\boldsymbol{\sigma}^{(-1)} + d\boldsymbol{\sigma}^{(-2)} + \cdots, \tag{71}$$

where the superscripts ∞, -1, -2, etc. denote respectively terms of zeroth, first, second, etc. orders in H^{-1}. With a corresponding notation for the components of $d\mathbf{j}$, we find that, for $k > 1$, the part of $d\mathbf{j}^{(-k)}$ perpendicular to **H** can be obtained in terms of $d\mathbf{j}^{(-k+1)}$ by taking the cross product of (46) with $\mathbf{u}^{(H)}$, and the part parallel to **H** from both this result and the dot product of (46) with $\mathbf{u}^{(H)}$. The general term can be written concisely but abstractly in the form

$$d\mathfrak{d}^{(-k)} = -\left(\frac{\pm c}{eH}\right)^k e^2 \left(\frac{\epsilon}{\langle\epsilon\rangle}\right) (\mathbf{G}\cdot\mathbf{U}\cdot\mathbf{S})^{k-1}\cdot\mathbf{G}\cdot\mathbf{U}\cdot\mathbf{G}^+ dn, \qquad (72)$$

if $k \geqq 1$; the direction of $\mathbf{E}$ is now unrestricted. Here $\mathbf{S}$ stands for the tensor $\mathbf{m}^*\cdot\boldsymbol{\tau}^{-1}$, while

$$G_{\alpha\beta} = \delta_{\alpha\beta} - S_{HH}{}^{-1} u_\alpha{}^{(H)} \sum_\lambda u_\lambda{}^{(H)} S_{\lambda\beta}, \qquad (73)$$

$\mathbf{G}^+$ is the transposed tensor, and

$$U_{\beta\gamma} = \sum_\mu \delta_{\beta\gamma\mu} u_\mu{}^{(H)}. \qquad (74)$$

By use of the identity $G^+S = SG$ one can easily show that (72) is symmetrical for even k, antisymmetrical for odd, as it should be.

B.8 *Limits of Q_e and Q_p at Large H*

For either Q_p or Q_e, or their sum, we have, from (6) and the Kelvin relation, the high-field limit $Q^{(\infty)}$ given by

$$TQ_{\alpha\alpha}{}^{(\infty)} = \sum_\varrho (\mathbf{\Pi}_\varrho\cdot\mathfrak{d}_\varrho{}^{(\infty)}\cdot\boldsymbol{\varrho}^{(\infty)})_{\alpha\alpha} + \sum_\varrho (\mathbf{\Pi}_\varrho\cdot\mathfrak{d}_\varrho{}^{(-1)}\cdot\boldsymbol{\varrho}^{(+1)})_{\alpha\alpha}, \qquad (75)$$

where α labels the rectangular direction in which Q is measured, and where, by analogy with the notation already used, $\rho^{(\infty)}$ is the limiting resistivity tensor at infinite H and $\rho^{(+1)}$ is the high-field Hall tensor (12).

When the α direction is parallel to $\mathbf{H}$, the only nonvanishing component of $\sigma_\varrho{}^{(\infty)}$ is, by (68), the $\alpha\alpha$ one. Moreover, in this case $\rho_{\beta\alpha}{}^{(+1)}$ vanishes for all β, so only the first term of (75) remains. In this term we can replace $\rho_{\alpha\alpha}{}^{(\infty)}$ by $(\sum_\varrho \sigma_{\varrho\alpha\alpha}{}^{(\infty)})^{-1}$, so we have

$$TQ_{\alpha\alpha}{}^{(\infty)} = \frac{\sum_i \langle\epsilon\Pi_{\alpha\alpha}{}^{(i)}/(\mathbf{m}^*\cdot\boldsymbol{\tau}^{-1})_{\alpha\alpha}{}^{(i)}\rangle}{\sum_i \langle\epsilon/(\mathbf{m}^*\cdot\boldsymbol{\tau}^{-1})_{\alpha\alpha}{}^{(i)}\rangle} \qquad \text{if } \mathbf{H} \parallel \alpha, \qquad (76)$$

where i labels the different valleys.

If the different components of $\boldsymbol{\tau}$ all have the same energy dependence, the relative magnitudes of the currents (68) for shells of different energies will be the same as for $H = 0$, so, as (76) and (50) show explicitly,

$$Q_e{}^{(\infty)} = Q_e(0) \text{ parallel to } \mathbf{H}. \qquad (77)$$

If the valleys have [111] orientations in a cubic crystal, the general form (76) becomes, for symmetry directions,

$$TQ_p^{(\infty)}\Big]_{001}^{001} = \frac{\langle \epsilon[\Pi_{p\parallel} + 2\Pi_{p\perp}][(m_\parallel^*/\tau_\parallel) + 2(m_\perp^*/\tau_\perp)]^{-1}\rangle}{3\langle \epsilon[(m_\parallel^*/\tau_\parallel) + 2(m_\perp^*/\tau_\perp)]^{-1}\rangle}, \tag{78}$$

$$TQ_p^{(\infty)}\Big]_{011}^{011} = \frac{\langle \epsilon\Pi_{p\perp}\tau_\perp/m_\perp^*\rangle + \langle \epsilon[\Pi_{p\perp} + 2\Pi_{p\parallel}][(m_\perp^*/\tau_\perp) + 2(m_\parallel^*/\tau_\parallel)]^{-1}\rangle}{\langle \epsilon\tau_\perp/m_\perp^*\rangle + 3\langle \epsilon[(m_\perp^*/\tau_\perp) + 2(m_\parallel^*/\tau_\parallel)]^{-1}\rangle}, \tag{79}$$

$$TQ_p^{(\infty)}\Big]_{111}^{111} = \frac{\langle \epsilon\Pi_{p\parallel}\tau_\parallel/m_\parallel^*\rangle + 3\langle \epsilon[\Pi_{p\parallel} + 8\Pi_{p\perp}][(m_\parallel^*/\tau_\parallel) + 8(m_\perp^*/\tau_\perp)]^{-1}\rangle}{\langle \epsilon\tau_\parallel/m_\parallel^*\rangle + 27\langle \epsilon[(m_\parallel^*/\tau_\parallel) + 8(m_\perp^*/\tau_\perp)]^{-1}\rangle}. \tag{80}$$

As usual, these equations also hold for Q_e and Q_p individually, if $\Pi_\parallel$ and $\Pi_\perp$ are given the corresponding subscript. Further simplifications are possible if the anisotropies are energy-independent, as assumed in Table III, or if the τ's are $\propto \epsilon^{-\frac{1}{2}}$, etc.

When the α direction is perpendicular to **H** and **H** is normal to a symmetry plane, (70) suffices for the evaluation of (75). For this case, the first term of (75) vanishes, since $\sigma_\varrho^{(\infty)}$ has only an HH component and $\rho^{(\infty)}$ has no αH component. We find easily

$$TQ_{\alpha\alpha}^{(\infty)} = N_V^{-1}\langle\epsilon\rangle^{-1}\sum_i \left\langle \left(\Pi_{\alpha\alpha}^{(i)} - \frac{S_{\alpha H}^{(i)}}{S_{HH}^{(i)}}\right)\Pi_{\alpha H}^{(i)}\right\rangle \qquad (\alpha \perp \mathbf{H}), \tag{81}$$

where i runs over the different valleys, N_V in number, and where, as above, $\mathbf{S}^{(i)}$ is the tensor $\mathbf{m}^*\cdot\boldsymbol{\tau}^{-1}$ for the ith valley. This holds for any multivalley structure when the symmetry is such that **E** is exactly $\perp$**H**. The entries of Tables III and IX are specializations of (81).

B.9 *Asymptotic Behavior of B as* $H \to \infty$

Let **H** he in the z-direction, ∇T in the x-direction. From (1), (5), (6) and the symmetries which we proved ahove from (72), we find

$$T\left[\frac{\partial(BH)}{\partial(H^{-1})}\right]_\infty = H\left[\sum_\varrho \Pi_\varrho\cdot(\sigma_\varrho^{(-2)}\cdot\rho^{(+1)} + \sigma_\varrho^{(-1)}\cdot\rho^{(\infty)})\right]_{xy}, \tag{82}$$

where, it will he remembered, the superscripts -2, -1, ∞, $+1$ denote quantities going as H^{-2}, H^{-1}, H^0, H as $H \to \infty$. Here we may use (12) for $\rho^{(+1)}$ and get $\sigma^{(-1)}$ from (70). Since $\rho^{(+1)}$ has only xy and yx components, the first term on the right of (82) involves just $(\sum_\varrho \Pi_\varrho\cdot\sigma_\varrho^{(-2)})_{xx}$. Use of the explicit evaluation of $\mathfrak{d}_\varrho^{(-2)} = d\mathfrak{d}^{(-2)}$ from (72) gives

$$(\mathbf{\Pi}_g \cdot d\mathfrak{d}^{(-2)})_{xx} = -\frac{c^2\epsilon\, dn}{H^2\langle\epsilon\rangle}\left[\left(\Pi_{gxy} - \frac{\Pi_{gxz}S_{zy}}{S_{zz}}\right)\left(S_{xy} - \frac{S_{xz}S_{yz}}{S_{zz}}\right) - \left(\Pi_{gxx} - \frac{\Pi_{gxz}S_{xz}}{S_{zz}}\right)\left(S_{yy} - \frac{S_{yz}^2}{S_{zz}}\right)\right], \tag{83}$$

where, as above, $\mathbf{S}$ is the tensor $\mathbf{m}^* \cdot \boldsymbol{\tau}^{-1}$ for group g. If the directions of $\mathbf{H}$ and ∇T are such that $\rho^{(\infty)}$ is diagonal in our coordinate system, the second term on the right of (82) involves $(\Pi_g \cdot \sigma_g^{(-1)})_{xy}$, for which we find

$$(\mathbf{\Pi}_g \cdot d\mathfrak{d}^{(-1)})_{xy} = \pm\frac{ce\epsilon\, dn}{H\langle\epsilon\rangle}\left(\Pi_{gxx} - \frac{\Pi_{gxz}S_{xz}}{S_{zz}}\right), \tag{84}$$

where, as always, the upper sign is for electrons, the lower for holes. By the use of (50) and the relation

$$\frac{c}{\mu} = \mp\frac{\rho^{(0)}}{R(\infty)} \tag{85}$$

we can evaluate (82) in the form,

$$\begin{aligned}\frac{1}{Q(0)}\left[\frac{\partial(BH)}{\partial(c/\mu H)}\right]_\infty &= \mp\frac{\langle\epsilon(S_\parallel^{-1} + 2S_\perp^{-1})\rangle^2}{3\left\langle\epsilon\left(\frac{\Pi_\parallel}{S_\parallel} + \frac{2\Pi_\perp}{S_\perp}\right)\right\rangle\langle\epsilon\rangle^2 N_V} \\ &\cdot \sum_i \left\langle\epsilon\left(\Pi_{xy}^{(i)} - \frac{\Pi_{xz}^{(i)}S_{zy}^{(i)}}{S_{zz}^{(i)}}\right)\left(S_{xy}^{(i)} - \frac{S_{xz}^{(i)}S_{yz}^{(i)}}{S_{zz}^{(i)}}\right)\right. \\ &\left. - \epsilon\left(\Pi_{xx}^{(i)} - \frac{\Pi_{xz}^{(i)}S_{zx}^{(i)}}{S_{zz}^{(i)}}\right)\left(S_{yy}^{(i)} - \frac{S_{yz}^{(i)2}}{S_{zz}^{(i)}}\right)\right\rangle \\ &\mp \frac{\langle\epsilon(S_\parallel^{-1} + 2S_\perp^{-1})\rangle}{\left\langle\epsilon\left(\frac{\Pi_\parallel}{S_\parallel} + \frac{2\Pi_\perp}{S_\perp}\right)\right\rangle\langle\epsilon\rangle N_V}\sum_i\left\langle\epsilon\left(\Pi_{xz}^{(i)} - \frac{\Pi_{xz}^{(i)}S_{xz}^{(i)}}{S_{zz}^{(i)}}\right)\right\rangle,\end{aligned} \tag{86}$$

where the superscript i labels the different valleys, N_V in number. This equation applies to B_e or B_p or their sum, if all Π's, B and Q are given the appropriate subscript; it is valid for any multivalley structure with over-all cubic symmetry if z is normal to a symmetry plane and x is along a two-fold or four-fold axis in the plane. The entries in Table II result from tedious but straightforward specializations of (86) to [111] valleys and energy-independent anisotropies.

B.10 *Maxwellian Averages*

As an appendix to this appendix we list here the Maxwellian averages of various powers of the energy, which are needed for the evaluation of

TABLE XV — MAXWELLIAN AVERAGES OF POWERS OF ENERGY

n	$\left\langle \left(\frac{\epsilon}{kT}\right)^n \right\rangle$
-1	2
$-\frac{3}{4}$	1.38
$-\frac{1}{2}$	$2\pi^{-1/2}$
$-\frac{1}{4}$	1.02
1	1
$\frac{1}{4}$	1.04
$\frac{1}{2}$	$2\pi^{-1/2}$
$\frac{3}{4}$	1.28
1	$\frac{3}{2}$
$\frac{5}{4}$	1.81
$\frac{3}{2}$	$4\pi^{-1/2}$
$\frac{7}{4}$	2.88
2	$\frac{15}{4}$
$\frac{9}{4}$	4.99
$\frac{5}{2}$	$12\pi^{-1/2}$

the various expressions we have derived when the τ's and Π's are assumed to have power-law dependences on energy. Since the number of Maxwellian carriers in the energy range ϵ to $\epsilon + d\epsilon$ is proportional to $\epsilon^{\frac{1}{2}} \exp(-\epsilon/kT)d\epsilon$, we have for any quantity Z

$$\langle Z \rangle \equiv \frac{\int_0^\infty Z\epsilon^{\frac{1}{2}} \exp(-\epsilon/kT)\, d\epsilon}{\int_0^\infty \epsilon^{\frac{1}{2}} \exp(-\epsilon/kT)\, d\epsilon}. \tag{87}$$

The results for various powers of the energy are given in Table XV.

REFERENCES

1. Herring, C., Geballe, T. H. and Kunzler, J. E., Phys. Rev., **111**, 1958, p. 36.
2. Herring, C., in *Halbleiter und Phosphore*, F. Vieweg & Sohn, Braunschweig, Germany, 1958, p. 184.
3. Herring, C. and Vogt, E., Phys. Rev., **101**, 1956, p. 944.
4. Herring, C., to be published.
5. Argyres, P. N. and Adams, E. N., Phys. Rev., **104**, 1956, p. 900.
6. Appel, J., Z. Naturforsch., **11a**, 1956, p. 892.
7. Argyres, P. N., J. Phys. Chem. Solids, **4**, 1958, p. 19.
8. Pollak, H. O. and Herring, C., unpublished calculations.
9. Klinger, M. I. and Voronyuk, P. I., J. Exp. Theor. Phys. (U.S.S.R.), **33**, 1957, p. 77. Translation: Soviet Phys. JETP, **6**, 1958, p. 59.
10. Argyres, P. N., Phys. Rev., **109**, 1958, p. 1115.
11. Wolff, P. A., unpublished work.
12. Furth, H. P. and Waniek, R. W., Phys. Rev., **104**, 1956, p. 343.

13. Herring, C., B.S.T.J., **34**, 1955, p. 237.
14. Dorn, D., Z. Naturforsch., **12a**, 1957, p. 18.
15. Herring, C., to be published.
16. Tanenbaum, M. and Hrostowski, H. J., unpublished measurements.
17. Goldberg, C., Phys. Rev., **109**, 1958, p. 331.
18. Goldberg, C. and Howard, W. E., Phys. Rev., **110**, 1958, p. 1035.
19. Glicksman, M., Phys. Rev., **108**, 1957, p. 264; *Progress in Semiconductors*, Vol. 3, Heywood & Co., London, 1958.
20. Conwell, E. M. and Weisskopf, V. F., Phys. Rev., **77**, 1950, p. 388.
21. Brooks, H., Phys. Rev., **83**, 1951, p. 879; *Advances in Electronics and Electron Physics*, Vol. 7, Academic Press, New York, 1955, p. 128.
22. Dingle, R. B., Phil. Mag., **46**, 1955, p. 831.
23. Sclar, Phys. Rev., **104**, 1956, p. 1548.
24. Blatt, F. J., J. Phys. Chem. Solids, **1**, 1957, p. 262.
25. Debye, P. P. and Conwell, E. M., Phys. Rev., **93**, 1954, p. 693.
26. Fan, H. Y., *Solid State Physics*, Vol. 1, Academic Press, New York, 1955, p. 283; Conwell, E. M., Proc. I.R.E., **46**, 1958, p. 1281.
27. Spitzer, L., Jr. and Härm, R., Phys. Rev., **89**, 1953, p. 977.
28. Madelung, O., *Handbuch der Physik*, Vol. 20, Springer-Verlag, Berlin, 1957, p. 1.
29. Dingle, R. B., Arndt, D. and Roy, S. K., Appl. Sci. Res., **B6**, 1956, p. 155.
30. Beer, A. C., Armstrong, J. A. and Greenberg, I. N., Phys. Rev., **107**, 1957, p. 1506.
31. Mansfield, R., Proc. Phys. Soc., **B69**, 1956, p. 862.
32. Herring, C., Phys. Rev., **95**, 1954, p. 954.
33. Brockhouse, B. N. and Iyengar, P. K., Phys. Rev., **111**, 1958, p. 747.
34. Pomeranchuk, I., J. Phys. (U.S.S.R.), **4**, 1941, p. 259; **6**, 1942, p. 237; Phys. Rev., **60**, 1941, p. 820.
35. Pomeranchuk, I., J. Phys. (U.S.S.R.), **4**, 1941, p. 529.
36. Dresselhaus, G., Kip, A. F. and Kittel, C., Phys. Rev., **98**, 1955, p. 368.
37. Morin, F. S., Geballe, T. H. and Herring, C., Phys. Rev., **105**, 1957, p. 525.